DISS. ETH NO. 25393

MICROFLUIDIC HANGING-DROP PLATFORMS FOR 3D MICROTISSUE CULTURE AND ANALYSIS

A thesis submitted to attain the degree of

DOCTOR OF SCIENCES of ETH ZURICH

(Dr. sc. ETH Zurich)

presented by

PATRICK MARK MISUN

M.Sc. Biotechnology, ETH Zurich

born on 18.09.1987

citizen of

Basel, BS, Switzerland

accepted on the recommendation of

Prof. Dr. Andreas Hierlemann

Prof. Dr. Petra S. Dittrich

Dr. Olivier Frey

2018

ABSTRACT

This thesis presents the concept and applications of microfluidic hanging-drop platforms for the culture and analysis of 3D microtissues – an emerging *in vitro* cell culture model. The motivation of this work was to bridge the gap between advances in 3D cell cultures and the commonly used cell culture platforms, which are designed prevalently for static and 2D cell cultures, and to demonstrate the potential of dedicated 3D cell culture platforms in providing suitable and reliable experimental conditions.

Hanging drops are used for the scaffold-free formation and culture of spherical 3D microtissues. These microtissues are easy to handle and feature many organotypic tissue functions, which renders them a suitable *in vitro* model system for both, basic research, and pharmaceutical industry. Despite the biological relevance and advantages of these microtissue model systems, the lack of optimized platforms for culturing and analysis still limits the widespread use and application of 3D microtissues in biomedical testing and pharmaceutical compound screening.

Microfabrication techniques offer a great toolbox to build next-generation cell culturing and analysis systems. The combination of microfluidics to realize physiologically-relevant culture conditions and microfabricated sensor units enables the realization of integrated systems for organ-, and body-on-a-chip applications.

This thesis presents the fabrication, working principle and operation of microfluidic hanging-drop networks for the culturing and analysis of 3D microtissues, and introduces three dedicated platforms for interrogating 3D models.

i. *Biosensing in hanging-drop networks.* Enzyme-based biosensors were integrated in hanging-drop networks for real-time *in situ* multi-analyte monitoring of 3D microtissue metabolism. The device enabled online detection of lactate secretion and glucose consumption of human colon cancer microtissues.

ii. *High-resolution imaging in hanging-drop networks.* Integration of hydrogels in hanging-drop networks enabled both, immobilization of 3D microtissues for high-resolution and long-term imaging, as well as providing fine control over the microenvironment of the 3D microtissues. The system allows for investigating complex

biological processes down to single-cell level and for observation of physiologically events at subcellular scale.

iii. *FlowGSIS in hanging drops.* A hanging-drop perfusion system was developed for studying the dynamics of glucose-stimulated insulin secretion (GSIS) of human endocrine pancreas islets. The device enabled high-temporal-resolution sampling to resolve the bi-phasic and pulsatile insulin release of single islets to study the effects of anti-diabetic medication.

The presented platforms represent a set of novel tools for culturing and interrogating 3D microtissues. The design and operation of each platform has been optimized for the respective application, ranging from precise stimulation of microtissues and subsequent metabolite detection, to long-term and high-resolution imaging. The broad range of applications served by these platforms and the platform complementarity greatly improve our capability of taking full advantage of 3D microtissues as organotypic *in vitro* model systems.

ZUSAMMENFASSUNG

Diese Dissertation behandelt das Prinzip und die Anwendung von mikrofluidischen Plattformen zur Kultur und Analyse von 3D-Mikrogeweben, einem aufkommenden *in vitro* Zellkulturmodell.

Die Motivation dieser Arbeit war es die Lücke zwischen neuen 3D-Zellkulturmodellen und herkömmlichen Zellkulturmethoden, welche vor allem für statische und 2D-Zellkulturen konzipiert waren, zu schliessen. Wir wollten die Vorteile und das Potential von neuen Plattformen aufzeigen, welche für 3D-Zellkulturen optimiert wurden, um geeignete und verlässliche experimentelle Bedingungen zu ermöglichen.

Hängende Tropfen werden für die gerüstfreie Formung und Kultur von sphärischen 3D-Mikrogeweben verwendet. Diese Mikrogewebe sind einfach in der Handhabung und weisen viele organtypische Eigenschaften auf, welche sie zu einem geeigneten *in vitro*-Model für die Grundlagenforschung und die Pharmaindustrie machen. Trotz der biologischen Relevanz und Vorteile dieser Mikrogewebe als Modellsystem mangelt es an optimierten Plattformen für deren Kultur und Analyse, was deren Anwendung in der Biomedizin, aber auch in der Pharmaindustrie für die Suche nach neuen Wirkstoffen beschränkt.

Mikrofabrikationsprozesse bieten eine Vielfalt an Möglichkeiten um Zellkultur-, und Analysesysteme der nächsten Generation zu entwickeln. Die Kombination von Mikrofluidik, um physiologisch relevante Kulturkonditionen zu erzeugen, und mikrofabrizierten Sensoreinheiten macht integrierte Systeme für Organ-Chip-, und Multi-Organ-Chip Anwendungen möglich.

Diese Dissertation beschreibt die Fabrikation, das Funktionsprinzip und den Einsatz von mikrofluidischen Netzwerken von hängenden Tropfen für die Kultur und Analyse von 3D-Mikrogeweben und präsentiert drei spezialisierte Plattformen für solche Zellkulturen.

i. *Biosensorik in Netzwerken von hängenden Tropfen.* Enzymbasierte Biosensoren wurden in Netzwerken von hängenden Tropfen für die Echtzeit *in situ* Überwachung des Metabolismus von 3D-Mikrogeweben integriert. Die Plattform erlaubt die online-Detektion von Laktatsekretion und Glukoseaufnahme von humanen Darmkrebsmikrogeweben.

ii. *Hochaufgelöste Bildgebung in Netzwerken von hängenden Tropfen.* Die Integration von Hydrogelen in Netzwerken von hängenden Tropfen erlaubt die Immobilisierung von 3D-Mikrogeweben für hochaufgelöste Bilderfassung über längere Zeiträume und erlaubt die präzise Kontrolle der Mikroumgebung von 3D-Mikrogeweben. Das System ermöglicht die Untersuchung von komplexen biologischen Vorgängen auf Einzelzellebene und ermöglicht die Überwachung von physiologischen Ereignissen auf subzellulärer Ebene.

iii. *FlussGSIS in hängenden Tropfen.* Ein Perfusionssystem auf Basis von hängenden Tropfen wurde für die Untersuchung der dynamischen Glukose-stimulierten Insulinsekretion von humanen Langerhans'schen Inselzellen der Bauchspeicheldrüse entwickelt. Die Plattform ermöglicht Probeentnahmen mit hoher zeitlicher Auflösung um die Zweiphasen- und die pulsierende Insulinsekretion von einzelnen Langerhans-Inseln zu detektieren und um die Effekte von Diabetesmedikamenten zu untersuchen.

Die präsentierten Plattformen stellen eine Auswahl von neuartigen Instrumenten für die Kultur und die Untersuchung von 3D-Mikrogeweben dar. Die Entwicklung jeder dieser Plattformen wurden für eine spezifische Anwendung optimiert. Diese reichen von der präzisen Stimulation von Mikrogeweben und der anschliessenden Detektierung von Metaboliten bis zu Langzeitbilderfassung in hoher Auflösung. Die vielfältige Anwendbarkeit dieser Plattformen und deren Komplementarität verbessern im hohem Masse die Möglichkeiten, das Potential von 3D-Mikrogeweben als organspezifische *in vitro* Modelle voll und ganz auszuschöpfen.

ACKNOWLEDGEMENTS

I am grateful to Prof. Andreas Hierlemann for giving me the opportunity to conduct my PhD at the Bio Engineering Laboratory and for always providing a very positive and motivating work environment. Moreover, I would like to thank him for giving me the freedom to develop and follow my own ideas which was an excellent and very valuable experience for me.

I am also very grateful to Dr. Olivier Frey. As an advisor and mentor, he introduced me to microfluidics, microtechnology and 3D microtissue cultures and thus provided me with the knowledge and skillset that was needed for this work. Moreover, I would like to thank him for providing valuable ideas, inputs and for having fruitful scientific discussions, which provided many times the basis for new projects and supported their successful outcome. It has been a great pleasure to work with him and he contributed a lot to my professional development.

I would like to thank Elise Aeby, Felix Forschler, Andrea Müller and Anna Ringauf for the work and contributions during their research and master projects, which supported the progress of this work.

A special thank goes to the people at BEL who joined me many times in coffee breaks in our Science Lounge, for having a very good time at our lab retreats and for the creative and technical discussions I had with you.

I would also like to extend my thanks to all members of the Bio Engineering Laboratory who helped and supported me in any way, through their knowledge, valuable inputs and scientific advices. Moreover, I would like to thank everyone at BEL to create this very pleasant and supportive working atmosphere.

A big thank goes to all the people working at D-BSSE. Especially the technical stuff, as well as the administration who provided a unique infrastructure and support since I joint this department at ETH.

Finally, I am very grateful for the support of my family, my brothers Roman and Simon, and especially to my parents for their inexhaustible support throughout my life.

AUTHOR CONTRIBUTIONS

Elise A. Aeby

Chapter 4: Developed the microfluidic hydrogel hanging-drop platform. Designed and fabricated microfluidic chips, planned and performed experiments, analyzed data and wrote the manuscript.

Axel K. Birchler

Chapter 2: Designed and fabricated microfluidic chips, planned and performed experiments, contributed to the manuscript.

Felix Forschler

Chapter 5: Co-developed the FlowGSIS platform. Designed and fabricated microfluidic devices, planned and performed experiments, and analyzed data.

Dr. Olivier Frey

Chapters 1-5: Conceived the concept of microfluidic hanging-drops. Provided ideas and contributed through consulting and guidance to all chapters of this thesis. He edited and revised all manuscripts.

InSphero: Dr. Burçak Yesildag, Aparna Neelakandhan, Adelinn Biernath

Chapter 5: Developed and characterized the re-aggregated human pancreas islet model. Helped to design experiments and contributed to the manuscript.

Moritz Lang

Chapter 2: Developed and implemented the automated hanging-drop feedback controller software in YouScope. Contributed to the manuscript.

Patrick M. Misun

Chapter 1-2: Developed the microfluidic hanging-drop network platform, designed and fabricated microfluidic devices, planned and performed experiments, analyzed data and wrote the manuscript.

Chapter 3: Developed the integrated hanging-drop biosensor platform, designed, fabricated and optimized the device, planned and performed experiments, analyzed data and wrote the manuscript.

Chapter 4: Initiated the hydrogel hanging-drop project, designed and fabricated microfluidic chips, planned and performed experiments, analyzed data, contributed to, and revised the manuscript.

Chapter 5: Co-developed the FlowGSIS platform. Designed and fabricated microfluidic chips, planned and performed experiments, analyzed data and wrote the manuscript.

Dr. Jörg Rothe

Chapter 3: Developed the CMOS-based multi-potentiostat and corresponding software. Provided support and instrumentation to build the experimental setup.

Nassim Rousset

Chapter 5: Modeled the flow characteristics in perfused hanging drops, simulated experimental measurements and contributed to the manuscript.

Yannick R.F. Schmid

Chapter 3: Designed and fabricated microfluidic-, and biosensor chips.

CONTENTS

1 INTRODUCTION

1.1 From 2D to 3D cell cultures – 3D microtissues

Physiologically relevant cell-based *in vitro* assays are fundamental in drug development and screening, as a means to identify new candidate compounds and to render this process reliable and efficient. Testing compounds and studying cellular responses in pre-clinical trials by using monolayer cell systems in standard well plates has the advantage that one can rely on established techniques and laboratory equipment for cell handling and imaging at high throughput. Conventional 2D cell cultures, however, have limitations in mimicking functional living tissue, as the native microenvironment including cell-to-cell interactions, mechanical cues and spatiotemporal biochemical gradients are not present.[1–3]

Tissue models that reproduce *in vivo* conditions as closely as possible are key for understanding organ-specific cell behaviour to investigate diseases and to find new compounds and therapies in the drug discovery process.[4–7] 3D spherical microtissues,[8] for example, are a popular choice as they represent a scaffold-free 3D cell culture model. They can be formed using different methods, which rely on promoting cell-to-cell interactions instead of cell-substrate interactions. The most efficient way of forming and culturing 3D microtissues is the hanging-drop approach,[9,10] where cells in suspension sediment to the liquid-air interface of a hanging drop.[11] The lack of a surface for cell attachment and the spherical drop shape promote the formation of 3D spherical microtissues. Different types of 3D microtissues exist and have been found to mimic functional tissue of several organs, while retaining specific organotypic characteristics and functions for extended periods of time.[12–16] Their simple formation, culturing, and handling make these organotypic 3D spherical microtissues a highly flexible and widely applicable relevant model system.

Parts of this introduction were published in the book chapter "Miniature Fluidic Microtissue Culturing Device for Rapid Biological Detection" by Patrick M. Misun, Andreas Hierlemann and Olivier Frey. Oh SH., Escobedo C., Brolo A. (eds). Integrated Analytical Systems. Springer, Cham, 2018. DOI: 10.1007/978-3-319-64747-0_8. The content of this text was adapted to the context of this thesis.

1.2 3D cell culture platforms – microfluidic hanging-drop networks

Currently, most cell culture platforms used for *in vitro* assays are designed to meet the requirements of static and 2D cell cultures. These cell culture platforms must be adapted for applications with 3D cell cultures in order to fully capitalize on the advantages of 3D cell culture formats. Microtechnology is a great tool for the miniaturization of cell culture devices and for the design of designated platforms for 3D microtissue cultures. The addition of microfluidic features allows for precise control of the microtissue microenvironments and better recapitulate of the *in vivo* milieu by reproducing physiologically relevant parameters, such as nutrient and metabolite turnover, perfusion rates and shear stresses. Additionally, miniaturization of cell-culture platforms allows adjustment to the liquid-to-cell ratios found *in vivo*.[17]

A hanging drop platform is a powerful method for achieving scaffold-free 3D cell culture. Microfluidic hanging-drop networks have been conceived for generating and culturing of 3D microtissues. Individual microtissues are kept at the liquid-air interface at the bottom of fluidically interconnected hanging drops.[18] The completely open microfluidic chip design allows for an easy loading of the microtissues, and their retrieval for endpoint assays. Additionally, this design overcomes common microfluidic issues related to bubble formation and trapping, and ensures, at the same time, optimal gas exchange. The latter is of fundamental importance to closely mimic the *in vivo* environment of microtissues and to maintain their full functionality and viability *in vitro* over extended time. Moreover, interconnected fluidic networks offer the possibility to combine different cell cultures or tissue types to realize "body-on-a-chip" configurations.[19–25]

Novel 3D cell culturing platforms, in combination with representative human *in vitro* models, can be used to test compounds in the drug development process and have the potential to replace 2D cell culture formats and reduce the need for animal models.[7,26,27]

1.3 Analysis of 3D microtissue cultures

The next aspect includes analysis methods, which have been predominantly designed to meet the requirements of 2D cell cultures. Analysis methods and assays, therefore, need to be adapted for 3D cell cultures and the corresponding platforms in order to be able to take full advantage of 3D cell culture formats. Metabolic processes are dynamic and can occur within short time frames, such as a few minutes. Thus, studying time-resolved responses of 3D cell cultures upon environmental changes or upon defined compound dosage often requires

continuous readout in order not to miss the occurrence of important events.[28] Non-invasive methods can be used to attain information from 3D microtissue cultures. Potential strategies include monitoring of the culture environment and quantitative determination of metabolites in the cell culture medium. In well-based approaches, medium is handled through discrete pipetting and sampling steps. Long sampling intervals entail a large risk to miss rare or rapid events which consequently remain undetected. Moreover, conventional cell assays usually include relatively large sample volumes. Frequent sampling of the cell culture medium interrupts and disturbs the overall culturing process and may entail extensive dilution of important markers or metabolites because of the addition of new medium. As medium-to-cell ratios are comparably high, frequent sampling also entails the risk that metabolite concentrations fall below the limit of detection. Microfluidics, in contrast, offer precise flow handling of small liquid volumes, which is important for analytics in cell culture devices.[29]

Another non-invasive method to attain information from 3D microtissues is microscopy imaging. However, most platforms with microfluidic features for culturing 3D microtissues are limited in spatiotemporal microscopy-imaging resolution. Either, they are not compatible with the latest-generation fluorescence microscopes, or perfusion flow induces a movement of the tissues, which makes high-resolution imaging and tracking of cellular and subcellular events within the tissue impossible. Without the access to time-lapse imaging, the dynamic nature of many morphological processes remains difficult to study.[30]

Invasive and complementary analysis methods for 3D microtissues exist, but require full access to the microtissues for harvesting after experiments. Advanced microfluidic 3D cell culturing systems oftentimes lack access to the cell culture for harvesting the microtissues and conducting downstream assays.

Microfabrication techniques offer the use of multiplexing capabilities and allow for realization of advanced 3D cell culturing platforms, while the fabrication of the different components can be kept be simple. All platform features and functions need to be ensured over the duration of an experiment; cell cultures need to stay viable and functional, microfluidic handling needs to be robust and precise. The use of 3D cell cultures in microfluidic setups and the realization of multi-tissue configurations increase platform complexity.

1.4 Scope and structure of this thesis

The focus of this thesis is on the development and application of microfluidic hanging-drop-based platforms for culturing and analysis of 3D microtissues. Three versatile platforms have

been conceived, and each one was optimized for a specific assay and readout technology which are relevant for cell-based assays. First, the fabrication and operation of hanging-drop networks was established. Second, electrochemical biosensors were developed and integrated into hanging-drops networks for the online monitoring of 3D microtissue metabolism. Third, a hanging-drop platform was devised, which is fully compatible with high-resolution microscopy setups. Fourth, a hanging-drop based perfusion system was designed, which allows for measuring the secretion dynamics of metabolites from single microtissues.

The thesis includes one book chapter and three publications:

1. **Fabrication and operation of microfluidic hanging-drop networks.** Patrick M. Misun, Axel K. Birchler, Moritz Lang, Andreas Hierlemann, Olivier Frey., in Methods in Molecular Biology, vol. 1771, P. Ertl and M. Rothbauer, Eds. New York, NY: Springer New York, 2018, pp. 183–202.

2. **Multi-analyte biosensor interface for real-time monitoring of 3D microtissue spheroids in hanging-drop networks.** Patrick M. Misun, Jörg Rothe, Yannick R. F. Schmid, Andreas Hierlemann, Olivier Frey. Microsystems & Nanoengineering 2, 16022 (2016).

3. **Microfluidic hydrogel hanging-drop network for long-term culturing of 3D microtissues and simultaneous high-resolution imaging.** Elise A. Aeby*, Patrick M. Misun*, Andreas Hierlemann, Olivier Frey. Advanced Biosystems 2, 1800054 (2018).

4. **Uniform reaggregated pancreatic islets in microfluidic hanging-drop perfusion system enable to study insulin release dynamics at single-islet level.** Patrick M. Misun, Felix Forschler, Nassim Rousset, Andreas Hierlemann Burçak Yesildag, Aparna Neelakandhan, Adelinn Biernath, Olivier Frey In preparation for submission.

1.5 Summary of major results

Integration of biosensors into hanging-drop networks

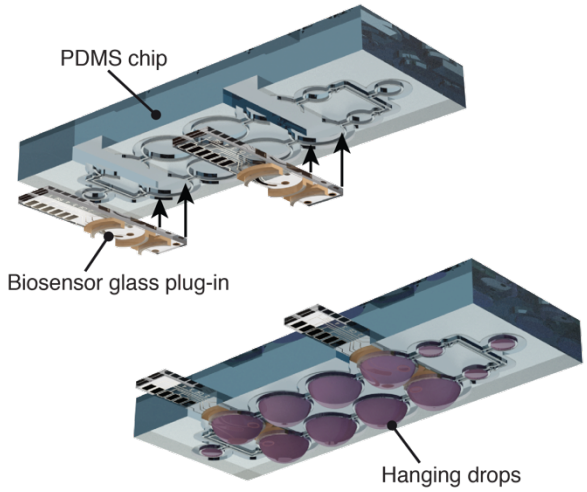

A biosensor-integrated microfluidic hanging-drop device was developed. Small glass modules were designed as versatile sensor plug-ins. These plug-ins feature four platinum working electrodes, one platinum counter electrode, and an Ag/AgCl reference electrode. Complementary microfluidic structures on the glass modules provided leakage-free and stable operation of the system, and the straightforward integration of the sensor units into the microfluidic hanging drop network. Electrodes were functionalized for the electrochemical detection of glucose and lactate, and these biosensors were characterized with on-chip and off-chip calibration measurements.

Real-time *in situ* monitoring of 3D microtissues metabolism

The integrated biosensors enabled microtissue-size-dependent detection of glucose consumption and lactate secretion from single human colon cancer microtissues cultured in the hanging drops. The impact of different culture conditions on the metabolism of cancer microtissues could be assessed in real time.

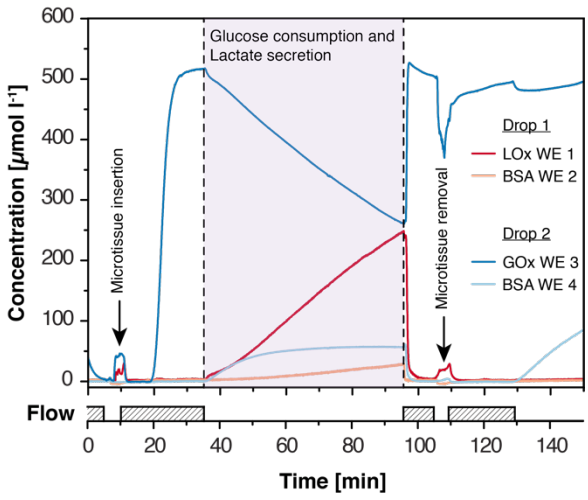

High-resolution time-lapse imaging of 3D microtissues

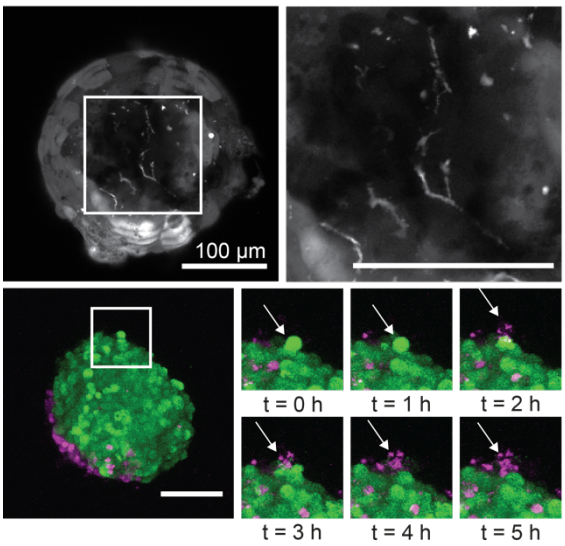

A microfluidic platform for long-term culture and high-resolution confocal imaging of 3D microtissues was developed. Hanging hydrogel drops enabled the precise placement and stable immobilization of microtissues at defined positions in the microfluidic network. Different types of hydrogels were used for hosting the tissues, and the perfusion capability allowed the application of drugs, staining and tissue-clearing solutions. The platform allows for monitoring of complex and highly dynamic processes from organotypic 3D microtissues down to the single-cell and subcellular scale.

Resolving the insulin secretion dynamics of islet microtissues

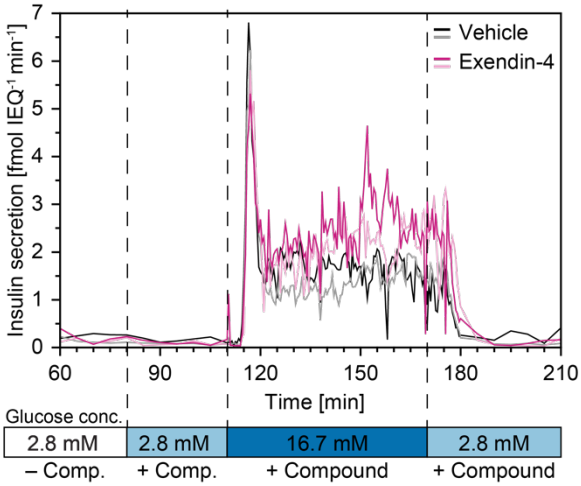

A hanging-drop based perfusion system was used with a standardized and uniform islet model to perform reproducible and dynamic glucose-stimulated insulin secretion assays. The physiologically relevant bi-phasic insulin release with a prominent first phase and a sustained, pulsatile second phase could be resolved with high temporal resolution. Furthermore, this platform was used to study the effects of anti-diabetic drugs on the dynamics of insulin secretion. The enabling feature is the open microfluidic channel and hanging-drop design, which provides precise fluid control and rapid liquid turnover, resulting in minimal sample dispersion in the platform so that rapid changes in secretion patterns can be observed.

1.6 References

1. Baharvand, H., Hashemi, S. M., Kazemi Ashtiani, S. & Farrokhi, A. Differentiation of human embryonic stem cells into hepatocytes in 2D and 3D culture systems in vitro. *Int. J. Dev. Biol.* **50,** 645–52 (2006).

2. Asthana, A. & Kisaalita, W. S. Microtissue size and hypoxia in HTS with 3D cultures. *Drug Discov. Today* **17,** 810–7 (2012).

3. Knight, E. & Przyborski, S. Advances in 3D cell culture technologies enabling tissue-like structures to be created in vitro. *J. Anat.* (2014). doi:10.1111/joa.12257

4. Pampaloni, F., Reynaud, E. G. & Stelzer, E. H. K. The third dimension bridges the gap between cell culture and live tissue. *Nat. Rev. Mol. Cell Biol.* **8,** 839–45 (2007).

5. Justice, B. A., Badr, N. A. & Felder, R. A. 3D cell culture opens new dimensions in cell-based assays. *Drug Discov. Today* **14,** 102–7 (2009).

6. Esch, M. B. *et al.* How multi-organ microdevices can help foster drug development. *Adv. Drug Deliv. Rev.* **69–70,** 158–169 (2014).

7. Polini, A. *et al.* Organs-on-a-chip: a new tool for drug discovery. *Expert Opin. Drug Discov.* **9,** 335–52 (2014).

8. Sutherland, R. M. Cell and environment interactions in tumor microregions: the multicell spheroid model. *Science* **240,** 177–84 (1988).

9. Carrel, A. & Burrows, M. T. Cultivation of tissues in vitro and its technique. *J. Exp. Med.* **13,** 387–96 (1911).

10. Potter, S. W. & Morris, J. E. Development of mouse embryos in hanging drop culture. *Anat. Rec.* **211,** 48–56 (1985).

11. Kelm, J. M., Timmins, N. E., Brown, C. J., Fussenegger, M. & Nielsen, L. K. Method for generation of homogeneous multicellular tumor spheroids applicable to a wide variety of cell types. *Biotechnol. Bioeng.* **83,** 173–80 (2003).

12. Tung, Y.-C. *et al.* High-throughput 3D spheroid culture and drug testing using a 384 hanging drop array. *Analyst* **136,** 473–8 (2011).

13. Hirschhaeuser, F. *et al.* Multicellular tumor spheroids: an underestimated tool is catching up again. *J. Biotechnol.* **148,** 3–15 (2010).

14. Messner, S., Agarkova, I., Moritz, W. & Kelm, J. M. Multi-cell type human liver

microtissues for hepatotoxicity testing. *Arch. Toxicol.* **87,** 209–13 (2013).

15. Rimann, M. *et al.* An in vitro osteosarcoma 3D microtissue model for drug development. *J. Biotechnol.* **189,** 129–35 (2014).

16. Beauchamp, P. *et al.* Development and Characterization of a Scaffold-Free 3D Spheroid Model of Induced Pluripotent Stem Cell-Derived Human Cardiomyocytes. *Tissue Eng. Part C. Methods* **21,** 852–61 (2015).

17. Esch, M. B., Sung, J. H. & Shuler, M. L. Promises, challenges and future directions of microCCAs. *J. Biotechnol.* **148,** 64–9 (2010).

18. Frey, O., Misun, P. M., Fluri, D. A., Hengstler, J. G. & Hierlemann, A. Reconfigurable microfluidic hanging drop network for multi-tissue interaction and analysis. *Nat. Commun.* **5,** 4250 (2014).

19. Maschmeyer, I. *et al.* A four-organ-chip for interconnected long-term co-culture of human intestine, liver, skin and kidney equivalents. *Lab Chip* **15,** 2688–2699 (2015).

20. Kim, J.-Y. *et al.* 3D spherical microtissues and microfluidic technology for multi-tissue experiments and analysis. *J. Biotechnol.* **205,** 24–35 (2015).

21. Zhang, C., Zhao, Z., Abdul Rahim, N. A., van Noort, D. & Yu, H. Towards a human-on-chip: culturing multiple cell types on a chip with compartmentalized microenvironments. *Lab Chip* **9,** 3185–92 (2009).

22. Van Midwoud, P. M., Merema, M. T., Verpoorte, E. & Groothuis, G. M. M. A microfluidic approach for in vitro assessment of interorgan interactions in drug metabolism using intestinal and liver slices. *Lab Chip* **10,** 2778–86 (2010).

23. Huh, D., Torisawa, Y., Hamilton, G. A., Kim, H. J. & Ingber, D. E. Microengineered physiological biomimicry: organs-on-chips. *Lab Chip* **12,** 2156–64 (2012).

24. Sung, J. H., Kam, C. & Shuler, M. L. A microfluidic device for a pharmacokinetic-pharmacodynamic (PK-PD) model on a chip. *Lab Chip* **10,** 446–55 (2010).

25. Sonntag, F. *et al.* Design and prototyping of a chip-based multi-micro-organoid culture system for substance testing, predictive to human (substance) exposure. *J. Biotechnol.* **148,** 70–5 (2010).

26. Bhatia, S. N. & Ingber, D. E. Microfluidic organs-on-chips. *Nat. Biotechnol.* **32,** 760–72 (2014).

27. Esch, E. W., Bahinski, A. & Huh, D. Organs-on-chips at the frontiers of drug discovery. *Nat. Rev. Drug Discov.* **14,** 248–60 (2015).

28. Link, H., Fuhrer, T., Gerosa, L., Zamboni, N. & Sauer, U. Real-time metabolome profiling of the metabolic switch between starvation and growth. *Nat. Methods* **12,** 1091–7 (2015).

29. El-Ali, J., Sorger, P. K. & Jensen, K. F. Cells on chips. *Nature* **442,** 403–11 (2006).

30. Aeby, E. A., Misun, P. M., Hierlemann, A. & Frey, O. Microfluidic Hydrogel Hanging-Drop Network for Long-Term Culturing of 3D Microtissues and Simultaneous High-Resolution Imaging. *Adv. Biosyst.* **2,** 1800054 (2018).

2 Fabrication and Operation of Microfluidic Hanging-Drop Networks

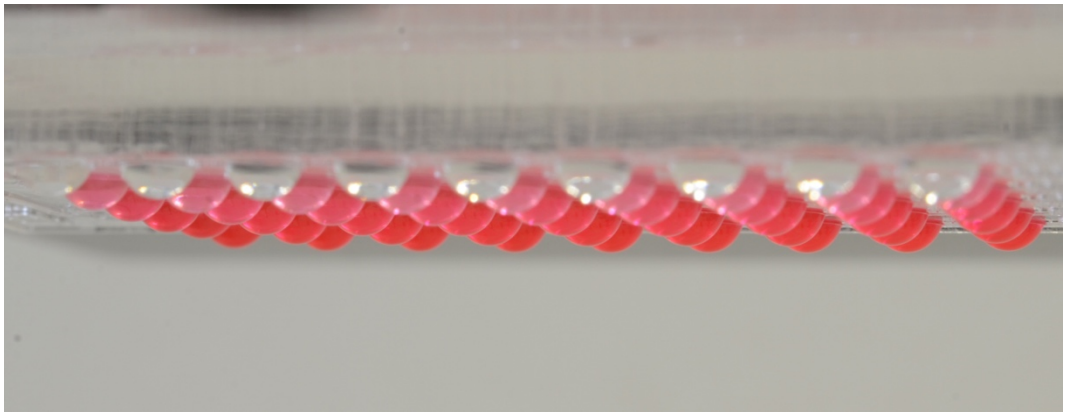

Patrick M. Misun, Axel K. Birchler, Moritz Lang, Andreas Hierlemann, Olivier Frey. Fabrication and Operation of Microfluidic Hanging-Drop Networks, in Methods in Molecular Biology, vol. 1771, P. Ertl and M. Rothbauer, Eds. New York, NY: Springer New York, 2018, pp. 183–202.

DOI: 10.1007/978-1-4939-7792-5_15

2.1 Abstract

The hanging-drop network (HDN) is a technology platform based on a completely open microfluidic network at the bottom of an inverted, surface-patterned substrate. The platform is predominantly used for the formation, culturing and interaction of self-assembled spherical microtissues (spheroids) under precisely controlled flow conditions. Here, we describe design, fabrication and operation of microfluidic hanging-drop networks.

2.2 Introduction

The hanging-drop technique enables the formation of scaffold-free 3D spherical microtissues by seeding a defined number of cells into hanging drops of a specific culture medium. Cells sediment by gravity force, aggregate, and form a spherical microtissue at the liquid-air surface.[1] Hanging-drop *networks* (HDNs) expand the isolated hanging drops towards a fully interconnected network of hanging drops and enable controlled liquid flow between the hanging drops.[2] Adding perfusion functions allows for continuous medium exchange, for application of compound dosage protocols and for interaction of different microtissue types to realize multi-tissue or so-called "body-on-a-chip" setups. The hanging-drop technology has also been tested for stem cell culturing.[3] Further, electrical impedance spectroscopy[4], biosensor readout methods,[5] and on-chip peristaltic pumps[6] have been integrated.

Hanging-drop networks are designed as completely open microfluidic systems at the bottom of an inverted, surface-patterned substrate (Figure 1). They inherently fully exploit the benefits of the liquid-air interface with respect to low cell adhesion and reduced compound adsorption. Further, their open nature ensures gas exchange, prevents bubble formation and gives access to the liquid phase and the microtissues at every position in the network. Finally, their fabrication is simple, and the design of the networks is very versatile.

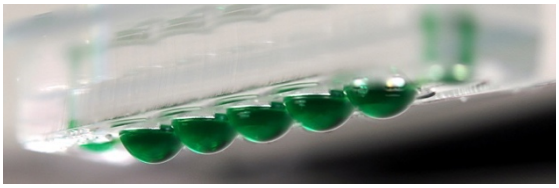

Figure 1 Photograph of a line of hanging drops filled with green food dye. As a result of surface energy minimization, all five hanging drops have the same radius and, therefore, comprise the same liquid volume.

The surface patterns underneath the inverted substrate guide the liquid by surface tension and capillary forces. Rim structures are used to distinguish wetted regions from dry regions and

prevent the liquid from flowing over the whole surface in an uncontrolled way. The design of the rim structures defines where drops are formed. Circular patterns induce the formation of hanging drops, whereas extended narrow structures produce a channel-like structure. Through the variation of the feature dimensions many different arrangements and configurations of hanging-drop networks can be realized. Robust operation of hanging-drop networks depends on a few basic principles that have to be followed during the design and arrangement of the hanging drops and interconnection channels; the respective features will be explained in Subheading 1.4.1.

The hanging-drop network structures are made of PDMS casted from a micropatterned SU-8 mold. The stability of the chips can be increased through bonding of the PDMS substrate onto a glass slide with fluid access holes. The chips are placed in a custom-made chip holder and connected to conventional pumps via tubing. All fabrication and setup steps are described in detail in Subheadings 1.4.2, 1.4.3 and 1.4.4. The fabrication of the SU-8 mold is done in a cleanroom. All other steps can be performed in a conventional laboratory.

The open nature of the HDN-systems ensures bubble-free initial liquid filling of the microfluidic network. Further, the loading of cells and preformed microtissues is straightforward and easy to perform. Different approaches for loading cells and spheroids are presented Subheading 1.4.5.

In comparison to the more common closed microfluidic systems, flow control is different in hanging-drop networks. For a stable drop size to be maintained over extended time, the liquid needs to be actively infused and actively withdrawn at both inlet and outlet, respectively, at a precision, which is not available in most commercial systems. We present two different methods that allow for robust perfusion over an extended culturing period. In the first method, described in Subheading 1.4.6, the outlet is conceived as a hanging drop and a needle is placed at the liquid-air interface. The position of the needle then defines the drop size in the whole network (we call it “needle-outlet” method, here). This method does not require a microscope and can be used for perfusion in a conventional incubator. In the second method, described in Subheading 1.4.7, we use microscopy to estimate the average drop height by (software) auto-focusing the individual microtissues. The microtissues are always located at the bottom of each drop on the liquid-air interface and the z-position of the objective with the microtissue in focus can be used as measure for the drop height. Based on this value the flow rate is adjusted online via proportional–integral feedback control (“feedback” method). Finally, in Subheading 1.4.8 we describe, how spheroids can be retrieved from the microfluidic system for further analysis.

2.3 Materials

2.3.1 SU-8 mold

1. Transparency masks of the design printed at 50'800 dpi resolution (Selba SA, Versoix, Switzerland).
2. 4-inch silicon wafer (525 μm thick, single-side polished).
3. Cleanroom equipped with mask aligner, spin coater, hotplate (*see* **Note 1**), ultrapure water bath, glass beakers, spiders, and covers.
4. Chemicals:
    a) Acetone (semiconductor grade).
    b) Isopropanol (semiconductor grade).
    c) SU-8 100 negative photoresist (Microchem Corp., Newton, MA, USA).
    d) mr-Dev 600 Developer (Micro Resist Technology GmbH, Berlin, Germany).
    e) Trichloro(1H,1H,2H,2H-perfluorooctyl)silane (Sigma-Aldrich, Buchs, Switzerland).

2.3.2 PDMS chip

1. Polydimethylsiloxane (PDMS), Sylgard 184, (Dow Corning GmbH, Wiesbaden, Germany).
2. Vacuum desiccator.
3. Scotch tape or custom-built wafer holder for PDMS casting.
4. Hotplate (*see* **Note 1**).
5. Cutter blade.
6. Hollow punchers 0.75 mm and 2.00 mm (Harris Uni-Core, Ted Pella, Inc., Redding, CA, USA).
7. Microscopy glass slides, standard size (1 mm thick, 25 mm x 75 mm or 50 mm x 75 mm).
8. Diamond drill of 1.2 mm diameter.
9. O_2 plasma cleaner/sterilizer 50 W at 0.3 mbar (Diener Electronic GmbH & Co., Ebhausen, Germany).
10. *(For needle-outlet)* N-124S Nanoport connector and F-124S Standard Head Fitting (Idex Health & Science GmbH, Wertheim, Germany).
11. *(For needle-outlet)* Araldite rapid two-component glue (Huntsman Advanced Materials GmbH, Basel, Switzerland).

2.3.3 Setup

1. Custom-built chip holder, or PDMS spacer blocks.
2. One-well culture dish (Nunc OmniTray, Thermo Fischer Scientific, Rochester, NY, USA).
3. Humidifier pad (InSphero AG, Schlieren, Switzerland).
4. Tubing and connectors:
    a) Polytetrafluoroethylene (PTFE) tubing, ID 0.3 mm/0.5 mm, OD 0.6 mm/1 mm, (Bola GmbH, Grünsfeld, Germany).
    b) Standard luer lock syringe-tubing connectors 22 GA. Bent 90 deg, (APM Technica AG, Heerbrugg, Switzerland).
    c) Standard luer lock syringe-tubing connectors 25 + 32 GA straight, (APM Technica AG).
    d) Silicon tubings Tygon LMT-55, ID 0.38 mm, Wall 0.91 mm (Idex Health & Science GmbH, Wertheim, Germany).
    e) Peristaltic tubing Tygon S3 E-LFL, ID 0.27 mm, 0.91 mm wall (Idex Health & Science GmbH).
5. neMESYS syringe pump base and dosing units (Cetoni GmbH, Korbussen, Germany).
6. Peristaltic pump (Ismatec, ISM935C, Idex Health & Science GmbH).

2.3.4 Microscopy

1. Automated inverted microscope (DMI6000B, Leica Microsystems).
2. Objectives (Leica Microsystems).
    a) 5x / 0.12 HCX FL Plan.
    b) 10x / 0.30 Ph1 HCX PL Floutar.
3. Camera (DFC340FX, Leica Microsystems).
4. *(Optional)* C-Mount 0.70x.
5. Environmental box for microscope (“The Box”, Life Imaging Services, Basel, Switzerland).
6. Temperature controller (“The Cube”, Life Imaging Services).
7. Stage-top incubator and automated gas mixer (“The Brick”, Life Imaging Services).

2.3.5 Microscope control software “YouScope”

1. Youscope version R2016 or higher, available at http://www.youscope.org/ for Windows 7 (32bit or 64bit) or higher.

2. The control software is necessary for the "feedback" method; optional for "needle-outlet" method (e.g. for imaging and/or switching flows).

2.4 Methods

2.4.1 Design of the chips

1. Design the microfluidic hanging-drop networks by using 2D CAD software (e.g. Clewin, AutoCAD). A very basic hanging-drop network is presented as an example in Figure 2A. The layout features one inlet, one outlet, and five drop-sites that are interconnected through short, semi-open connection channels. The drop structures have a diameter of 3.5 mm and are arranged in a row (*see* **Note 2**). The drop pitch is 4.5 mm, which corresponds to the 384-well-plate format, making it compatible with routine imaging and pipetting. A 200-µm-wide circular rim defines the drop sites and guides the liquid on the microfluidic chip. Cross sections 1, 2 and 3 in Figure 2B illustrate the surface pattern of the inverted substrate. The depth of the fluidic structure is 500 µm. The groove around the rim is 250 µm deep and 800 µm wide. Inlet and outlet areas have a diameter of 1.5 mm. The small channels between the drops are 1 mm long, 200 µm wide, and 500 µm deep.
2. Printing of two high-resolution transparency masks is required for the fabrication process of the SU-8 mold. Figure 2C shows both layers for the hanging-drop line in Figure 2A.

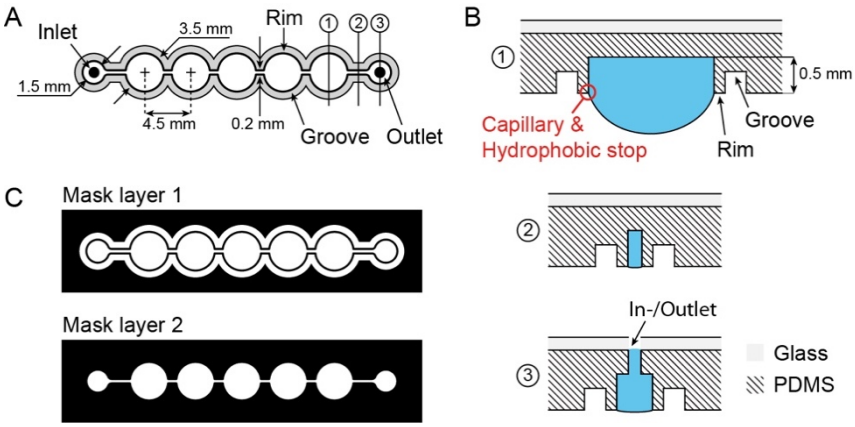

Figure 2 Design of the hanging-drop network. (**A**) Line of 5 hanging drops with single inlet and outlet. All important dimensions are indicated. (**B**) Schematic cross sections of drop, channel and outlet site. (**C**) Masks required for fabrication of the negative-tone SU-8 mold of the hanging-drop line in (**A**).

3. The reported dimensions for drops and channels have been optimized with regard to drop and network stability and media perfusion characteristics (*see* also ref.[2]). Design custom hanging-drop network configurations (e.g., larger arrays, different interconnections, other inlet and outlet position) respecting the guidelines given above. Arrays larger than 8-by-8 drops and more than 8 inlets and outlets become rather difficult to realize. An example of a 4-by-4 array is presented in Figure 3A. The array includes also a microfluidic gradient generator allowing for exposing spheroids to different compound concentrations[7]. Additional microfluidic features may be devised, but then have to be tested. The channel dimensions should, in general, include a width of 200 µm and a height of 500 µm.
4. The integration of capillary stop valves enables sequential filling of the microfluidic network and subsequent reconfiguration. An example is given in Figure 3B. The 4-by-6-drop array has 4 inlets and 4 outlets. Each column can be loaded with a different liquid or cell suspension through the cell loading ports located at the top of the columns. After loading, the columns are connected by adding liquid through the connecting ports (*see* also Subheading 3.5). The optimized design and respective mask layers of the capillary stop valves are shown in Figures 3C,D.

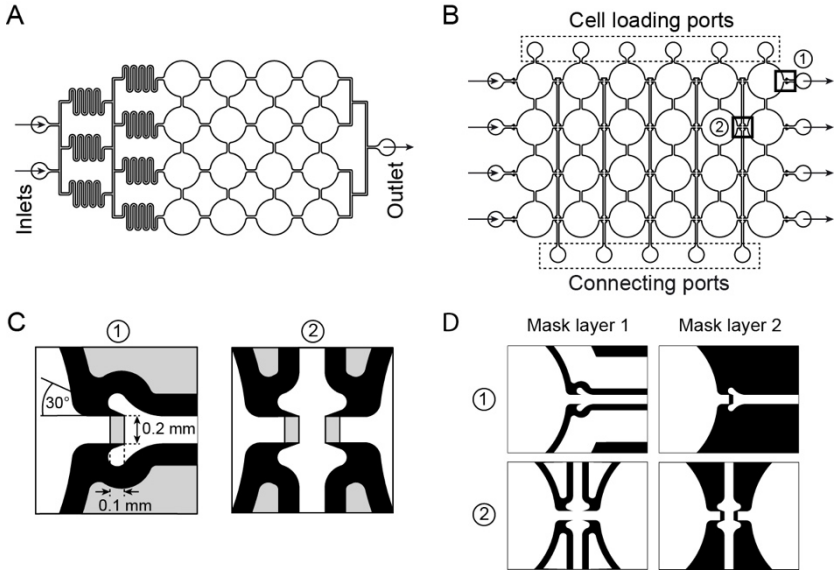

Figure 3 Examples of different hanging-drop networks. (**A**) 4-by-4 interconnected hanging-drop array with preceding microfluidic gradient generator structure. (**B**) 4-by-6 hanging-drop array including the reconfiguration option, so that every column can be loaded independently. (**C**) Details of the valves indicated in (**B**). (**D**) Design and of the masks for fabricating the valves.

2.4.2 Fabrication of the SU-8 mold

1. Take a 4-inch polished silicon wafer and perform a dehydration bake for 5 min at 200 °C on a hot plate. Proceed right afterward with SU-8 spin coating.
2. Spin-coat the first layer of SU-8 100 (~250 µm height, Figure 4A): Pour SU-8 100 directly from the 500-mL bottle onto the wafer (*see* **Note 3**). Use the following two-step spin-coating program: (1) Spreading step with a ramp (500 rpm/s) to 500 rpm held for 5 s, (2) spinning step with a ramp (500 rpm/s) to 1500 rpm held for 30 s. After coating, remove the wafer from the spin coater and clean the backside of the wafer by using a tissue and acetone (*see* **Note 4**).
3. Soft-bake the wafer on a leveled hot plate using the following protocol: 15-min ramp from RT to 65 °C, hold for 30 min, 15-min ramp from 60 °C to 95 °C, hold for 90 min, slow cool down to RT in ~60 min. Slow ramps reduce internal stress and improve the adhesion of SU-8 to the silicon substrate.
4. UV-expose the first SU-8 layer on a mask aligner through the first mask (Figure 4B). SU-8 is a negative-tone resist; exposed areas are cross-linked and remain on the wafer after development. Use soft-contact mode and a broadband exposure dose of 400 mJ/cm^2 (*see* **Note 5**).
5. After exposure, perform the postexposure bake on a hot plate using the following protocol: 15-min ramp from RT to 65 °C, hold for 5 min, 15-min ramp from 60 °C to 95 °C, hold for 30 min, slow cool down to RT in ~60 min (Figure 4C).
6. Spin-coat the second layer of SU-8 100 (~250 µm height) onto the first SU-8 layer using the same procedure described in **steps 2** and **3** (Figure 4D).
7. Align the second mask with respect to the SU-8 structures on the wafer and UV-expose the second SU-8 layer using a broadband exposure dose of 400 mJ/cm^2 (Figures 4E,F). After exposure, perform the postexposure bake using the same parameters described in **step 5** (*see* **Note 6**).
8. Develop the unexposed SU-8 in a glass beaker by using mr-Dev 600 developer. Put the wafer upside down on a spider and fill the beaker with developer until the wafer is completely immersed. Cover the beaker. Develop for about 60 min and agitate the developer from time to time (Figure 4G) (*see* **Note 7**). Once all unexposed resist has been dissolved, rinse the wafer with fresh developer followed by isopropanol and then rinse it thoroughly in an ultrapure water bath. Spin-dry the wafer for 60 s at 2500 rpm or let it dry in air.

9. Vapor silanization of the SU-8 mold: Put the clean wafer, together with 5 µl of trichloro(1H,1H,2H,2H-perfluorooctyl)silane applied on a glass slide, into a desiccator. Apply house vacuum or a pump vacuum for 2-3 min and close the valve. Leave the wafer in the silane atmosphere for 2 h. Purge the chamber with air and remove the wafer.

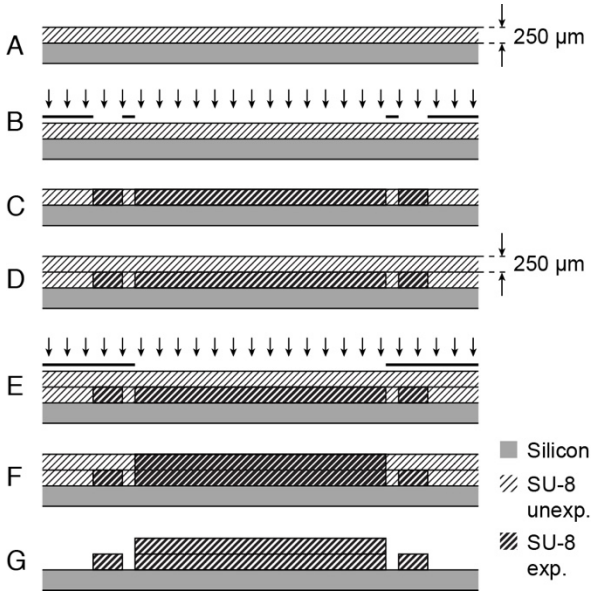

Figure 4 Fabrication of the SU-8 mold. (**A**) Spin coating of the first SU-8 layer. (**B**) Exposure through the first mask. (**C**) Postexposure bake and cross-linking. (**D**) Spin-coating of the second SU-8 layer. (**E**) Alignment and exposure through the second mask. (**F**) Postexposure bake and (**G**) development of un-exposed SU-8.

2.4.3 Fabrication of the PDMS hanging-drop network

1. Add Sylgard 184 silicone elastomer and Sylgard 184 silicone elastomer curing agent at a ratio of 10 : 1 (e.g., 44 g in total) into a dust-free plastic cup and mix thoroughly. Place the cup into a vacuum desiccator for ~30 min until no air bubbles are visible anymore.
2. Add tape as a wall around the wafer or place the wafer in a petri dish to create a containment for the PDMS with the wafer at the bottom (*see* **Note 8**). Custom-built wafer holders may also be used.
3. Pour 20 g of degassed PDMS on the wafer (3 mm thick, Figure 5A). Pour 10 g of PDMS in an empty petri dish (1 mm thick), which is later used as a mask for the surface activation. Degas the PDMS under vacuum for additional 30 min to remove all bubbles.

4. Place wafer and petri dish on a leveled hot plate for 2 h at 75 °C to fully cure the PDMS (*see* **Note 1**).
5. After curing and cool down, carefully remove the structured PDMS from the mold and the PDMS layer out of the petri dish (Figure 5B). Cut the PDMS into single-chip pieces using a cutter blade and punch holes at inlet and outlet using a 0.75-mm hollow puncher.
6. Prepare the PDMS mask by cutting the thin PDMS layer into slides fitting the hanging-drop network array by using a cutter blade. Punch holes at the corresponding drop positions using a 2-mm hollow puncher (Figure 5C and 6).
7. Take a microscopy glass slide and drill holes with a diameter of 1.2 mm at the inlet and outlet positions by using a diamond drill (*see* **Note 9**).
8. Clean the PDMS bonding surface as well as the glass slide with soap and successively rinse it with DI water, acetone and isopropanol and dry the two parts with an air gun.
9. Place the PDMS chip and the glass slide into the plasma cleaner with the bonding surfaces facing upwards. Activate the surfaces for 25-30 s using oxygen plasma at 50 W and 0.5 mbar.
10. Remove the parts from the plasma cleaner and place the PDMS chip onto a dust-free paper with the non-structured surface at the top. Align the microscopy glass slide to the chip by eye and bring them into contact starting at one side so that no air bubbles are trapped. Slightly press them together (Figure 5D).
11. *(For needle-outlet)* Glue an N-124S Nanoport connector on the glass slide at the outlet hole. Use a two-component glue (Araldite), which cures rapidly. Apply slight pressure on the connector from the top for several minutes to tightly fix it (Figure 5E) (*see* **Note 10**).
12. *(For needle-outlet)* Remove the plastic part of a 32-GA and a 25-GA standard luer lock syringe-tubing connector. Glue the 32-GA needle tip inside the 25-GA needle tip by carefully adding glue to the thinner tip and sliding it into the thicker one. Make sure that approximately 5 mm of the inner needle stays uncovered. Glue the combined needle into a F-124S standard head fitting with the uncovered part in front (Figure 5F).

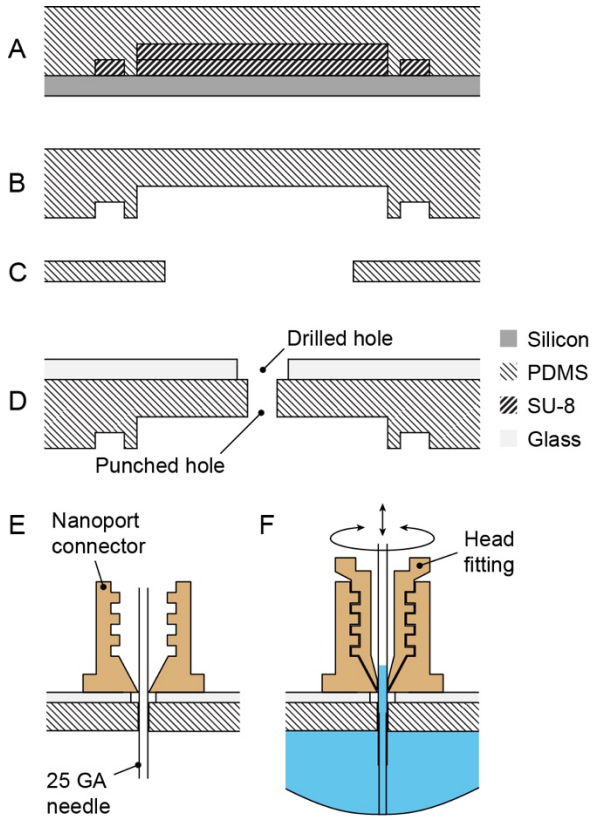

Figure 5 Fabrication of the PDMS chip. (**A**) Molding of PDMS from the SU-8 structure. (**B**) PDMS chip with SU-8 replica. (**C**) PDMS mask for chip preparation. (**D**) PDMS chip bonded on a glass slide. (**E**, **F**) Application of the needle outlet.

2.4.4 Chip preparation

1. Carefully clean the PDMS chip and the PDMS mask with soap, water, acetone, isopropanol and dry the two parts with an air gun (*see* **Note 11**).
2. Align the holes in the PDMS mask with the circular hanging-drop areas on the PDMS chip before plasma activation and press them slightly together so that a good contact of the PDMS mask and the rim is ensured (Figure 6) (*see* **Note 12**).
3. Put the chip into the plasma cleaner with the openings of the mask facing upward. Activate the chip for 45-60 s using an oxygen plasma at 50 W and 0.5 mbar. In this step, the inside of the circular areas and channels is turned hydrophilic, while the rim structures covered by the PDMS mask remain hydrophobic.
4. Remove the mask from the PDMS chip and affix it to a custom-built holder with the hanging-drop structures facing down. *Alternative:* Use pre-fabricated PDMS blocks to support the flipped chip (*see* Figure 9) (*see* **Note 13**).

5. *(For needle-outlet)* Insert the prepared needle fitting into the Nanoport connector (Figure 5F). Visually adjust the needle so that the tip is 0.5 – 1.0 mm below the rim structure.
6. Take a sterile one-well culture dish (OmniTray box) and place a humidifier pad inside. Soak it with sterile DI water. Place the PDMS chip and custom-built holder inside.

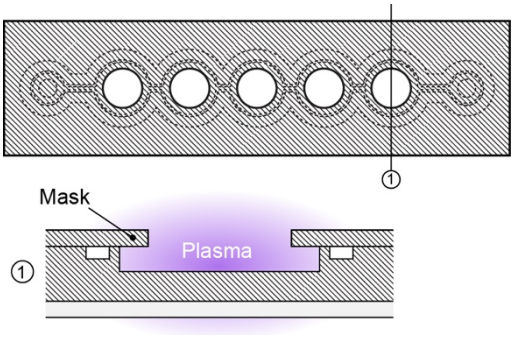

Figure 6 Preparation of the chip. A PDMS mask with holes is used to selectively activate the inside of the circular hanging-drop areas and channels, while the rim is protected and remains hydrophobic.

2.4.5 Cell and spheroid loading

Option 1 – Loading of a cell suspension

1. Perform the loading sequence within 15 min after oxygen plasma activation.
2. Prepare the cell suspension and adapt the cell concentration with respect to the final cell numbers required per hanging drop.
3. Calculate a volume of 8 µl per drop and load the total liquid volume that is required for filling of the selected drop (sub) array into a conventional pipet (200-µl tip).
4. Load liquid or the prepared cell suspension through one of the inlets (*see* **Note 14**). The liquid will automatically spread over the whole network, and hanging drops will simultaneously develop below all circular structures (Figure 7A). For large networks, one or more additional inlets at drops inside the network may be used to achieve a more homogeneous cell distribution.
5. For hanging-drop networks that can be reconfigured through capillary stop valves, load the defined cell suspensions through the respective loading ports (Figures 7B, C). Let the cells sediment for 5-10 min and then load a small amount (~5 µl) of medium through the connection port to connect the different subarrays.

Option 2 – Loading of preformed microtissues

1. Seal inlet and outlet with sticky tape.
2. Flip the chip so that the hanging-drop structures are facing upward.
3. Load medium into the network until standing drops are formed at all circular areas. The medium can be loaded at several positions in the network (Figure 7D).
4. Pick up the selected spheroids from your dish or well plate into the tip of a 100/200 µl pipet tip together with 20 µl of medium.
5. Observe and wait until the spheroid settles at the bottom of the tip at the liquid-air interface (Figure 7E).
6. Hold the tip vertically and bring the tip into contact with the selected standing drop. The spheroid will transfer without any pipetting actuation.
7. Load all spheroids into the network. If the drops have been designed with the required pitch, a multichannel pipet may be used for parallel spheroid transfer (*see* **Note 15**).
8. Flip the chip back into hanging drop mode and place it onto the holder (*see* **Note 16**).
9. Remove the sticky tape at inlet and outlet.

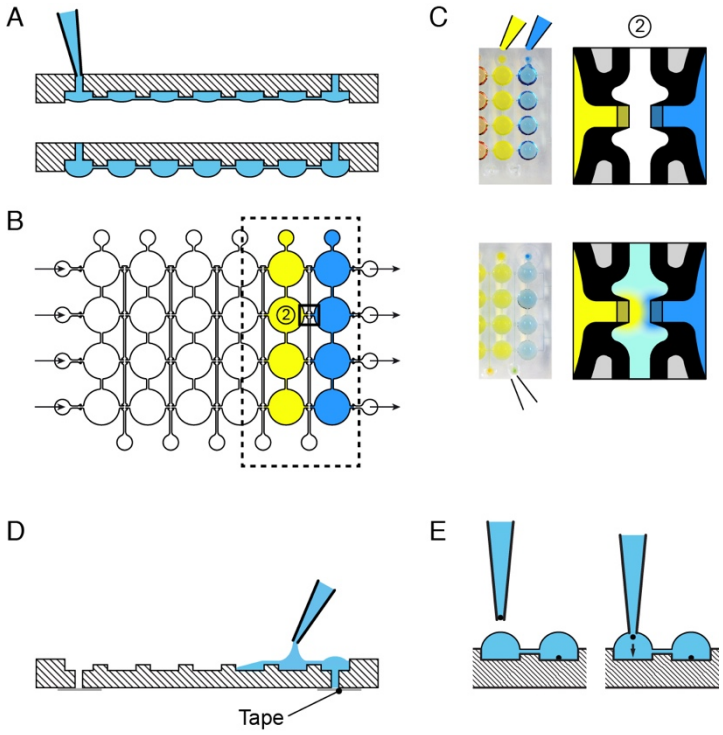

Figure 7 Cell and spheroid loading. (**A**) Loading of liquid or cell suspension through the inlet and formation of hanging drops of uniform size. (**B**) Sequential loading of subarrays of hanging drops (here columns) and subsequent connection. (**C**) Photograph of the loading using food

dye and details on the capillary stop valve function. (**D**) Loading of the network with drops facing upwards. (**E**) Transfer of a spheroid into a standing drop.

2.4.6 Operation using "Needle-Outlet" method

1. Choose an appropriate incubator for your experiments with 5% CO_2 and >95% humidity. The incubator should have the possibility to insert tubing from the outside.
2. Place the syringe pump and the peristaltic pump as close to the incubator as possible.
3. Prepare the tubing connections from the syringe pumps to the PDMS chip with polytetrafluoroethylene (PTFE) tubing of appropriate length (ID 0.3 mm). Connecting pieces are prepared by removing plastic and glue from standard luer lock syringe-tubing connectors (22 GA Bent 90). They are then connected to the PTFE tubing by short flexible silicon tubing (ID 0.38 mm) (Figure 9B).
4. Fill glass syringes with culture medium and mount the tubing to the syringe, which is then mounted onto the neMESYS syringe pumps. Prefill the tubing with medium to remove any air bubbles before connecting it to the hanging-drop chip.
5. Use special peristaltic tubing (ID 0.27 mm) for the peristaltic pump. A PTFE tubing of appropriate length is directly inserted in the peristaltic tubing. The other end of the PTFE tubing is inserted in a short silicon tubing adapter piece (ID 0.38 mm), which is later used to connect to the outlet needle (Figure 8).
6. Put the one-well culture dish (OmniTray box), including the PDMS chip prepared in Subheading 3.4, into the incubator. Connect inlet and outlet tubing to the chip. Check the horizontal position of the PDMS chip (*see* **Note 17**).
7. Close the lid of the culture dish and the incubator. Make sure that none of the tubing is squeezed.
8. In this operation mode, the drop size is controlled by the position of the outlet needle. Liquid is removed from the chip if the drop size increases and the liquid-air interphase moves below the needle tip. The liquid removal stops as soon as the liquid-air interface then again reaches the needle tip. This back and forth between liquid withdrawal and no withdrawal ensures a constant drop height (Figure 8). As indicated in the figure, the outlet produces a segmented flow with alternating air and liquid plugs.
9. Start the perfusion of the chip. The programed withdrawal rate should always be set higher than the inlet rate for stable chip operation (1.5–2 times the inlet rate). A continuous flow rate of 0.5–10 µl/min has been successfully tested. As an alternative, pulsed inlet flow can be applied. The average input volume should, however, always

compensate for the evaporation in the incubator and to guarantee a constant liquid volume in the chip and never exceed the continuous withdrawal rate.

10. *(For needle-outlet)* If the volume of the hanging drops is increasing too much, decrease the needle length by turning the needle fitting counter-clockwise. Turn the fitting in the opposite direction to increase the volume of the hanging drops.
11. *(Optional)* The withdrawn liquid can be sampled by simply guiding the tubing downstream of the peristaltic pump into a sampling device or container.

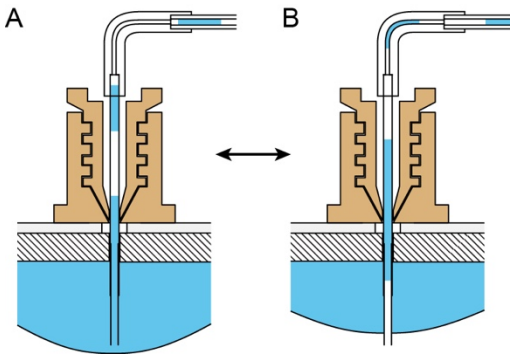

Figure 8 A back and forth between liquid withdrawal (**A**) and no withdrawal (**B**) is used to control the drop volume and the overall liquid volume in the chip.

2.4.7 Operation using "Feedback" method

1. Install YouScope and Qmix SDK (first time). Configure YouScope as described in [8] and add a "NemesysPump" device.
2. Switch on the microscope and set the temperature controller of the environmental box to 37 °C for 3-4 h before starting the experiment.
3. Select a 5x or 10x objective (Figure 9).
4. Set the culturing conditions inside the stage-top incubator with an automated gas mixer to 5% CO_2 and >95% humidity and a gas flow rate of 10 l/h.
5. Prepare the tubing connections from the syringe pumps to the PDMS chip with polytetrafluoroethylene (PTFE) tubing (ID 0.3 mm, OD 0.6 mm) and metal connecting pieces. Connecting pieces are prepared by removing plastic and glue from standard luer lock syringe-tubing connectors (22 GA Bent 90). They are then connected to the PTFE tubing by short flexible silicon tubing (ID 0.38 mm).
6. For the inlet, fill glass syringes with culture medium and mount the tubing to the syringe with standard luer lock syringe-tubing connectors (22 GA), which are then affixed to the neMESYS syringe pumps. Prefill the tubing with medium. Remove any air bubbles.

7. Special peristaltic tubing (ID 0.27 mm) is used for the peristaltic pump. All the other part of the tubing remains the same as described in **step 4**. Prefill the peristaltic tube with medium. The outlet of the tube can be used for sampling of the medium.
8. Affix the one-well culture dish (OmniTray box) including the PDMS chip prepared in Subheading 3.4 to the microscopy stage. Connect all inlet and outlet tubes to the chip. Close the dish with a lid and put the stage-top incubator on top (*see* **Note 18**).
9. Check the horizontal position of the PDMS chip by checking the z-position on all four edges of the chip. Adjust if needed.
10. Check if all channels and capillary stop valves are filled with liquid.
11. Check the size of the hanging drops and adjust the drop height if needed by slowly infusing (~5 µl/min) additional medium through the syringe pumps (*see* **Note 19**).
12. Identify autofocus settings for feedback control in YouScope (first time): Manually focus on a microtissue inside a drop. Create a "simple measurement" with #executions = 1. Add an autofocus job using "exhaustive search," with upper and lower bounds approximately plus/minus half the drop height. Before starting the measurement, double-click on "autofocus results". Display a plot with x-column = "relative focus," y-column = "focus score," and "scatter plot," and start the measurement. Adjust the imaging settings and the focal score algorithm until the focus-score plot becomes bell-shaped, with a single maximum around zero and a good signal-to-noise ratio (*see* **Note 20**).
13. For time-lapse imaging and drop-height control (Figure 9), create a microplate measurement in YouScope. Choose the 384-well-plate format, or create a custom microplate if using a nonstandard chip format. Select microplate positions corresponding to the drop layout, and manually focus the microtissues in each drop. Add a "droplet-based microfluidic" job, and select all connected syringes. Use "Brent Optimization" for the autofocus, and all other settings as previously identified. Select "syringe-table" as the controller strategy, select the target flow rate (*see* **Note 21**), and allow the controller to deviate approximately half the target flow rate to adjust the drop height. Measure or estimate (based on the chip design) the first-order relationship between drop height and volume around the target height. Choose at least one syringe to generate the inflow (the target flow is distributed equally between all selected syringes). If using the peristaltic pump to generate the outflow, do not choose "outflow" for any syringes. By adding rows to the "syringe table," one can switch during the measurement between syringes containing different media. To take additional images,

e.g., for quantifying fluorescence, add the respective imaging jobs to the imaging protocol after the "droplet-based microfluidic" job.

14. Start the measurement and, at the same time, the withdrawal through the peristaltic pump with a flow rate equal the target flow rate of the controller (*see* **Note 22**). If necessary, stop the measurement and the flow to adjust the controller settings (*see* **Note 21**).

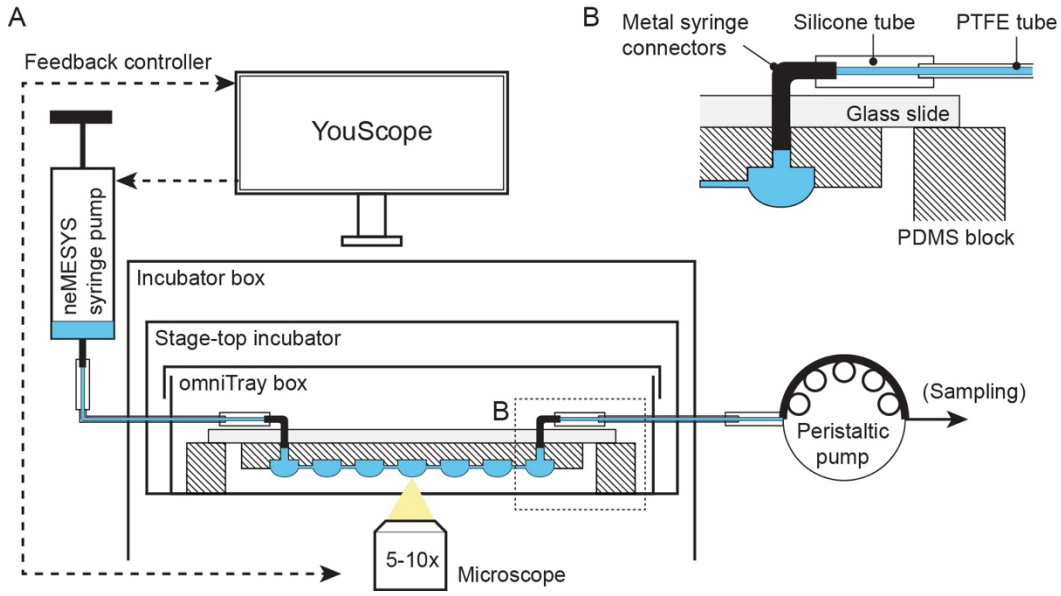

Figure 9 Experimental setup on the microscope. (**A**) The hanging-drop chip is placed on PDMS blocks inside an OmniTray box. The stage-top incubator and the incubator box ensure high humidity and a constant temperature to minimize evaporation. The inflow is provided by neMESYS syringe pumps. Flow rates into the microfluidic chip are adjusted through a feedback controller, which has been implemented in YouScope to keep the drop height constant. Outflow is generated by a peristaltic pump and is constant during the experiment. (**B**) Enlarged view on the outlet of the chip.

2.4.8 Retrieval

1. Collect a selected microtissue from a single drop using a conventional pipet.
2. *(Alternative)* Bring the hanging drop network into contact with the surface of a petri dish and collect the microtissues from there by using a pipette. The petri dish can be filled with medium. By using this alternative collection method the order and registration of the microtissues will be lost.
3. *(Alternative)* Transfer all microtissues in parallel to a special receiver plate. The receiver plate features hydrophilic spots at the locations of the hanging drops. In this

way, the registration of the microtissues is maintained (for more details please refer to [3]).

2.5 Notes

1. Make sure to horizontally level the hot plate.
2. Hanging drops can be designed and operated under stable conditions if they feature diameters between 2.5 mm and 5 mm.
3. SU-8 is very viscous. The final height has ~10% variation. The amount poured onto the wafer needs to be the more or less the same for each layer.
4. If small air bubbles appear on the wafer, simply prick them with a small needle.
5. The resolution depends on the print quality of the mask. Use chromium masks on glass if critical features are smaller than 30 µm. For larger structures, such as presented here, 50'800-dpi foil masks are sufficient.
6. Special alignment structures are placed at the sides of both mask layers and promote precise alignment.
7. When the developer becomes yellow, exchange it for fresh one.
8. Make sure that the PDMS is not going underneath the wafer.
9. For precise positioning of the holes, place the punched PDMS chip onto the microscopy glass slide and mark the positions of the access holes directly on the glass.
10. For precise alignment, use a 25-GA needle tip inside the Nanoport connector that protrudes into the punched PDMS hole during fixation so that the connector and outlet are cocentered.
11. A toothbrush can be used with soap to remove persistent dust or other debris in the channels and drop structures.
12. No contact of the mask will lead to plasma activation of the rim and potential failure of the chip during operation.
13. Height of the PDMS block should be ~8 mm, yielding a total distance of the drops from the OmniTray bottom of approximately 3-4 mm.
14. Loading flow rates of 300-400 µl/min can be applied. The total chip volume depends on the chip design. In general, one drop (without channel) with a diameter of 3.5 mm has a volume of ~8 µl. This yields a drop size/height of ~800 µm (measured from the rim structure).
15. Place the network on a heating mat, if the procedures take longer. Be quick to minimize evaporation.

16. Do the flipping fast and with a uniform rotation rate along the axis of the drop rows.
17. Due to the additional height of the Nanoport connector, a small window needs to be removed from the lid of the culture dish to provide access for the outlet tubing.
18. Properly tape the tubing on the microscope stage.
19. The drop height can be measured through the difference in the z-position of the rim structure of the chip and the specimen located at the bottom of the hanging drop.
20. Small improvements in autofocus quality can significantly improve long-term stability of the controller. Try to slightly over-expose the autofocus search images, clean the optics, use pre-filtered medium, switch off lights, use Köhler illumination, and consider to decrease magnification. In our experience, auto-correlation based focus scores with lags between one and eight showed the best results.
21. If the average drop height and the target flow rate show long-lasting oscillations, increase the "mean droplet's height learn speed" of the observer, and increase the time-constants for the proportional and integral parts of the controller. If individual drop height measurements are noisy, decrease the "individual droplet's height learn speed" to avoid high frequency fluctuations in the flow. If only small flow adjustments are necessary, manually switch on the flow and let the droplets settle before configuring and starting the controller.
22. The maximal flow rate highly depends on the array design and the volume of the interconnecting channels, and, in general, on the flow resistance between inlet and outlet. Up to 20 µl/min for a single drop line can be applied without problems. In some cases, high flow rates can lead to substantially different drop sizes (smaller drops towards the outlet) as a result of the pressure drop over the interconnecting channels in the network. (for more details *see* ref.[2]).

2.6 Acknowledgements

This work was financially supported by FP7 of the EU through the project 'Body on a chip', ICT-FET-296257, and the ERC Advanced Grant 'NeuroCMOS' (contract 267351), as well as by an individual Ambizione Grant 142440 from the Swiss National Science Foundation for Olivier Frey. The research leading to these results also received funding from the People Programme (Marie Curie Actions) of the European Union's Seventh Framework Programme (FP7/2007-2013) under REA grant agreement n° [291734]. We would like to thank Alexander Stettler, ETH Zurich for his expertise and support in the cleanroom and we acknowledge the Single Cell Unit of D-BSSE, ETH Zurich for assistance in microscopy issues. ML is grateful

to the members of the Guet and Tkačik groups, IST Austria, for valuable comments and support.

2.7 References

1. Kelm, J. M., Timmins, N. E., Brown, C. J., Fussenegger, M. & Nielsen, L. K. Method for generation of homogeneous multicellular tumor spheroids applicable to a wide variety of cell types. *Biotechnol. Bioeng.* **83,** 173–80 (2003).

2. Frey, O., Misun, P. M., Fluri, D. A., Hengstler, J. G. & Hierlemann, A. Reconfigurable microfluidic hanging drop network for multi-tissue interaction and analysis. *Nat. Commun.* **5,** 4250 (2014).

3. Birchler, A. *et al.* Seamless Combination of Fluorescence-Activated Cell Sorting and Hanging-Drop Networks for Individual Handling and Culturing of Stem Cells and Microtissue Spheroids. *Anal. Chem.* **88,** 1222–9 (2016).

4. Schmid, Y. R. F., Bürgel, S. C., Misun, P. M., Hierlemann, A. & Frey, O. Electrical Impedance Spectroscopy for Microtissue Spheroid Analysis in Hanging-Drop Networks. *ACS Sensors* **1,** 1028–1035 (2016).

5. Misun, P. M., Rothe, J., Schmid, Y. R. F., Hierlemann, A. & Frey, O. Multi-analyte biosensor interface for real-time monitoring of 3D microtissue spheroids in hanging-drop networks. *Microsystems Nanoeng.* **2,** 16022 (2016).

6. Rismani Yazdi, S. *et al.* Adding the 'heart' to hanging drop networks for microphysiological multi-tissue experiments. *Lab Chip* **15,** 4138–4147 (2015).

7. Jeon, N. L. *et al.* Generation of Solution and Surface Gradients Using Microfluidic Systems. *Langmuir* **16,** 8311–8316 (2000).

3 Multi-Analyte Biosensor Interface for Real-Time Monitoring of 3D Microtissue Spheroids in Hanging-Drop Networks

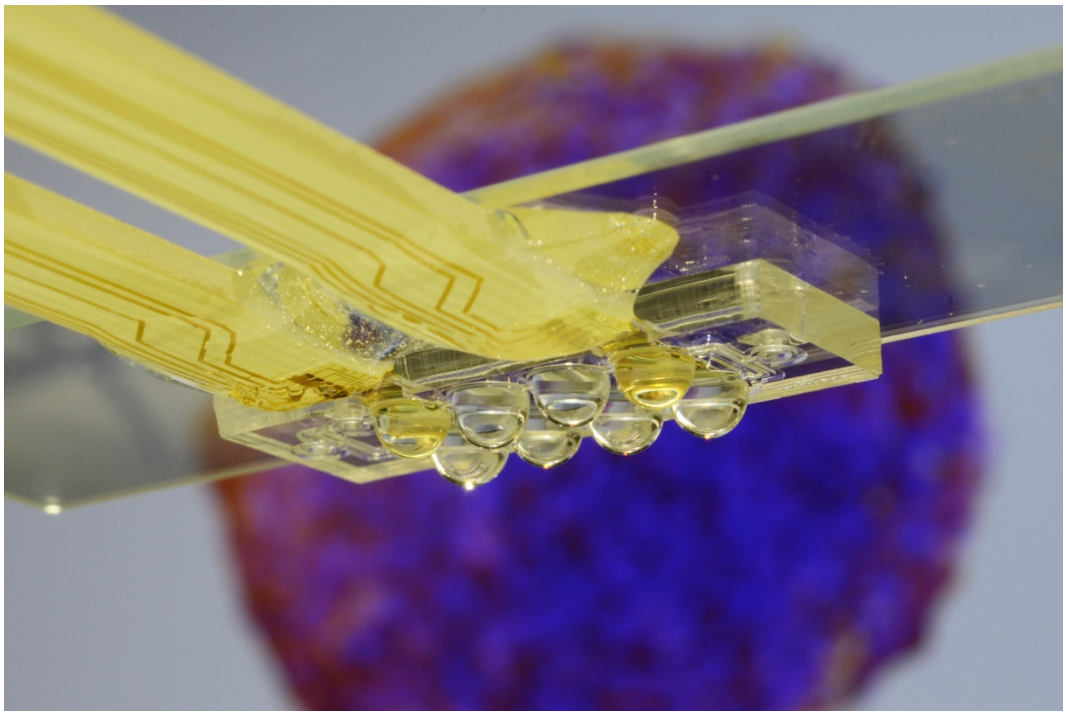

Patrick M. Misun, Jörg Rothe, Yannick R. F. Schmid, Andreas Hierlemann, Olivier Frey. Multi-analyte biosensor interface for real-time monitoring of 3D microtissue spheroids in hanging-drop networks. Microsystems & Nanoengineering 2, 16022 (2016).

DOI: 10.1038/micronano.2016.22

3.1 Abstract

Microfluidics is becoming a technology of growing interest for building microphysiological systems with integrated read-out functionalities. Here, we present the integration of enzyme-based multi-analyte biosensors into a multi-tissue culture platform for "body-on-a-chip" applications. The microfluidic platform is based on the technology of hanging-drop networks, which is designed for the formation, cultivation and analysis of fluidically interconnected organotypic spherical three-dimensional (3D) microtissues of multiple cell types. The sensor modules were designed as small glass plug-ins featuring four platinum working electrodes, a platinum counter electrode, and an Ag/AgCl reference electrode. They were placed directly into the ceiling substrate from which the hanging drops that host the spheroid cultures are suspended. The electrodes were functionalized with oxidase enzymes to enable continuous monitoring of lactate and glucose through amperometry. The biosensors featured high sensitivities of 322 ± 41 nA mM^{-1} mm^{-2} for glucose and 443 ± 37 nA mM^{-1} mm^{-2} for lactate; the corresponding limits of detection were below 10 µM. The proposed technology enabled tissue-size-dependent, real-time detection of lactate secretion from single human colon cancer microtissues cultured in the hanging drops. Furthermore, glucose consumption and lactate secretion were monitored in parallel, and the impact of different culture conditions on the metabolism of cancer microtissues was recorded in real-time.

3.2 Introduction

Microsystems technology offers a variety of new approaches to culturing and analysing human cells and functional tissue structures.[1,2] Tissue models that reproduce *in vivo* conditions as closely as possible are key for understanding organ-specific cell behaviour, for investigating diseases, and for discovering new agents and therapies during the drug development process.[3–6]

Simple organ models for testing new compounds and studying cellular response and metabolism in preclinical trials consist of two-dimensional (2D) cell culture systems. Culturing cells in a monolayer has certain advantages; the cells are simple to handle and image, and one can rely on established techniques and standard laboratory equipment. Two-dimensional cell cultures, however, have certain limitations in mimicking functional living tissue, as original microenvironmental inputs, such as cell-to-cell interaction and spatiotemporal biochemical gradients, are absent.[7–9] Three-dimensional (3D) cell cultures offer the potential to overcome many of these limitations and are therefore finding increasing applications in the

pharmaceutical industry and basic research.[10] A wide spectrum of 3D cell culture methods and materials are currently being developed to reproduce tissue-specific properties.[11–13] The hanging-drop technique, for example, is a popular method of growing scaffold-free 3D microtissues of spherical shape. Different types of spheroids can be formed to mimic the functional tissues of various organs while retaining their specific characteristics and functions over an extended period of time.[14–19]

Two additional aspects are closely related and of high interest. The first is that advanced culture systems with continuous perfusion capabilities and the possibility to integrate fluid-dynamic and mechanodynamic cues offer the possibility to even better mimic the *in vivo* environment.[20] Perfusion, for example, can be modulated to provide tissue-specific environmental conditions[21,22] and to simulate the shear forces that are present at the interfaces of tissues in their fluidic environments[23–25]. Flexible substrates can be implemented to mimic the oscillatory mechanical stress in lung aveoli.[26,27] Finally, interconnected fluidic networks offer the possibility to combine different cell cultures or tissue types to realize "body-on-a-chip" configurations.[28–34]

The second aspect is related to established analysis methods, which have been designed primarily to meet the requirements of 2D cell cultures. These analysis methods and assays must be adapted for application to 3D cell cultures and the corresponding platforms to fully capitalize on the advantages of 3D cell culture formats.

Most metabolic processes are dynamic and occur on time scales of a few minutes. Thus, studying time-resolved responses of cell cultures to environmental changes or upon the application of a defined compound dosage often requires continuous read-out to ensure that occurrences of important events are not missed.[35] In well-based approaches, liquid handling is discrete, which engenders a high risk of missing events. Moreover, conventional cell assays usually involve rather large sample volumes. Frequent sampling of the cell culture medium interrupts and disturbs the overall culturing process, increases the risk of contamination, and may cause extensive dilution of important markers or metabolites in the process because of the addition of new medium. As the cell-to-medium ratios are extremely low, frequent sampling also incurs a risk that metabolite concentrations may fall below the limit of detection.

Microfluidics, in contrast, offer precise flow handling of small liquid volumes and accurate control over microenvironmental parameters that are important in analytical cell culture devices.[1] In addition, microfabrication techniques offer multiplexing capabilities and allow

straightforward integration of novel modules, such as pumping systems, actuators, and microsensors.[36,37] Microsensor technologies have been developed over the past several decades for a variety of applications. Their miniature size and versatile features as well as their high sensitivity and low-detection limits enable monitoring of various analytes in cell and tissue culture set-ups at high temporal and spatial resolution.

Many multi-sensor systems were designed as probes, mostly comprising electrochemical biosensors, and have been applied to conventional cell culture assays to monitor microphysiological conditions over time.[38–41] Miniaturized versions have been used as scanning probes to monitor the glucose and lactate metabolism of single cells.[42,43] Flow-through-type sensor systems have been devised to analyse cell culture conditions and metabolites in liquid samples downstream of cell cultures.[44–51] Silicon-based sensor chips for multi-parameter online monitoring have been mounted in a perfused cell culture unit,[52] and multiple sensing electrodes have been directly incorporated into transparent microfluidic systems to measure the glucose consumption of single cardiac cells[53] or the lactate production of cells of various types[54] and, combined with optical read-out, for monitoring cancer cell metabolism.[55]

The combination and integration of microfluidics and microsensors with cell culturing units poses challenges. The fabrication methods for the different components need to be compatible, and all target features and functions must be preserved over the duration of an experiment; the cell cultures must remain viable and functional, the microfluidic handling needs to be robust and precise, and the sensors must satisfy the detection specifications, including sensitivity and selectivity. The use of 3D microtissues in microfluidic set-ups and the realization of multi-tissue configurations render this integration even more complex.

In this paper, we present a highly versatile, modular, and scalable analytical platform technology that combines microfluidic hanging-drop networks with multi-analyte biosensors for the *in situ* monitoring of 3D microtissue metabolism. Hanging-drop networks consist of arrays of interconnected hanging drops that are specifically designed for 3D microtissue aggregation and culture.[56] They allow precise control of microtissue culture conditions and enable on-chip intertissue communication, which is of fundamental importance for realizing 3D microtissue body-on-a-chip configurations. Sensor modules were implemented as small glass plug-ins to allow convenient functionalization and calibration of the sensors and to avoid interference with microfluidic functions. We demonstrated the detection of lactate secreted by single-microtissue spheroids, the amount of which depends on the tissue size.

Moreover, we were able to monitor the variations in lactate secretion with changing nutrient availability by applying different microfluidic perfusion protocols. Finally, we also showed that it is possible to monitor microtissue lactate secretion and glucose consumption in parallel.

3.3 Materials and Methods

3.3.1 Microfluidic hanging-drop network fabrication

A microfabricated SU-8 master mould was used to fabricate microfluidic polydimethylsiloxane (PDMS) chips (Supplementary Figure S1). Three layers of SU-8 100 (Microchem Corp., Newton, USA) were successively spin-coated onto a 4-inch silicon wafer and processed using a standard photolithographic protocol. The rotation speeds were adjusted to obtain the desired layer thicknesses of h_1=250 µm, h_2=250 µm, and h_3=500 µm. The first two layers were used to pattern the rim and drop structures. The third layer was used to create a recess in the microfluidic PDMS chip architecture for the insertion of the sensor glass plug-in during device assembly.

After soft baking, each SU-8 layer was exposed to ultraviolet light through different transparency masks and post-exposure baked for cross-linking. Development was performed at the end of the fabrication procedure for all SU-8 layers simultaneously. A vapour silanization process with trichloro(1H,1H,2H,2H,-perfluorooctyl)silane (Sigma-Aldrich, Buchs, Switzerland) was used to reduce the adhesion of the PDMS during casting.

The PDMS was prepared by mixing Sylgard 184 Silicone Elastomer and Sylgard 184 Silicon Elastomer Curing Agent (Dow Corning Corp., Billerica, USA) at a 10:1 (w/w) ratio. The mixture was then poured onto the SU-8 master mould, degassed for 1 h and cured on a hotplate for 2 h at 80 °C. The cured 3-mm-thick PDMS replica was cut into individual microfluidic chips, and holes were punched at predefined access sites to enable fluidic connections via tubing. Microscopy slides (26 mm x 76 mm x 1 mm) were prepared with liquid access holes, and the PDMS chips were bonded to these slides after 25 s of oxygen plasma surface activation (Harrick Plasma PDC-002, Harrick Plasma, Ithaca, NY, USA). The glass slide improves the planarity and mechanical stability of the system. Finally, the microfluidic PDMS chips were sterilized with 70% ethanol and isopropanol and cleaned with oxygen plasma for a duration of 3 min (Diener Electronic GmbH & Co., Ebhausen, Germany).

3.3.2 Sensor glass plug-in fabrication

A 4-inch glass wafer (0.5-mm thick) was used to fabricate the sensor glass plug-ins using standard photolithography processes (Supplementary Figure S2). Lift-off resist (LOR3B, Microchem Corp., Newton, USA) and positive photoresist (S1813, Rohm-Haas, Schwalbach, Germany) were sequentially spin-coated and soft baked to form layers with thicknesses of 300-400 nm and 1.5 µm, respectively. Metal patterns were transferred into the resist via ultraviolet exposure through a transparency mask. The wafer was developed in MF319 Developer (Rohm-Haas, Schwalbach, Germany) for 60 s. The under-etching of the LOR layer facilitated the lift-off process after metal deposition. A sputtering process was applied to deposit 200 nm of platinum with a 20-nm TiW adhesion layer (Ionfab 300, Oxford Instruments, Abingdon, UK). Lift-off was executed in Remover 1165 (Rohm-Haas, Schwalbach, USA) using ultrasound. A 500-nm-thick Si_3N_4 passivation layer was then deposited onto the wafer using a plasma-enhanced chemical vapour deposition process (Plasmalab 80, Oxford Instruments). This passivation layer was re-opened at specified electrode sites using a patterned S1813 positive photoresist mask and reactive-ion etching (RIE; Plasmalab 100, Oxford Instruments).

Complementary rim structures and rings surrounding the electrodes on the sensor glass plug-in were fabricated using SU-8 resist. The 20-µm SU-8 rings were fabricated with SU-8 3025 (Microchem Corp.). The rim structures were fabricated with 2 layers of SU-8 100 following the same procedure described for the PDMS mould. After development, the glass wafer was diced into single sensor glass plug-ins (2.8 mm x 13 mm) using a precision saw.

The individual glass plug-ins were glued onto a printed circuit board (PCB, 8 mm x 91 mm x 1.5 mm), wire bonded and packaged using epoxy glue (EPOTEK 302-3M, Dow Corning GmbH, Wiesbaden, Germany). Connector pins were soldered to the PCB to provide electrical connections.

3.3.3 Electrode preparation

All sensor units were initially sterilized with 70% ethanol and isopropanol and cleaned with oxygen plasma for a duration of 3 min (Diener Electronic GmbH & Co., Ebhausen, Germany). The electrodes were tested by recording cyclic voltammograms (Compactstat, IVIUM Technologies, Eindhoven, The Netherlands). The electrodes were cycled in N_2-bubbled, 1 M sulfuric acid solution between -0.25 and 1.60 V vs. Ag/AgCl at 100 mV s^{-1} at least 10 times. The reference electrode (RE) was coated with silver (Ag) via galvanostatic electrodeposition at -0.1 mA mm^{-2} for 300 s using an Ag wire as a combined counter/reference electrode; the

silver on the RE was subsequently partially transformed into AgCl through the application of a constant current of 5 µA mm^{-2} for 1500 s in a 50-mM KCl solution. All four working electrodes (WEs) were coated with an m-polyphenylenediamine layer (mPPD; Sigma-Aldrich) using a 0.1 M mPPD solution in PBS. The polymer was deposited over 15 voltammetry cycles (0–0.9 V vs. Ag/AgCl). To improve the adhesion of the sensor hydrogel to the working electrodes, an additional (3-aminopropyl)triethoxysilane layer (Sigma-Aldrich) was deposited via vapour deposition for a duration of 2 h.

3.3.4 Biosensor functionalization

The working electrodes were functionalized to detect glucose and L-lactate. Two different hydrogels, containing either glucose oxidase (GOx) or lactate oxidase (LOx), were prepared and deposited onto the electrodes under sterile conditions. The membrane hydrogel was prepared by adding the enzymes to an aqueous solution containing bovine serum albumin (BSA) and glutaraldehyde 25% (GA) to initiate cross-linking for hydrogel formation. For the glucose biosensor, 5 mg GOx (Sekisui Diagnostics, Kingshill, UK), 20 mg BSA (Sigma-Aldrich), 500 µl deionized (DI) water, 10 µl Triton X-100 (3 g l^{-1}) (AppliChem GmbH, Darmstadt, Germany), and 20 µl GA (Sigma-Aldrich) were used. For the L-lactate biosensor, 10 mg LOx (Sekisui Diagnostics, Kingshill, UK), 30 mg BSA, 500 µl DI water, 10 µl Triton X-100 (3 g l^{-1}), and 20 µl GA were used. An enzyme-free control hydrogel was formed using 30 mg BSA, 500 µl DI water, 10 µl Triton X-100 (3 g l^{-1}), and 20 µl GA. The catalase membrane solution contained 1 mg catalase (Sigma-Aldrich), 30 mg BSA, 500 µl DI water, 10 µl Triton X-100 (3 g l^{-1}), and 20 µl GA. GA was added at the end, after all other compounds had been thoroughly mixed for 15 min. The final solution was mixed for an additional 5 min using a magnetic stirrer.[48]

Sub-microliter volumes of these solutions were manually transferred onto the electrodes by touching the small rim structure surrounding the electrodes with a 2-µl pipette using appropriate tips. The hydrogel was formed directly on the electrodes by curing the solution at room temperature for at least 3 h before use. For the preparation of multi-layer hydrogel electrodes, solutions were consecutively transferred to the electrodes using the same drop-coating technique, with 10 min of curing time in between.

3.3.5 Device assembly

For the final assembly of a device, the sensor modules were inserted into the designated recesses on the microfluidic PDMS chip. Epoxy adhesive (Araldite, Huntsman, Everberg, Belgium) was poured between the microscopy slide hosting the PDMS structures and the PCB to fix and stabilize the device. As an alternative, double-sided adhesive tape could be used to reversibly affix the sensor module.

Prior to each experiment, the assembled device was activated by means of a 30-s oxygen plasma treatment (Diener Electronic GmbH & Co., Ebhausen, Germany), during which a thin PDMS mask with openings at the inlet, outlet, and all drop sites was used to cover all rim structures of the microfluidic hanging-drop device. This selective plasma treatment caused the inherently hydrophobic PDMS inside the circular drop structures and channel locations to enter a hydrophilic state. The covered rim structures remained hydrophobic, ensuring that the liquid would stay contained between them.

3.3.6 Device operation

The assembled device was clamped upside down onto a custom-made chip holder and placed into an OmniTray cultivation box, covered with a lid; wet cotton pads were also placed in the box to provide additional humidity and minimize evaporation. The sensor unit was electronically connected to an in-house-fabricated CMOS-based multi-potentiostat for parallel current read-out[57] and operated at a constant potential of 0.65 V between each working electrode and the on-chip RE. Precision syringe pumps (neMESYS, Cetoni GmbH, Korbussen, Germany) were used for flow control. The reported flow rates are given for single-drop rows. The device was placed in an incubation box with a controlled atmosphere of 37 °C, 5% CO_2, and 95% humidity for optimal culture conditions. Inlet tubing was connected to a heatable perfusion cannula (PH01&TC02, Multichannel Systems, Reutlingen, Germany) to ensure a constant temperature.

3.3.7 Sensor calibration

Off-chip calibrations were performed by immersing each functionalized biosensor unit in either 50 ml 1x phosphate-buffered saline (PBS) of pH 7.4 (Gibco, Life Technologies, Zug, Switzerland) or 50 ml RPMI 1640 cell culture medium (Chemie Brunschwig AG, Basel, Switzerland), including 100 IU ml^{-1} penicillin and 100 µg ml^{-1} streptomycin (Chemie Brunschwig). The temperature was set to 37 °C, and the liquid was constantly stirred using a

magnetic stirrer. Defined volumes of prepared 100 mM D-glucose (Sigma-Aldrich) and 100 mM L-lactate (Sigma-Aldrich) solutions were added in a stepwise manner.

On-chip calibrations were performed using the same stock solutions. Lactate and glucose solutions were diluted to 0.25, 0.50, and 1.00 mM and loaded into glass syringes. The liquids were successively perfused through the device.

3.3.8 Cell culture

All cell-based experiments were conducted using the fluorescent human colon carcinoma cell line HCT116 eGFP (Sirion Biotech, Munich, Germany). The cells were cultured in RPMI 1640 growth medium (Chemie Brunschwig) supplemented with 10% fetal bovine serum (FBS, Sigma-Aldrich), 100 IU ml^{-1} penicillin, 100 µg ml^{-1} streptomycin (Chemie Brunschwig), and 0.3 mg ml^{-1} puromycin (Sigma-Aldrich). The cell line was cultured in a humidified incubator (CB 60, Binder, Tuttlingen, Germany) at 37 °C, 5% CO_2, and 95% humidity. When the cell culture reached a confluence of 80% in the 5-ml culture flasks, the cells were diluted with fresh medium and transferred to a new culture flask to ensure constant proliferation and long-term maintenance of the cell line.

Prior to an experiment, cells were collected from the culture flasks for microtissue fabrication. Old medium was removed from the cell culture flask, and the adherent cells were washed with 1x PBS of pH 7.4 (Gibco). The cells were treated with a 0.25% Trypsin-EDTA solution (Gibco) at 37 °C for 4 min to detach them from the culture plate. The cell suspension was diluted with fresh RPMI 1640 growth medium containing all supplements. The cell concentration was measured using a haemocytometer and adjusted with regard to the experimental requirements and desired microtissue sizes.

GravityPLUS plates (InSphero AG, Schlieren, Switzerland) were used to form and grow microtissues from HCT116 eGFP cell suspensions inside hanging drops. The cell concentrations were adjusted such that different hanging drops contained 250, 500, 1000, and 2000 cells each to modify the initial microtissue size. A multichannel pipette was used to transfer 40 µl of cell suspension to each hanging-drop site on the 96 GravityPLUS plate. After 3 days of incubation in the incubator at 37 °C, 5% CO_2, and 95% humidity, microtissues of different sizes were formed and transferred to a GravityTRAP plate (InSphero) for maintenance and media exchange every 3 days.

3.3.9 Measurement of analyte secretion

The glucose and lactate biosensors were calibrated to determine the specific sensitivity per area (nA $mmol^{-1}$ L mm^{-2}) of each electrode. During the experiments, the current density (nA mm^{-2}) was constantly measured at a 10-Hz sampling rate. The corresponding analyte concentration was then calculated according to the previously determined sensitivity of the electrode in question. This procedure enabled continuous monitoring of the analyte concentration (mmol L^{-1}) in the hanging drops over time.

Continuous measurements were performed as perfusion was periodically switched on or off, and the concentration changes in the 10-µl hanging-drop compartment were recorded in real-time (mmol L^{-1} h^{-1}). The secretion rates (mmol h^{-1}) were finally obtained by taking the volume of 10 µl into account.

3.4 Results and Discussion

3.4.1 Device concept and design

The biosensors are integrated into the hanging-drop network using a modular approach. The final device consists of two parts, a microfluidic PDMS chip and small glass plug-ins featuring the biosensor electrodes, as shown in Figure 1a. The hanging-drop network consists of eight circular regions, each with a diameter of 3.5 mm, at a pitch compatible with the 384-well-plate format (4.5 mm). The hanging drops form underneath these circular regions, which are interconnected by narrow channels. They are arranged in two rows of four drops, with three inlets and one outlet. In this configuration, medium can be guided in parallel through the microfluidic structures, allowing, for example, two different experimental conditions to be tested simultaneously. The PDMS substrate is biocompatible and transparent and offers the possibility to locally modify its wetting properties through O_2-plasma treatment, such that hydrophilic surface regions surrounded by hydrophobic rim patterns can be realized. The rim structures stabilize the completely open microfluidic network.

The sensor plug-ins each extend over two drops and comprise six platinum electrodes and connection pads located on a 13 mm x 2.8 mm glass substrate (Figure 1b). Two of these plug-ins can be inserted into one microfluidic PDMS chip. Two circular working electrodes (400 µm diameter) are integrated into each drop. Furthermore, a counter electrode and an Ag/AgCl pseudo-RE are integrated into one of the drops. SU-8 structures on the glass plug-in complete the rim patterns on the PDMS to obtain a leakage-free operation of the fluidic network. The

sensor unit is inserted into a small rectangular recess in the PDMS chip such that the electrodes are located at the ceiling of the hanging drop in the final assembly (Figure 1c, cross section A, Supplementary Figure S4).

The device is loaded by pipetting 120 µl of liquid into one of the access holes, and eight hanging drops then form below the circular regions (Figure 1c, cross section B; Figure 1d). Each hanging drop has a volume of 10 µl, which includes the liquid in the cylindrical recess in the glass/PDMS substrate and the spherical drop fraction (Supplementary Figure S1). The remaining liquid volume is located in the channel and connection structures. The completely open PDMS chip architecture allows easy access to the fluidic system and facilitates the loading and harvesting of samples and spheroids during experiments.

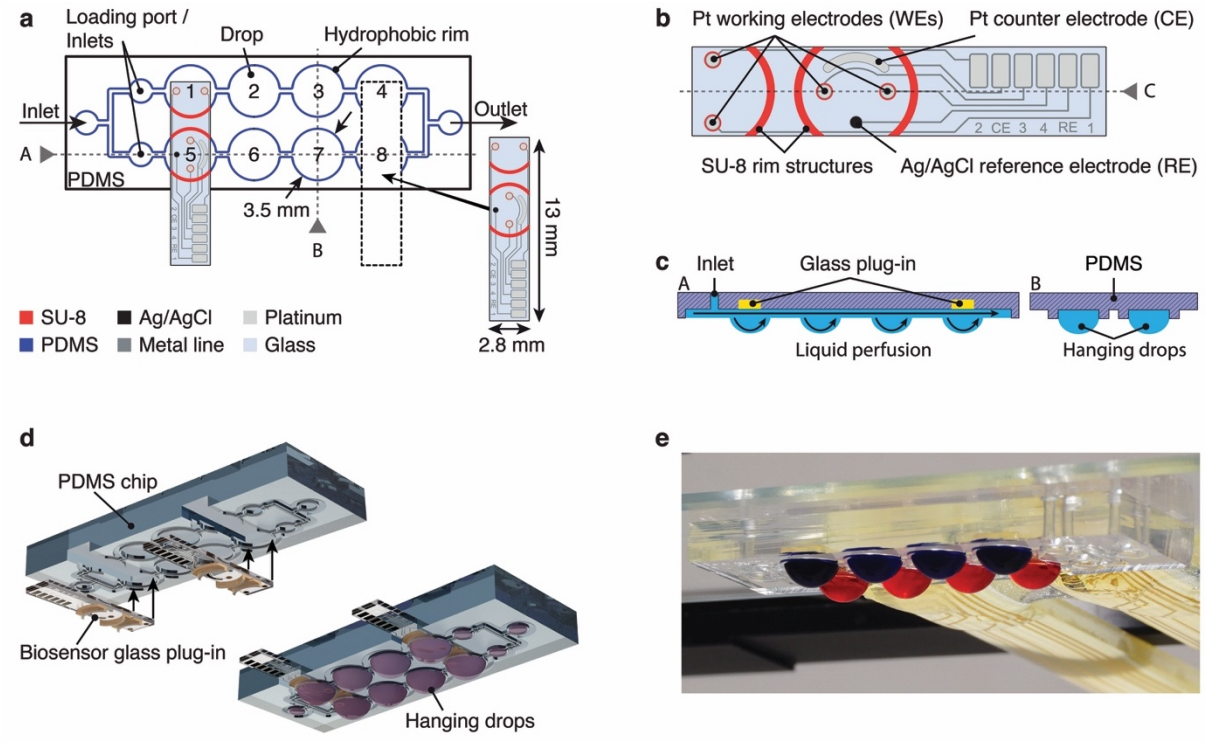

Figure 1 Design and assembly of the microfluidic hanging-drop network and sensor glass plug-ins. (**a**) Schematic two-dimensional (2D) top view of the microfluidic 2x4-hanging-drop chip showing the hydrophobic polydimethylsiloxane (PDMS) rim structures (blue). The dashed lines indicate a PDMS recess, into which a sensor plug-in is inserted. SU-8 structures on the glass plug-in complete the microfluidic network structures (red). (**b**) Close-up view of the sensor unit featuring four working electrodes (WEs), one counter electrode (CE), and one Ag/AgCl pseudo-reference electrode (RE), with the SU-8 rim structures indicated in red. (**c**) Cross section of the completely open microfluidic network showing the hanging drops, the inserted sensor glass plug-ins, and the perfusion flow. (**d**) Three-dimensional (3D) exploded

view showing the device assembly (see Supplementary Figure S3 for an enlarged version). (**e**) Photograph of an assembled device loaded with coloured liquid to better visualize the two rows of drops.

A cross section of an assembled microfluidic hanging-drop device and sensor unit is shown in Figure 2a. The sensing electrodes allow monitoring of the medium around the microtissues in the corresponding drops. A simple drop-coating process was used to coat and functionalize the platinum working electrodes with a hydrogel containing immobilized glucose oxidase (GOx) or lactate oxidase (LOx). These enzymes catalyse an oxidation reaction of glucose or lactate that produces hydrogen peroxide, which, in turn, is amperometrically detected on the Pt electrodes at a potential of 0.65 V vs. Ag/AgCl. The current signal is directly correlated with the analyte concentration of interest (Figure 2b, reaction schemes in Supplementary Figure S5). A coated working electrode is shown in Figure 2c. The enzyme hydrogel is precisely located on the electrode area within the SU-8 ring structure. The ring structure facilitates the coating procedure and ensures uniform hydrogel deposition on all electrodes.

An important advantage of the modular approach is that the functionalization and calibration of the sensor can be performed independently and before plugging the sensor unit into the microfluidic PDMS substrate.

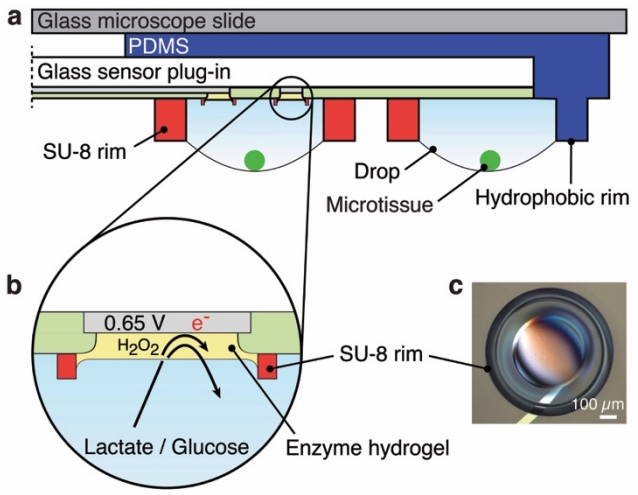

Figure 2 Configuration of the biosensor. (**a**) Schematic cross-sectional view of the biosensor inserted into the microfluidic hanging-drop network device (cross-section C in Figure 1b). Hanging drops form between the SU-8 rims on the glass substrate and the polydimethylsiloxane (PDMS) structure. The biosensors are located at the ceilings of the hanging drops. (**b**) Close-up view illustrating the working principle of the enzyme-based biosensors. Glucose oxidase (GOx) or lactate oxidase (Lox) transforms glucose or lactate to produce hydrogen peroxide,

which is electrochemically detected on the Pt surface at 0.65 V vs. Ag/AgCl. (**c**) Photograph of a hydrogel-coated platinum working electrode showing the SU-8 ring structure, which facilitates precise hydrogel deposition.

3.4.2 Characterization of the glucose and lactate biosensors

The biosensors were characterized through multiple calibration experiments off-chip and were characterized on-chip after mounting in the microfluidic network. Raw data from an off-chip calibration of three functionalized LOx working electrodes and one blank BSA electrode in a conventional 50-ml beaker are shown in Figure 3a. After 20 min of settling at the beginning of the recording, lactate was added stepwise to the RPMI 1640 medium to introduce an increasing lactate concentration. A specific current response to lactate was recorded. The limit of detection (LoD) for the lactate biosensors was calculated to be 7.07 ± 2.73 µM (three times the background noise at the end of the settling time) during off-chip calibration at 37 °C under continuous stirring.

The biosensors showed reproducible characteristics with regard to linearity, sensitivity, and reproducibility for both glucose and lactate (Figure 3b and c). A linear relationship was observed for up to 2 mM glucose for an electrode coated with a single GOx membrane ($R^2 > 0.99$). This sensor exhibited a high sensitivity of 322 ± 41 nA mM^{-1} mm^{-2}. The biosensor characteristics could be tuned by implementing additional layers on top of the enzyme membrane. Adding, for example, a diffusion-limiting BSA layer on top of the enzyme hydrogel membrane increased the linear range up to 7 mM while decreasing the sensitivity to 88 nA mM^{-1} mm^{-2}. Adding a catalase membrane on top of the enzyme membrane further increased the linear range to 11 mM. The sensitivity was determined to be 30 nA mM^{-1} mm^{-2}. Figure 3c shows that the lactate sensor, with a simple LOx membrane coating on the electrode, showed similar linear response characteristics and sensitivity in RPMI 1640 cell culture medium (435 ± 66 nA mM^{-1} mm^{-2}) and PBS solution (443 ± 37 nA mM^{-1} mm^{-2}). The sensor exhibited a linear response for up to 1 mM lactate.

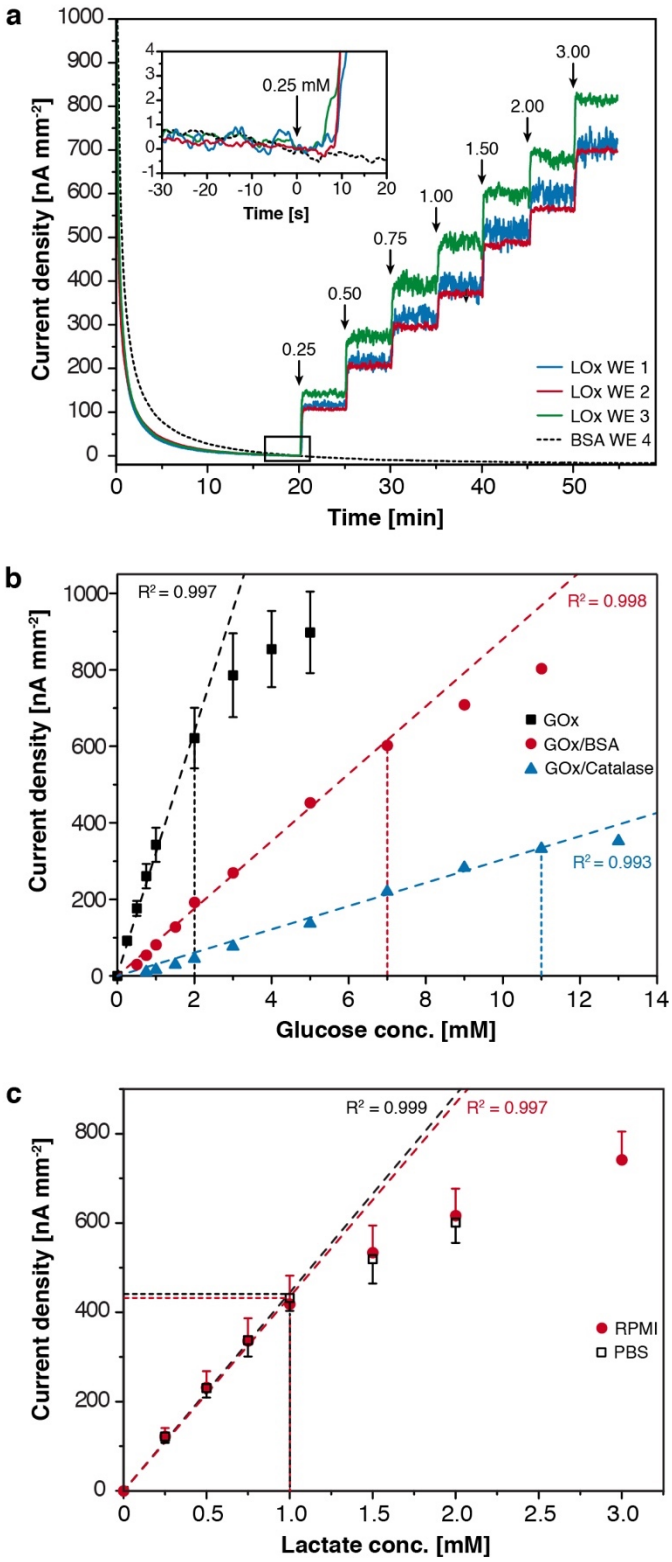

Figure 3 Off-chip calibration results for glucose and lactate biosensors at 37 °C for different biosensor compositions in various solutions. (**a**) Transient lactate current signals of three LOx-functionalized electrodes and one blank bovine serum albumin (BSA) electrode as a control in RPMI 1640 cell culture medium. The inset shows a zoomed-in view of the curves before the

first lactate injection (the solutions were continuously stirred). (**b**) Glucose calibration curves showing the effects of different electrode functionalization protocols on sensitivity and linearity; an additional diffusion-limiting BSA hydrogel layer or a catalase membrane was applied (n=4 for glucose oxidase (GOx) coating; error bars represent standard deviation (s.d.)). (**c**) Lactate calibration in RPMI 1640 cell culture medium (n=3) and PBS (n=4; error bars represent s.d.).

The biosensors were then tested in the chip system in flow-through mode. Figure 4a displays raw signal traces simultaneously recorded by lactate biosensors and blank sensors during consecutive on-chip perfusion of 0, 0.25, and 0.50 mM lactate in PBS at a flow rate of 10 µl min^{-1}. The response of the biosensors was selective and reversible. The two lactate sensors showed slightly different sensitivities, which can be attributed to variations in the manual membrane deposition process. These variations demonstrate the importance of performing calibrations before any biological measurement. For this characterization experiment, several syringe pumps supplying the various calibration solutions were connected to the device inlet via tubing. An artefact caused by the switching of the infusing syringe pump indicates a change in the calibration solution (Figure 4b). The presence of the tubing between the syringes and the microfluidic device produced a delayed sensor signal response. Based on the background noise, an LoD of 1.84 ± 0.34 µM was calculated for this calibration.

Figure 4c presents raw signal traces recorded by a lactate and a glucose biosensor located in the same drop in response to consecutive perfusion of PBS containing 1 mM glucose and 1 mM lactate at a constant flow rate of 5 µl min^{-1}. No sensor cross-talk was observed in the continuous-flow mode.

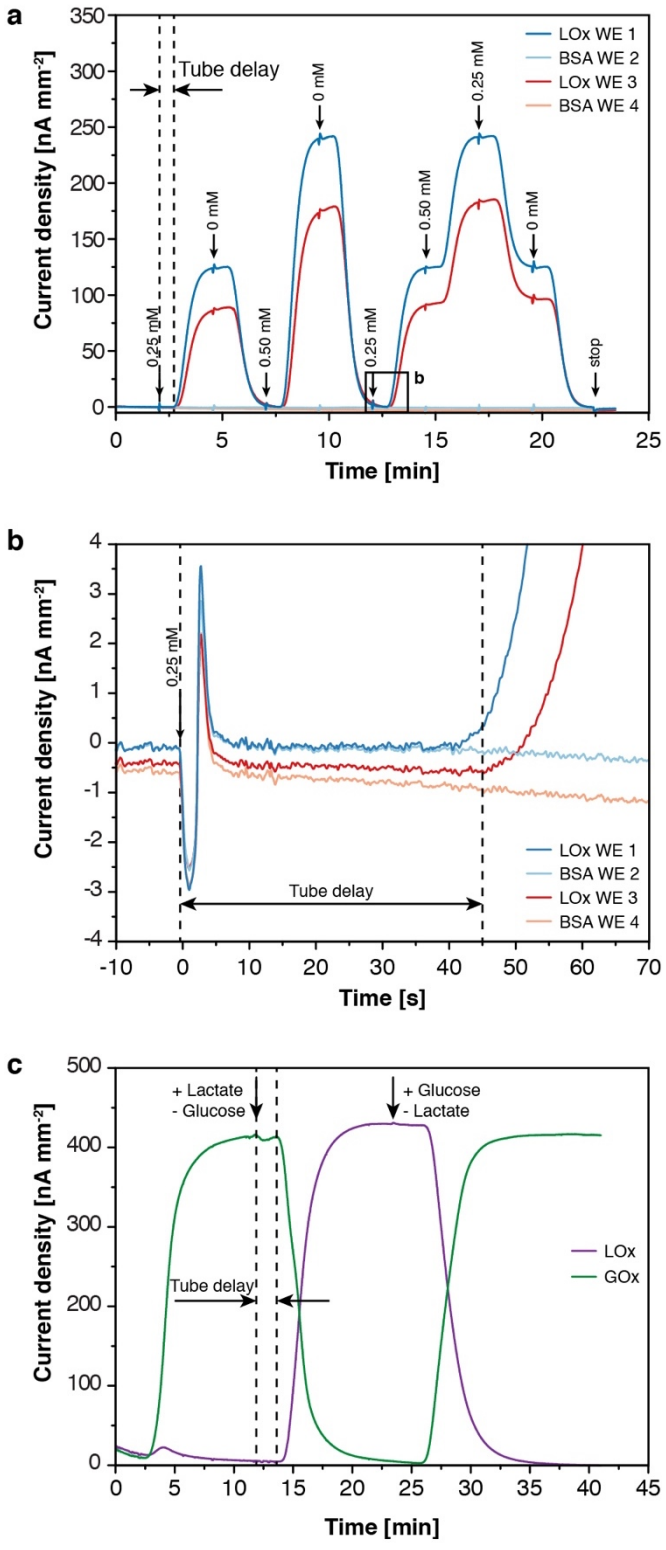

Figure 4 Sensor chip response curves for lactate and glucose in PBS at 37 °C. (**a**) Lactate signal recorded in a configuration featuring one lactate oxidase (Lox)-functionalized electrode and one blank BSA electrode per drop. The same liquid was infused in both rows in parallel at a flow rate of 10 µl min^{-1}. The tube delay represents the time needed for the medium from the syringe to reach the hanging drop instrumented with the sensor. The arrows indicate the

instances when syringes were switched to introduce a different concentration/solution. (**b**) Close-up view showing the artefact observed upon syringe switching, the sensor response observed upon lactate reaching the hanging drop, and the low background noise levels of all four electrodes. The data have been offset-corrected to t = 0 s. Negative current values can be attributed to incomplete settling at the beginning of the measurement. (**c**) On-chip lactate and glucose signals simultaneously recorded in phosphate-buffered saline (PBS) under an alternating analyte flow of glucose and lactate at a flow rate of 5 µl min^{-1}.

3.4.3 Real-time online analyte recording

A typical characteristic of cancerous tissue is an enhanced glucose uptake rate due to an increased glycolysis metabolism, through which pyruvate is fermented to lactate under aerobic conditions.[58] Therefore, the performance of the device was assessed by measuring the metabolism of spherical GFP-induced human colon cancer microtissues (HCT116 eGFP). Glucose uptake and lactate secretion were recorded in real time in the microfluidic hanging-drop network using the two developed biosensors.

Figure 5a presents measurements of the lactate that was secreted from an HCT116 eGFP microtissue (480 µm in diameter) inserted into one of the sensor drops. The measurement was performed in PBS supplemented with 10 mM glucose while perfusion was stopped. After perfusion had been stopped, the lactate signal reproducibly increased to 73.8 ± 4.4 µmol l^{-1} as a result of lactate accumulation in the drop and then decreased again during the washing phase, when the liquid volume in the drop was exchanged with fresh PBS at a flow rate of 5 µl min^{-1}. A lactate secretion rate of 2.21 nmol h^{-1} was calculated. This value is comparable to the lactate secretion rates of growing HCT116 microtissues reported in the literature.[59] As a negative control, the microtissue was removed from the hanging drop after four perfusion cycles. No lactate was detected after removal, thereby confirming that the microtissue was the source of the lactate. Furthermore, no signal that might have originated from any other electroactive species was recorded on the blank electrode. A three-point calibration was performed prior to microtissue loading and after the experiment for the calculation of lactate concentrations.

In a second experiment, we investigated variations in the lactate secretion rate and their correlation with microtissue size. The experimental set-up and the microtissue arrangement are shown in Figure 5b. Two biosensors were inserted into the microfluidic network, and four HCT116 eGFP microtissues of different sizes were loaded into separate sensing drops. Figure 5c presents the raw signal curves of the lactate concentrations that were simultaneously

recorded in all four hanging drops hosting the different microtissues. The following average lactate production rates were determined: 33.4 nmol h^{-1} for the largest, 541-µm-diameter microtissue; 23.9 nmol h^{-1} for the 450-µm-diameter microtissue; 21.1 nmol h^{-1} for the 404-µm-diameter microtissue; and 19.4 nmol h^{-1} for the smallest, 344-µm-diameter microtissue. The corresponding microtissue-size-dependent lactate secretion rates are plotted in Figure 5d.

Again, a washing step with fresh culture medium was performed by applying a perfusion flow of 5 µl min^{-1}. The peaks observed in the signals from the sensors in drops 3 and 4 during the washing step are due to carry-over of the lactate and hydrogen peroxide that were produced and accumulated in the two sensing drops upstream of these drops in the microfluidic system. Similar peaks are not present in the sensor signals from drops 1 and 2.

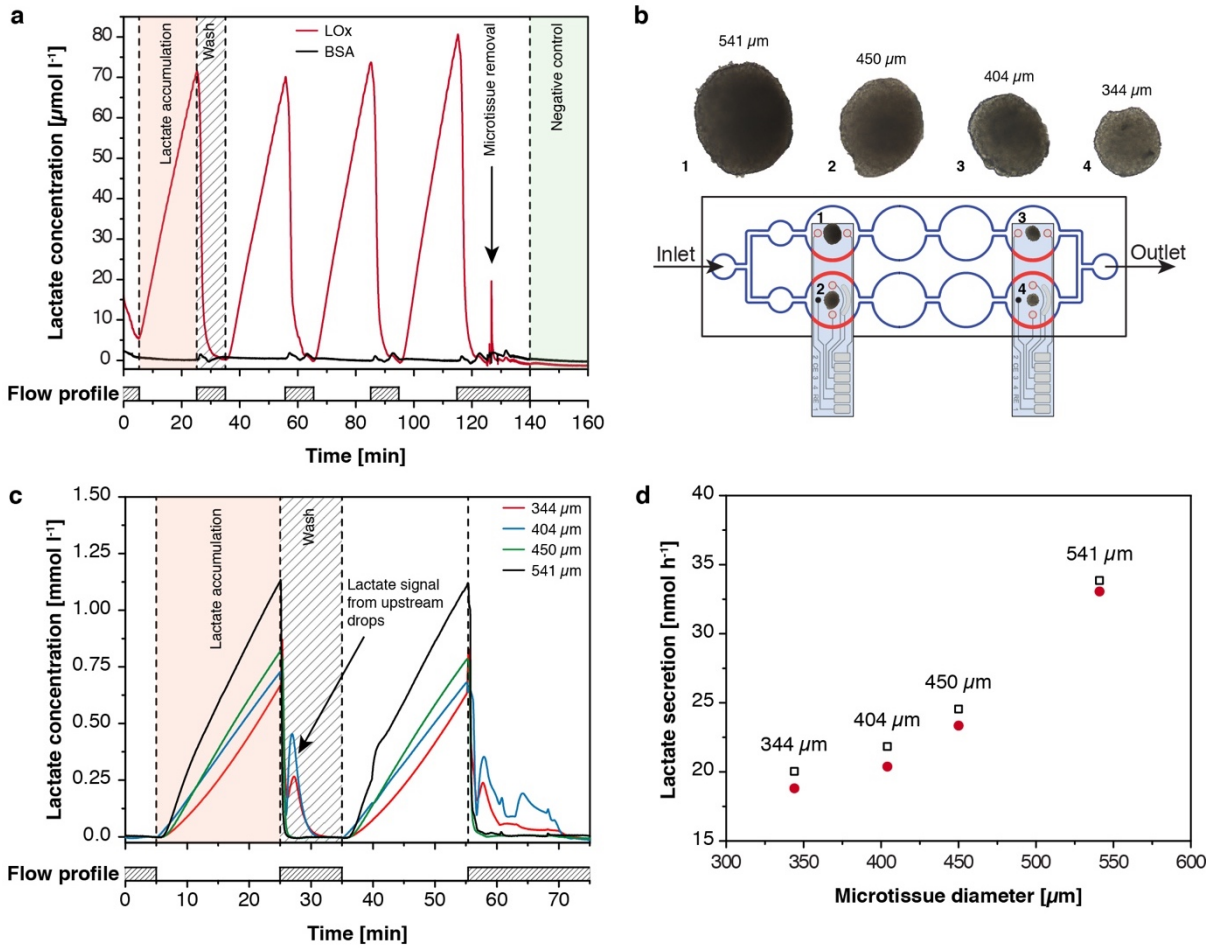

Figure 5 Measured lactate accumulation in hanging drops hosting HCT116 eGFP microtissues. (**a**) Lactate secretion from one microtissue sample cultured in phosphate-buffered saline (PBS) at 37 °C as measured during an on-off medium perfusion protocol, schematically depicted below the response curves. (**b**) Experimental arrangement and device set-up, with micrographs of the different HCT116 eGFP microtissue (not to scale) cultured in the different

sensing drops in the hanging-drop network. The microtissues were located at the bottom of the hanging drops, at an approximate distance of 1 mm to the electrodes. (**c**) Lactate secretion of different microtissues cultured in RPMI 1640 cell culture medium at 37 °C during on-off perfusion (schematically depicted below the response curves). Carry-over signal peaks during the washing phase are clearly visible in the two downstream drops. (**d**) Microtissue-size-dependent lactate secretion rates (black boxes and red dots indicate secretion rates obtained from two consecutive measurements).

Figure 6a presents *in situ* real-time measurements of the glucose consumption and simultaneous lactate production of four HCT116 eGFP microtissues of similar size (274 ± 9 µm), which were inserted in pairs into two separate sensing drops. One drop contained a glucose sensor and a blank BSA electrode for glucose detection. In the other drop, the electrodes were functionalized to act as a lactate sensor and a blank BSA electrode. The measurement was performed by switching between PBS and glucose-supplemented PBS solution (0.5 mM) using an on-off perfusion protocol and a flow rate of 5 µl min^{-1}. After microtissue insertion and the infusion of the glucose solution (clearly visible from the steep increase in the glucose signal), the microtissues were cultured for 60 min without flow. The glucose signal decreased from its initial value of 500 µM. The consumption rate for two microtissues was calculated to be 2.57 nmol h^{-1}. Simultaneously, lactate was secreted at a rate of 2.40 nmol h^{-1}. Comparable values for lactate secretion[59] and glucose consumption[59,60] have been reported in the literature. The blank BSA working electrodes showed slight cross-talk. This cross-talk signal originated from hydrogen peroxide diffusion in the same hanging drop. The liquid was exchanged after 1 h, restoring the initial sensor signal values for both sensor types. The microtissues were then removed from both sensing-drop sites. Perfusion was stopped again, and subsequent measurements confirmed that the recorded analyte transients indeed originated from the metabolism of the microtissues.

The developed microfluidic PDMS chip features separate inlet holes for each drop row (Figure 1a). These inlets can be used to perfuse different solutions in parallel. This configuration permits direct comparison of the effects of medium variations or the different dosages of compounds on the metabolic activity of cultured microtissues. Figure 6b shows the lactate secretion from HCT116 eGFP microtissues (553 and 566 µm) observed while changing from RPMI medium to glucose-free PBS in one of the two drop rows (green curve). The lactate secretion rate of the microtissue immediately began to decrease from its initial value of 22.5–25.0 nmol h^{-1} to 3.0 nmol h^{-1}, whereas no change in the secretion rate was observed for the

control microtissue that was continuously cultured in RPMI (violet curve). Switching the flow back to RPMI stimulated the lactate secretion to nearly the initial rate of approximately 20.0–22.5 nmol h^{-1}. The lactate measurements were performed by applying an on-off perfusion protocol (similar to previous experiments) that consisted of measuring the lactate secretion over 10 min under static conditions and then perfusing fresh medium for 5 min at 2.5 µl min^{-1}.

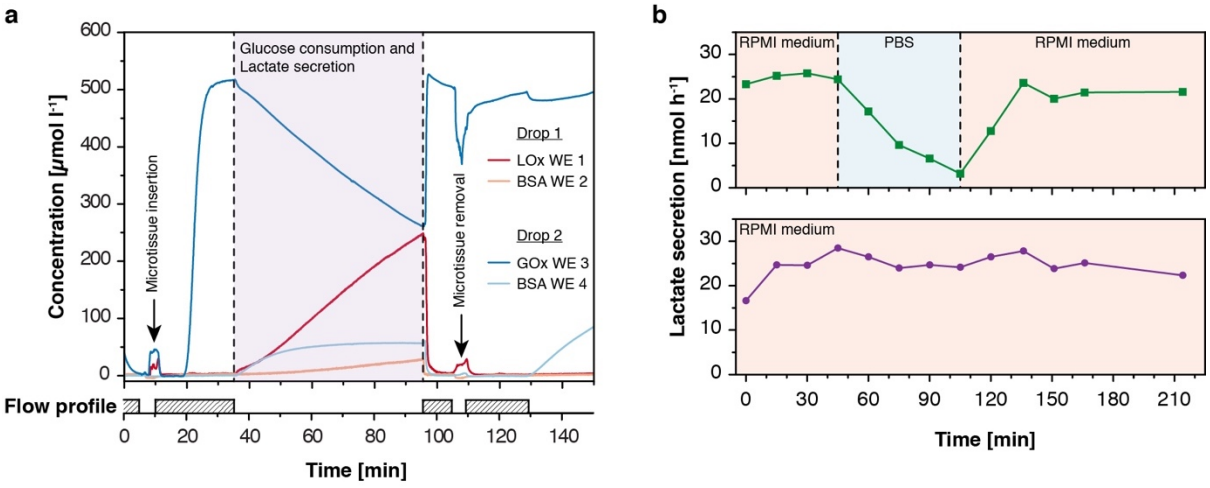

Figure 6 Monitoring the metabolism of HCT116 eGFP microtissues and their response to medium changes. (**a**) Glucose consumption and lactate secretion of HCT116 eGFP microtissues in phosphate-buffered saline (PBS) supplemented with 0.5 mM glucose at 37 °C under static culture conditions (sampling rate: 10 Hz). (**b**) The altered metabolism of a microtissue caused by the replacement of RPMI medium with glucose-free PBS in one of the drops and the recovery of lactate secretion after resupplementing with glucose (green curve). The other drop row on the same polydimethylsiloxane (PDMS) chip hosted a second microtissue (violet curve) and was continuously supplied with RPMI medium as a control.

3.5 Conclusion

We introduced an analytical platform for the real-time *in situ* multi-analyte monitoring of 3D microtissue spheroids by integrating sensor features into a microfluidic culture device. The implementation is based on a modular approach, in which glucose and lactate multi-electrode biosensor modules can be inserted as plug-ins into a microfluidic hanging-drop network. Through this approach, all advantages of the hanging-drop network technology can be fully exploited, including the adhesion-free liquid-air interface for spheroid cultures, precise control of the liquid flow, bubble-free operation, inherent gas exchange, and full continuous access to the fluidic network for the loading and harvesting of liquid samples and spheroids for downstream analysis.

The decoupling of the sensor unit from the microfluidic chip substantially reduces the fabrication, assembly, and operational complexity of the integrated multi-functional platform. Critical procedures, such as biosensor functionalization and calibration, can be performed independently off-chip. Biosensors can, for example, be prepared and stored and then plugged in immediately before use, when the microtissue structures are ready for experimentation. The developed functionalization procedure is simple, and its reproducibility has been improved through the implementation of SU-8 electrode rims that support drop deposition.

The lactate and glucose metabolism of individual GFP-induced human colon carcinoma microtissues was successfully measured *in situ* inside small, 10-µl volumes using an automated perfusion set-up, such that any disturbance from or influence of external effects could be effectively excluded. The obtained data provided real-time information on a time scale of minutes regarding the metabolic state of the microtissues under different culture conditions.

This technological approach is highly versatile. Different versions of the microfluidic chip were fabricated, in which the biosensor modules could be plugged in at different locations in the hanging-drop network. The approach can be applied in larger and more complex hanging-drop networks including different spheroid types in multi-tissue configurations. Furthermore, the read-out capability of the system can be easily expanded through the integration of additional plug-ins comprising more and/or tissue-specific sensor types. The platform is very flexible in how the sensors and the hanging drops hosting the microtissues can be arranged.

Although the presented approach allows continuous sensor operation at good sensitivity for ~1 day, biosensors always face challenges related to extending their lifetimes and achieving good measurement reproducibility. We attempted to address this challenge by using the plug-in approach, which allows sensors with satisfactory characteristics to be selected and permits pre- and post-calibration to be performed off-chip or by using an automated on-chip perfusion protocol during longer experiments. Thus, a variety of biological questions can be addressed using the presented method; for experiments extending over longer time spans, optimization of the sensors with respect to long-term stability will be required.

With the presented design for biosensor integration, we have introduced an important feature into the hanging-drop network technology. The proposed sensors enhance the data and information that can be collected from such systems and enable new insight into multi-tissue or “body-on-a-chip” experiments.

3.6 Acknowledgements

This work was financially supported by FP7 of the EU through the project “Body on a chip”, ICT-FET-296257, and the ERC Advanced Grant “NeuroCMOS” (contract 267351) as well as by an individual Ambizione Grant 142440 from the Swiss National Science Foundation for Olivier Frey.

3.7 Supplementary Information

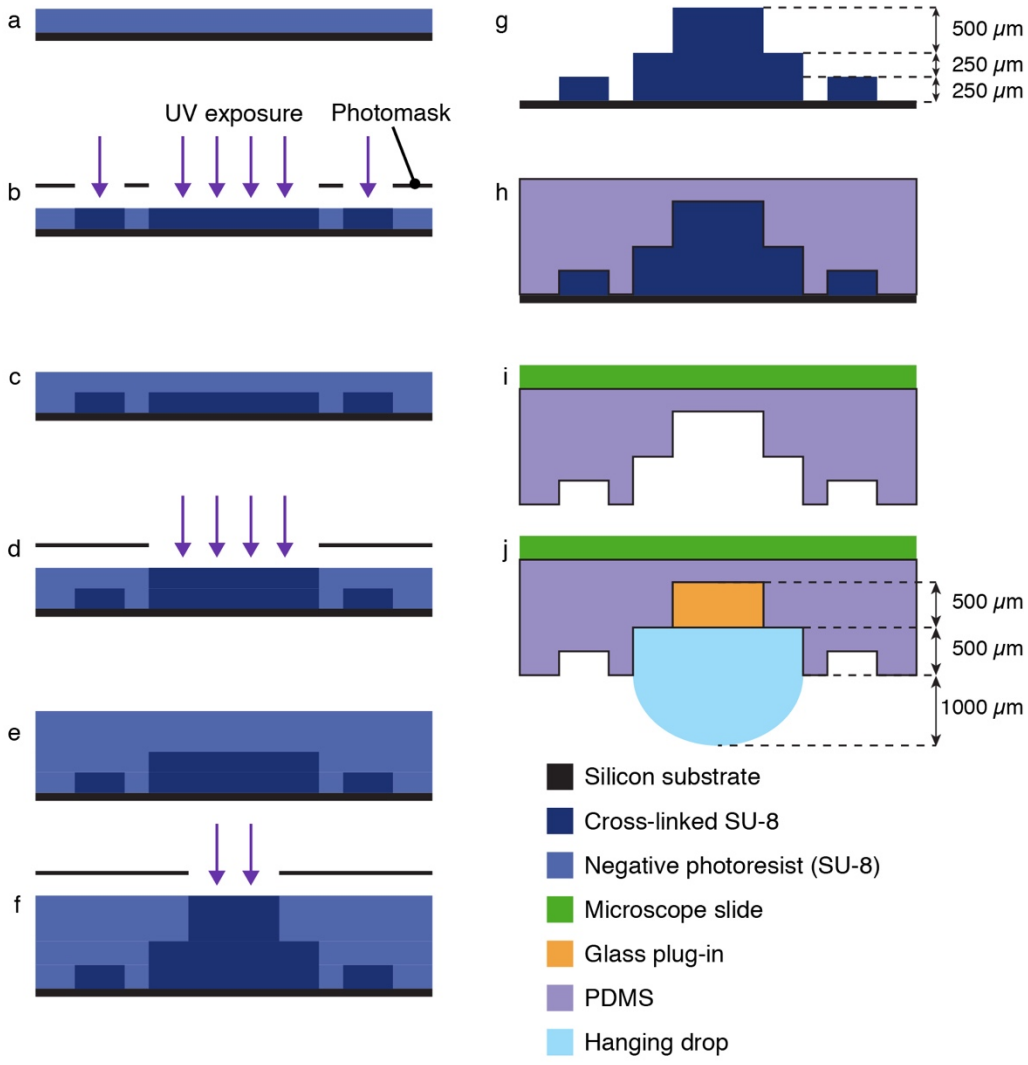

Figure S1 Fabrication of the SU-8 master mold for casting the microfluidic hanging-drop network. (**a**) Spin-coating of the first SU-8 layer (250 µm) on the silicon substrate. (**b**) UV exposure and patterning through a transparency mask and cross-linking of exposed SU-8. (**c-f**) Repeated process for SU-8 layers 2 (250 µm) and 3 (500 µm). (**g**) Development of non-crosslinked SU-8 of all layers. (**h**) PDMS casting and curing. (**i**) Bonding of PDMS onto a glass slide to improve stability. (**j**) Insertion of sensor glass plug-in and liquid loading.

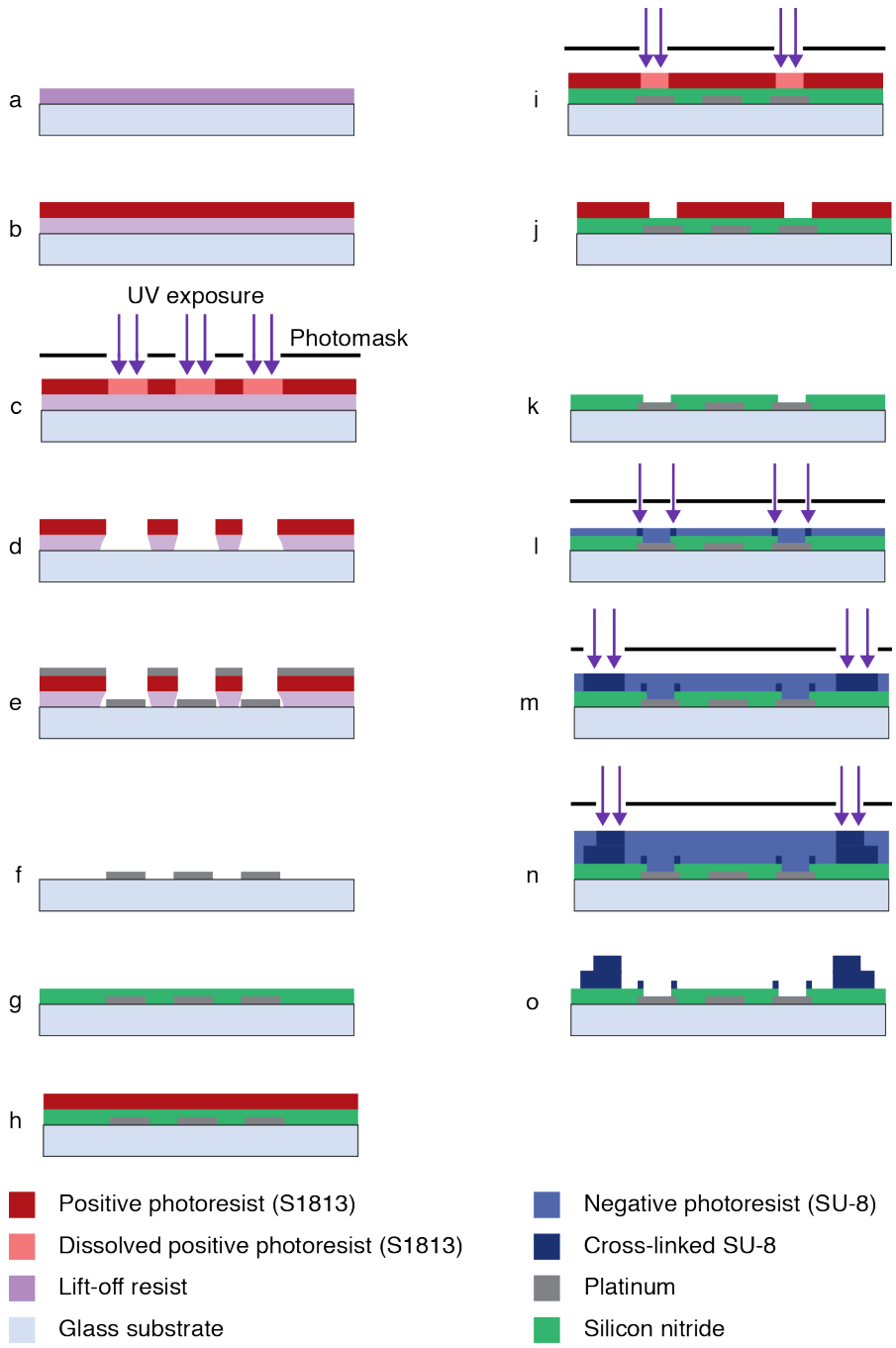

Figure S2 Fabrication of the sensor glass plug-in. (**a**) Spin-coating of the lift-off resist on the glass substrate. (**b**) Subsequent spin-coating of positive photoresist (S1813). (**c**) UV exposure through a transparency mask for metal patterning. (**d**) Development of photoresist and lift-off resist (exposed photoresist is dissolved) (**e**) Sputtering of the metal layer (20 nm TiW, 200 nm Pt). (**f**) Lift-off. (**g**) Plasma-enhanced vapor deposition of silicon nitride for passivation. (**h** and **i**) Spin-coating of positive photoresist (S1813) and UV exposure through a transparency mask. (**j**) Development of the exposed resist. (**k**) Reactive-ion etching to open platinum electrode sites. Remaining photoresist is removed by oxygen plasma. (**l-n**) Consecutive spin-coating of

three SU-8 layers (20, 250, and 250 µm), and UV exposure through transparency masks. (**o**) Development of all SU-8 structures.

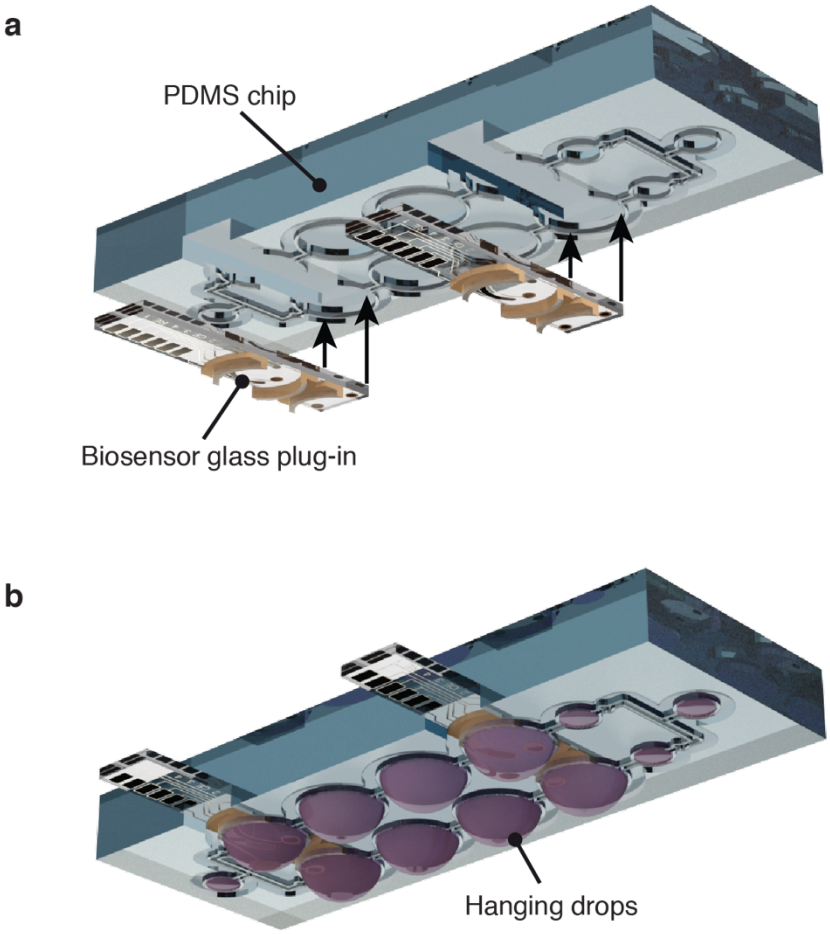

Figure S3 3D exploded view showing the device assembly. (**a**) Insertion of sensor glass plug-ins into a microfluidic PDMS hanging drop network (PCB is not shown). (**b**) Hanging drops are formed underneath the PDMS chip after liquid loading so that analyte measurements can be performed on four drops in parallel.

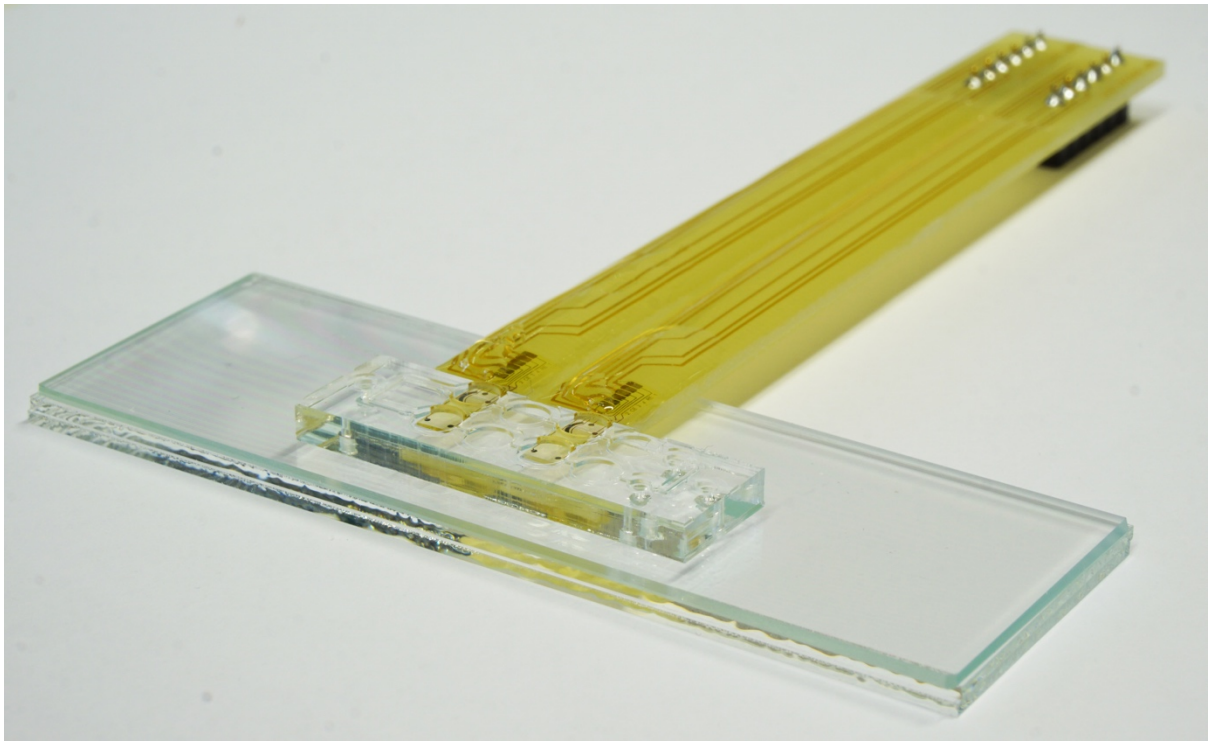

Figure S4 2x4 Hanging-drop network device with two sensor modules inserted into the microfluidic PDMS chip before liquid loading. The sensor glass plug-ins are glued to a small PCB and wire-bonded to connector pins at the end of the PCB to facilitate electric connection. Different PDMS chip layouts were designed, which allowed for inserting one or two identical sensor modules in parallel into different drops (in this image in columns 1 and 3).

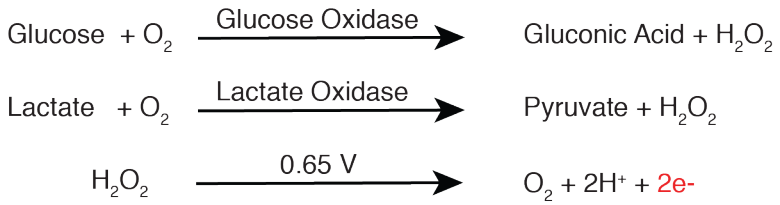

Figure S5 Analyte detection principle and reaction scheme of the sensor. Glucose oxidase (GOx) and lactate oxidase (LOx) catalyze an oxidation reaction of the analytes, i.e., glucose and lactate react to gluconic acid and pyruvate in the presence of oxygen. Hydrogen peroxide is produced as a side product and is oxidized on the electrodes at a potential of 0.65 V vs. Ag/AgCl. This oxidation process can be quantitatively monitored by amperometry, and the obtained signals directly correlate with the analyte concentration.

3.8 References

1. El-Ali, J., Sorger, P. K. & Jensen, K. F. Cells on chips. *Nature* **442,** 403–11 (2006).
2. Kovarik, M. L. *et al.* Micro total analysis systems for cell biology and biochemical assays. *Anal. Chem.* **84,** 516–40 (2012).
3. Pampaloni, F., Reynaud, E. G. & Stelzer, E. H. K. The third dimension bridges the gap between cell culture and live tissue. *Nat. Rev. Mol. Cell Biol.* **8,** 839–45 (2007).
4. Justice, B. A., Badr, N. A. & Felder, R. A. 3D cell culture opens new dimensions in cell-based assays. *Drug Discov. Today* **14,** 102–7 (2009).
5. Esch, M. B. *et al.* How multi-organ microdevices can help foster drug development. *Adv. Drug Deliv. Rev.* **69–70,** 158–169 (2014).
6. Polini, A. *et al.* Organs-on-a-chip: a new tool for drug discovery. *Expert Opin. Drug Discov.* **9,** 335–52 (2014).
7. Baharvand, H., Hashemi, S. M., Kazemi Ashtiani, S. & Farrokhi, A. Differentiation of human embryonic stem cells into hepatocytes in 2D and 3D culture systems in vitro. *Int. J. Dev. Biol.* **50,** 645–52 (2006).
8. Asthana, A. & Kisaalita, W. S. Microtissue size and hypoxia in HTS with 3D cultures. *Drug Discov. Today* **17,** 810–7 (2012).
9. Knight, E. & Przyborski, S. Advances in 3D cell culture technologies enabling tissue-like structures to be created in vitro. *J. Anat.* (2014). doi:10.1111/joa.12257
10. Breslin, S. & O'Driscoll, L. Three-dimensional cell culture: the missing link in drug discovery. *Drug Discov. Today* **18,** 240–9 (2013).
11. Tibbitt, M. W. & Anseth, K. S. Hydrogels as extracellular matrix mimics for 3D cell culture. *Biotechnol. Bioeng.* **103,** 655–63 (2009).
12. Lee, J., Cuddihy, M. J. & Kotov, N. A. Three-dimensional cell culture matrices: state of the art. *Tissue Eng. Part B. Rev.* **14,** 61–86 (2008).
13. Griffith, L. G. & Swartz, M. a. Capturing complex 3D tissue physiology in vitro. *Nat. Rev. Mol. Cell Biol.* **7,** 211–24 (2006).
14. Kelm, J. M., Timmins, N. E., Brown, C. J., Fussenegger, M. & Nielsen, L. K. Method for generation of homogeneous multicellular tumor spheroids applicable to a wide variety of cell types. *Biotechnol. Bioeng.* **83,** 173–80 (2003).

15. Tung, Y.-C. *et al.* High-throughput 3D spheroid culture and drug testing using a 384 hanging drop array. *Analyst* **136,** 473–8 (2011).

16. Hirschhaeuser, F. *et al.* Multicellular tumor spheroids: an underestimated tool is catching up again. *J. Biotechnol.* **148,** 3–15 (2010).

17. Messner, S., Agarkova, I., Moritz, W. & Kelm, J. M. Multi-cell type human liver microtissues for hepatotoxicity testing. *Arch. Toxicol.* **87,** 209–13 (2013).

18. Rimann, M. *et al.* An in vitro osteosarcoma 3D microtissue model for drug development. *J. Biotechnol.* **189,** 129–35 (2014).

19. Beauchamp, P. *et al.* Development and Characterization of a Scaffold-Free 3D Spheroid Model of Induced Pluripotent Stem Cell-Derived Human Cardiomyocytes. *Tissue Eng. Part C. Methods* **21,** 852–61 (2015).

20. Young, E. W. K. & Beebe, D. J. Fundamentals of microfluidic cell culture in controlled microenvironments. *Chem. Soc. Rev.* **39,** 1036–48 (2010).

21. Powers, M. J. *et al.* Functional behavior of primary rat liver cells in a three-dimensional perfused microarray bioreactor. *Tissue Eng.* **8,** 499–513 (2002).

22. Esch, M. B. *et al.* Multi-cellular 3D human primary liver cell culture elevates metabolic activity under fluidic flow. *Lab Chip* **15,** 2269–77 (2015).

23. Van der Meer, A. D., Poot, A. A., Feijen, J. & Vermes, I. Analyzing shear stress-induced alignment of actin filaments in endothelial cells with a microfluidic assay. *Biomicrofluidics* **4,** 11103 (2010).

24. Lu, H. *et al.* Microfluidic shear devices for quantitative analysis of cell adhesion. *Anal. Chem.* **76,** 5257–64 (2004).

25. Balcells, M., Fernández Suárez, M., Vázquez, M. & Edelman, E. R. Cells in fluidic environments are sensitive to flow frequency. *J. Cell. Physiol.* **204,** 329–35 (2005).

26. Huh, D. *et al.* Reconstituting organ-level lung functions on a chip. *Science* **328,** 1662–8 (2010).

27. Stucki, A. O. *et al.* A lung-on-a-chip array with an integrated bio-inspired respiration mechanism. *Lab Chip* **15,** 1302–10 (2015).

28. Maschmeyer, I. *et al.* A four-organ-chip for interconnected long-term co-culture of human intestine, liver, skin and kidney equivalents. *Lab Chip* **15,** 2688–2699 (2015).

29. Kim, J.-Y. *et al.* 3D spherical microtissues and microfluidic technology for multi-tissue experiments and analysis. *J. Biotechnol.* **205,** 24–35 (2015).

30. Zhang, C., Zhao, Z., Abdul Rahim, N. A., van Noort, D. & Yu, H. Towards a human-on-chip: culturing multiple cell types on a chip with compartmentalized microenvironments. *Lab Chip* **9,** 3185–92 (2009).

31. Van Midwoud, P. M., Merema, M. T., Verpoorte, E. & Groothuis, G. M. M. A microfluidic approach for in vitro assessment of interorgan interactions in drug metabolism using intestinal and liver slices. *Lab Chip* **10,** 2778–86 (2010).

32. Huh, D., Torisawa, Y., Hamilton, G. A., Kim, H. J. & Ingber, D. E. Microengineered physiological biomimicry: organs-on-chips. *Lab Chip* **12,** 2156–64 (2012).

33. Sung, J. H., Kam, C. & Shuler, M. L. A microfluidic device for a pharmacokinetic-pharmacodynamic (PK-PD) model on a chip. *Lab Chip* **10,** 446–55 (2010).

34. Sonntag, F. *et al.* Design and prototyping of a chip-based multi-micro-organoid culture system for substance testing, predictive to human (substance) exposure. *J. Biotechnol.* **148,** 70–5 (2010).

35. Link, H., Fuhrer, T., Gerosa, L., Zamboni, N. & Sauer, U. Real-time metabolome profiling of the metabolic switch between starvation and growth. *Nat. Methods* **12,** 1091–7 (2015).

36. Dittrich, P. S. & Manz, A. Lab-on-a-chip: microfluidics in drug discovery. *Nat. Rev. Drug Discov.* **5,** 210–8 (2006).

37. Nge, P. N., Rogers, C. I. & Woolley, A. T. Advances in Microfluidic Materials, Functions, Integration, and Applications. *Chem. Rev.* **113,** 2550–2583 (2013).

38. Grieshaber, D., Mackenzie, R., Vörös, J. & Reimhult, E. Electrochemical Biosensors - Sensor Principles and Architectures. *Sensors* **8,** 1400–1458 (2008).

39. Eklund, S. E., Taylor, D., Kozlov, E., Prokop, A. & Cliffel, D. E. A microphysiometer for simultaneous measurement of changes in extracellular glucose, lactate, oxygen, and acidification rate. *Anal. Chem.* **76,** 519–27 (2004).

40. Hafner, F. Cytosensor Microphysiometer: technology and recent applications. *Biosens. Bioelectron.* **15,** 149–58 (2000).

41. McKenzie, J. R., Palubinsky, A. M., Brown, J. E., McLaughlin, B. & Cliffel, D. E.

Metabolic multianalyte microphysiometry reveals extracellular acidosis is an essential mediator of neuronal preconditioning. *ACS Chem. Neurosci.* **3,** 510–8 (2012).

42. Ciobanu, M., Taylor, D. E., Wilburn, J. P. & Cliffel, D. E. Glucose and lactate biosensors for scanning electrochemical microscopy imaging of single live cells. *Anal. Chem.* **80,** 2717–27 (2008).

43. Pitta Bauermann, L., Schuhmann, W. & Schulte, A. An advanced biological scanning electrochemical microscope (Bio-SECM) for studying individual living cells. *Phys. Chem. Chem. Phys.* **6,** 4003 (2004).

44. Arquint, P., Koudelka-Hep, M., van der Schoot, B. H., van der Wal, P. & de Rooij, N. F. Micromachined analyzers on a silicon chip. *Clin. Chem.* **40,** 1805–9 (1994).

45. Talaei, S., van der Wal, P. D., Ahmed, S., Liley, M. & de Rooij, N. F. Enzyme SU-8 microreactors: simple tools for cell-culture monitoring. *Microfluid. Nanofluidics* **19,** 351–61 (2015).

46. Moser, I., Jobst, G. & Urban, G. A. Biosensor arrays for simultaneous measurement of glucose, lactate, glutamate, and glutamine. *Biosens. Bioelectron.* **17,** 297–302 (2002).

47. Boero, C., Olivo, J., De Micheli, G. & Carrara, S. New approaches for carbon nanotubes-based biosensors and their application to cell culture monitoring. *IEEE Trans. Biomed. Circuits Syst.* **6,** 479–85 (2012).

48. Frey, O., Talaei, S., van der Wal, P. D., Koudelka-Hep, M. & de Rooij, N. F. Continuous-flow multi-analyte biosensor cartridge with controllable linear response range. *Lab Chip* **10,** 2226–34 (2010).

49. Dempsey, E. *et al.* Design and development of a miniaturised total chemical analysis system for on-line lactate and glucose monitoring in biological samples. *Anal. Chim. Acta* **346,** 341–349 (1997).

50. Perdomo, J. *et al.* Miniaturized real-time monitoring system for L-lactate and glucose using microfabricated multi-enzyme sensors. *Biosens. Bioelectron.* **15,** 515–22 (2000).

51. Satoh, W. *et al.* Integrated Electrochemical Analysis System with Microfluidic and Sensing Functions. *Sensors* **8,** 1111–1127 (2008).

52. Brischwein, M. *et al.* Functional cellular assays with multiparametric silicon sensor chips. *Lab Chip* **3,** 234–40 (2003).

53. Ges, I. a. & Baudenbacher, F. Enzyme electrodes to monitor glucose consumption of single cardiac myocytes in sub-nanoliter volumes. *Biosens. Bioelectron.* **25,** 1019–24 (2010).

54. Ges, I. a. & Baudenbacher, F. Enzyme-coated microelectrodes to monitor lactate production in a nanoliter microfluidic cell culture device. *Biosens. Bioelectron.* **26,** 828–33 (2010).

55. Weltin, A. *et al.* Cell culture monitoring for drug screening and cancer research: a transparent, microfluidic, multi-sensor microsystem. *Lab Chip* **14,** 138–46 (2014).

56. Frey, O., Misun, P. M., Fluri, D. A., Hengstler, J. G. & Hierlemann, A. Reconfigurable microfluidic hanging drop network for multi-tissue interaction and analysis. *Nat. Commun.* **5,** 4250 (2014).

57. Rothe, J., Frey, O., Stettler, A., Chen, Y. & Hierlemann, A. Fully integrated CMOS microsystem for electrochemical measurements on 32 × 32 working electrodes at 90 frames per second. *Anal. Chem.* **86,** 6425–32 (2014).

58. Gatenby, R. a & Gillies, R. J. Why do cancers have high aerobic glycolysis? *Nat. Rev. Cancer* **4,** 891–9 (2004).

59. Timmins, N. E., Dietmair, S. & Nielsen, L. K. Hanging-drop multicellular spheroids as a model of tumour angiogenesis. *Angiogenesis* **7,** 97–103 (2004).

60. Aykin-Burns, N., Ahmad, I. M., Zhu, Y., Oberley, L. W. & Spitz, D. R. Increased levels of superoxide and H2O2 mediate the differential susceptibility of cancer cells versus normal cells to glucose deprivation. *Biochem. J.* **418,** 29–37 (2009).

4 Microfluidic Hydrogel Hanging-Drop Network for Long-Term Culturing of 3D Microtissues and Simultaneous High-Resolution Imaging

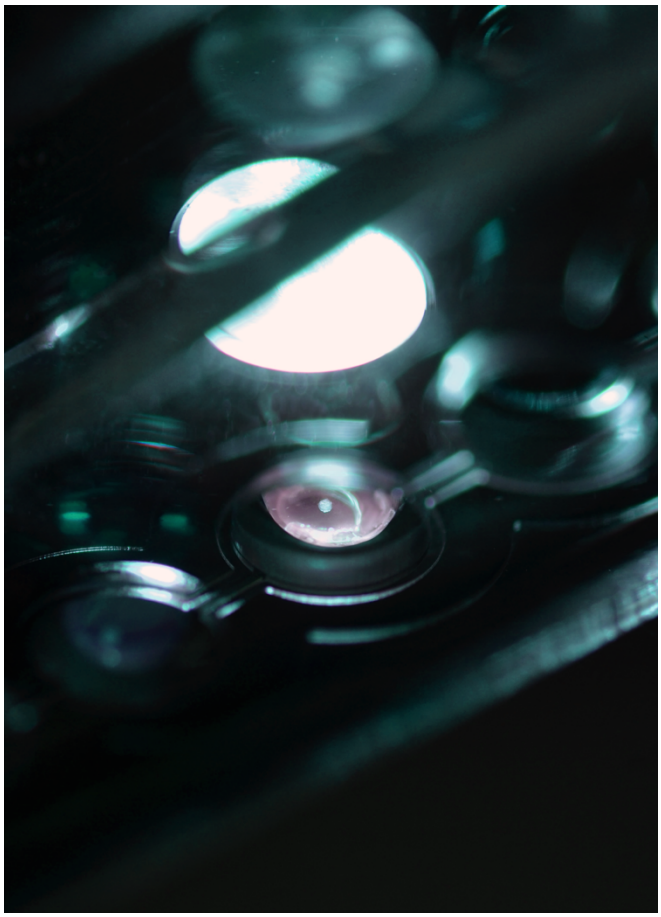

Elise A. Aeby*, Patrick M. Misun*, Andreas Hierlemann, Olivier Frey. Microfluidic hydrogel hanging-drop network for long-term culturing of 3D microtissues and simultaneous high-resolution imaging. Advanced Biosystems 2, 1800054 (2018).

DOI: 10.1002/adbi.201800054

* Both authors contributed equally.

4.1 Abstract

Three-dimensional (3D) microtissues, cultured in microfluidic platforms, enable to study complex biological mechanisms that cannot be replicated in two-dimensional cell cultures. Deeper insights can be obtained if these 3D culture systems are rendered compatible with high-resolution time-lapse imaging systems, which requires precise placement and immobilization of the specimen while ensuring high viability and functionality of the 3D cell constructs. This article presents a versatile microfluidic platform for long-term culturing and analysis of 3D microtissues. The platform is compatible with time-lapse high-resolution confocal microscopy. Hanging hydrogel drops enabled the precise placement and stable immobilization of the microtissues in the microfluidic chip. The chip includes perfusion capability to apply drugs, staining and clearing solutions. The features of the chip are demonstrated by studying (i) colon cancer microtissues to monitor tissue growth and cell death; on-chip clearing was used to augment the penetration depth for endpoint imaging; (ii) primary human liver microtissues were exposed to cytochalasin D to observe its effect on the bile canaliculi. The results obtained with both sample types demonstrate the suitability of the system for investigating complex processes in organotypic 3D microtissues, down to single-cell level, and for observation of physiologically relevant processes at subcellular scale.

4.2 Introduction

Over the last decade, the relevance of 3D cell cultures for reproducing *in vivo* functions and mechanisms has been widely established within the scientific community.[1,2] The reproducibility and *in vivo* relevance with respect to gene expression, protein expression and drug susceptibility, render 3D cell cultures the model of choice for *in vitro* studies.[3,4] Numerous methods to create 3D cell cultures exist[5]: i) culturing of cells in a non-adhesive environment to form 3D microtissues,[6] ii) culturing of the cells in or on an extracellular scaffold,[7] and iii) arranging the cells into a 3D tissue using microstructures[8–10] to obtain complex models of organs, such as lung,[11] airways,[12] liver,[13] kidney,[14] and organ-on-a-chip models for the gastrointestinal tract.[15,16] Additionally, membrane structures were created and have been used as models for selective barriers in the body, such as the blood-brain-barrier[17] and the placental barrier.[18] Spherical microtissues (MTs), also called spheroids, are 3D cell constructs that form spontaneously within 3-4 days by self-aggregation of the cells cultivated in a non-adhesive environment.[19,20] They feature tissue-specific phenotypes and functionality[21,22] including an

extracellular matrix (ECM),[23] or cell polarization in liver microtissues.[24] In addition, 3D spheroids are comprised of cells in various stages, including proliferating, quiescent, apoptotic, hypoxic, and necrotic cells.[25,26] Consequently, functional tissues of various organs can be generated in the form of microtissues,[20,27,28] including diseased tissues, such as cancerous tissue[21,29,30] or fatty liver.[31] Furthermore, the presence of cell-cell interactions,[32] a 3D biomechanical microenvironment[33] and the ECM[34] leads to an enhanced viability and/or functionality of the cultivated microtissues, which then closely resemble *in vivo* tissue.[2] The simple formation, culturing, and handling makes MTs a highly flexible and applicable organotypic model system for academia and industry.

The combination of 3D cell cultures with perfused analytical platforms further increases the relevance of these *in vitro* models[35–37] as it provides additional features.[37] Microfluidic technology allows for a precise control of the flow to exchange medium, enables to interconnect different types of tissues, and allows for the rapid change of the culturing conditions. An accurate control over microenvironmental parameters enables a broad range of new cell culturing applications.[38] Different microfluidic platforms for culturing MTs exist. Those platforms either trap pre-formed MTs in microstructures,[39] or MTs are formed directly inside the microfluidic systems.[40–42] An alternative approach is to use hanging-drop networks, where individual MTs are cultured at the bottom of interconnected hanging drops so that full access to the tissues is guaranteed.[43] In the past, we integrated different features in those hanging-drop networks in order to enhance the readout options.[44–46] Applications in drug screening and examples of multi-tissue interactions were reported and demonstrate the relevance of perfused and easy-to-operate MT culturing systems.[47–49]

A major draw-back of many setups is their limitation in spatiotemporal microscopy-imaging resolution. Despite the availability of fluorescent markers to study biological processes in a quantitative manner and to visualize cells and specific proteins, the full benefits of these techniques currently cannot be fully exploited. Either, the 3D tissue structures are not technically compatible with the latest-generation fluorescence microscopes, or perfusion flow induces the movement of MTs, which makes high-resolution imaging and tracking of cellular and subcellular events within the tissue impossible. Without the access to time-lapse imaging, the dynamic nature of many processes and the interplay of different cells within a tissue remain difficult to study. Additionally, versatile integrated systems that feature complementary assays can increase the breadth and impact of achievable experimental results.[50]

In this paper, we present a simple and highly versatile microfluidic system for culturing and analysis of organotypic MTs. The system is specifically designed for the use with high-resolution confocal microscopy. The enabling feature is a hanging hydrogel drop, into which single microtissues can be loaded. This system provides several advantages: i) the MT is automatically positioned at the bottom of the drop making it easy to locate the MT, ii) the hydrogel immobilizes the microtissues for long-term observation, iii) the hydrogel technology with its broad range of natural and synthetic components can be used to add biomechanical and chemical features to mimic tissue and cellular structural microenvironments.[51–54] The hydrogel drops are located at the ceiling of individual culture chambers. Multiple drops are arrayed in a microfluidic chip system and interconnected through microchannels, which enables controlled perfusion flow and multiplexed or parallel experiments. The flow enables nutrient supply and removal of waste products, which enhances MT viability and functionality. Staining solutions and compounds can be perfused through the microfluidic system to investigate the behavior and response of microtissues in real-time. Microtissues can be cleared directly within the system for endpoint imaging at higher penetration depth. Furthermore, the microtissues are fully accessible and can be harvested at the end of experiments for further downstream analysis.

4.3 Materials and Methods

4.3.1 Design and fabrication

The microfluidic chips were designed with CAD software (AutoCAD, Autodesk, San Rafael, California, U.S.). The mask designs were printed on a transparency mask provided by Selba (Versoix, Switzerland) at a resolution of 50800 dpi. As previously reported, a micro-fabrication process was used for fabricating the SU-8 mold (Figure S11, Supporting Information).[43] The first 250 µm thick layer was used to form the vacuum channel, the culture chamber, and the microchannels, which interconnected the chambers. The second layer was used to enlarge the culture chamber to have enough space for the hydrogel droplets. This layer was spin-coated in two subsequent steps with an intermediate soft-bake. The total thickness of the second layer was 1 mm. The third and last layer was 100 µm thick. It was used to form the circular rim structure at the ceiling of the culture chamber, which facilitated the hydrogel droplet deposition. The microfabricated molds were silanized by gas-phase deposition using trichloro(1H,1H,2H,2H-perfluorooctyl)silane (448931, Sigma-Aldrich, Buchs, Switzerland) during 12 h before molding the PDMS. This step was used to reduce PDMS adhesion to the mold. The silicone elastomer and the curing agent (Sylgard 184 Silicone elastomer kit, Dow

Corning, USA) were mixed in a 10:1 ratio, degassed, and poured over the SU-8 mold. The mold and PDMS were then degassed and placed on a hotplate at 75 °C for 2 h to polymerize the PDMS. Single chips were then cut from the master PDMS piece, and holes were punched to access the vacuum channels (diameter of 1 mm), and to create the in- and outlets (diameter of 0.5 mm).

The microfluidic chip was connected to precision syringe pumps (Harvard Pump PHD ULTRA, Harvard Apparatus, Holliston, United States). A standard luer lock syringe-tubing connector (22 GA ½", APM Technica AG, Heerbrugg, Switzerland) was connected to the syringe. Polytetrafluoroethylene (PTFE) tubing (ID 0.3 mm, OD 0.6 mm, Bohlender GmbH, Grünsfeld, Germany) was connected to the tubing connectors via a 2 cm long flexible silicon tubing (Tygon R3607, ID 0.25 mm, Idex Health & Science GmbH, Wertheim, Germany). A metal connection piece of a standard luer lock syringe-tubing connector (22 GA ½" Bent 90 Deg, APM Technica AG, Switzerland) was then used to access the microfluidic chip through the inlet. The outlet was connected in a similar way, and the end of the PTFE tubing was placed in a small container to collect the medium.

The connection to the vacuum channel was realized through a metallic connector that was taken from a standard luer lock syringe-tubing connector (18 GA, ½'' Bent 90 Deg, APM Technica AG, Switzerland). Flexible silicon tubings (Tygon LMT-55, ID 0.95 mm, Idex Health & Science GmbH, Germany) were interconnected using Y-connectors to plug into the main vacuum line.

4.3.2 Hydrogels

Low gelling agarose (A9414, Sigma-Aldrich, Switzerland) was added to 1x phosphate-buffered saline (PBS) of pH 7.4 (Gibco, Life Technologies, Zug, Switzerland) while stirring. Solutions were heated up until agarose was fully dissolved. Multiple concentrations of agarose in PBS were tested. The final concentrations of the solutions were 0.5% and 1%. The various agarose preparations were autoclaved and liquefied before the loading of MTs by boiling in a microwave. The gelling then occurred after settling the entire chip system at room temperature for 20 min.

Alginate (A0682, Sigma-Aldrich, Switzerland) was mixed with deionized (DI) water to a final concentration of 2.5% and filtered twice with a pressure of 5 bar and a pore size of 0.2 μm to homogenize the mixture and sterilize the solution. Final alginate concentrations of 0.5%, 1.0%, 1.5%, and 2.0% were reached by diluting the 2.5% alginate stock solution with sterile 0.9%

saline solution. A sterile 100 mM solution of $CaCl_2$ (C1016, Sigma-Aldrich, Switzerland) in DI water was pipetted on top of a glass slide, in the approximate shape of the microfluidic structure. The microfluidic structure was then placed on top of the $CaCl_2$ solution onto the substrate to crosslink the alginate solution. After 5 min of crosslinking, the channels and culture chambers were perfused with either PBS or culture medium.

PEGDA (average Mw 700 g mol^{-1}, 455008, Sigma-Aldrich, Switzerland) was mixed with PBS to make a 5% and 10% solution. Photoinitiator I2959 (410896, Sigma-Aldrich, Switzerland) was dissolved in methanol and added to the PEGDA solution to reach a final concentration of 0.01%. A UV lamp (365 nm) was used to polymerize the polymer for 2 min under nitrogen atmosphere. The microfluidic chip was subsequently flushed with PBS to wash out potential cytotoxic species.

Mebiol Gel (Advanced BioMatrix, San Diego, USA) is a synthetic hydrogel called Poly(N-isopropylacrylamide)-polyethylene glycol (PNIPAAm-PEG). It was prepared by following the manufacturer's instructions. PBS (10 mL) was added to the flask containing the dry gel (1 g), and the gel was allowed to dissolve overnight at 4 °C. Gelling occurred after the temperature of the hydrogel was raised to 37 °C for 20 min.

4.3.3 Staining

Staining of the MTs was performed in two ways: i) on-chip staining with low concentrations of fluorophores for real-time visualization of biological processes, and ii) pre-staining off-chip in a well plate to achieve a strong fluorescent signal right from the beginning of the experiment, and to avoid strong background signals in the chip from the stain in solution and in the hydrogel.

Hoechst 33342 (ThermoFisher Scientific, NucBlue Live ReadyProbes Reagent, R37605) was used for nuclear staining of HCT-116 MTs on-chip. Based on the manufacturer's directions, which recommend 1 drop per mL, we lowered the concentration by one order of magnitude for real-time imaging, i.e., 1 drop per 10 mL of culture medium.

Dead staining of hLiMTs and HCT-116 MTs was done by using PT (P4864, Sigma-Aldrich, Switzerland) at a concentration of 1.5 μM, which was demonstrated not to be cytotoxic.[55]

CellTracker Green (CMFDA, C2925, ThermoFisher Scientific, Waltham, USA) was used to stain hLiMTs at a concentration of 12 μM for 45 min in the well plate prior to the experiment.

SiR-actin (Spirochrome AG, Stein am Rhein, Switzerland) staining was used at a concentration of 1 μM for 45 min in the well plate to stain hLiMTs before loading them into the chip. The staining was used at a lower concentration of 100 nM in culture medium for on-chip real-time staining.

4.3.4 Clearing

The solution Scale U2[56] was prepared with a final urea concentration of 4 M (51459, Sigma-Aldrich, Switzerland), 10% (w/v) glycerin (AppliChem BioChemica, St. Louis, USA) and 0.1% (w/v) Triton X-100 (AppliChem BioChemica, St. Louis, USA). The solution was prepared in DI water. Complete clearing of HCT-116 MTs was observed after 24 h of incubation.

4.3.5 Cell Culture

Primary hLiMTs (InSight™ Human Liver Microtissues, MT-02-302-01, monoculture) were obtained from InSphero AG (Schlieren, Switzerland) and kept in a GravityTRAP plate (InSphero AG, Switzerland). Medium was exchanged every other day with hLiMM-TOX (CS-07-001-01, InSphero, Switzerland). The primary human liver cells were obtained from Bioreclamation IVT (Brussels, Belgium). In all instances, consent was obtained from all donors. For ethical and privacy reasons no information was provided which might identify the donor.

HCT-116 colon carcinoma cells induced with eGFP (Sirion, Biotech, Germany) were cultivated in a T25 flask and passaged twice a week, following a standard adherent-cell-culture protocol.

HCT-116 eGFP MTs were formed with cells that underwent a prolonged trypsinization (4 min) to avoid cellular clumps and form equal-size MTs. The cell suspension was diluted to concentrations of 250, 500, and 750 cells per drop and pipetted into the GravityPLUS plate (InSphero AG, Switzerland). MTs were formed in RPMI 1640 medium (Chemie Brunschwig AG, Switzerland), supplemented with 10% fetal FBS (Sigma-Aldrich, Switzerland), 100 IU mL^{-1} penicillin, 100 mg mL^{-1} streptomycin (P/S, Chemie Brunschwig AG, Switzerland) and 0.3 mg mL^{-1} Puromycin for 3 d until being transferred into the GravityTRAP plate (InSphero AG, Switzerland). Medium exchange was performed every 3 days.

4.3.6 Biological assays

The ATP content of the MTs was measured with CellTiter-Glo 3D cell viability assay (Promega, Madison, USA) at the end of the experiments. MTs were harvested from the chip, and the ATP content was measured, following the manufacturer's manual. The success rate for harvesting and transferring the MTs from the chip could be largely improved from 62% to 100% using a small spatula to collect the MTs including the hydrogel drop directly from the chip instead of aspirating the MTs from the hydrogel by using a pipette.

An enzyme linked immunosorbent assay (ELISA) albumin quantification set (Bethyl laboratories, Montgomery, USA) was used for the quantification of albumin in the culture medium of the hLiMTs. Perfused medium was collected from the outlet of the chip for 5 h each day, directly frozen and stored at -80 °C until ELISA measurements were conducted. In the static well plate control, the medium was exchanged and collected every 24 h.

4.3.7 Drug assays

Cytochalasin D (CCD, C2618, Sigma-Aldrich, Switzerland) was used to assess the role of actin microfilaments on the canaliculi structures as well as the dynamics and motility of the cells in the MTs. This drug is well established in stopping actin polymerization and, therefore, obviating actin-related cellular processes.[57] A 100 μM CCD solution was prepared in hLiMM-TOX and perfused through the microfluidic chip at a flow rate of 1 μL min^{-1}.

4.3.8 Image acquisition

Confocal imaging was performed with a Nikon A1 confocal microscope with a motorized xy-stage and operated with the Nikon NIS-Elements software (Nikon, Switzerland). Two objectives were used for 20x and 40x acquisition: Plan Apo VC 20x DIC (NA 0.75, WD 1 mm) and S Plan Fluor ELWD 40x Ph2 (NA 0.60, WD 2.8-3.6 mm). The excitation lasers had the following wavelengths: 403.1 nm (Hoechst stain), 487.5 nm (eGFP and CMFDA stain), and 561.2 nm (PI and SiR-actin stains).

A Leica DMI 6000 B with a motorized xy-stage (Leica Microsystems, Switzerland) was used for the multi-position time-lapse acquisition in combination with YouScope[58] software. The setup consisted of a Leica DFC340FX camera with a 0.70x C-mount. A halogen lamp was used for bright-field images and a mercury arc lamp for fluorescence images (GFP: 470/40 nm excitation wavelength, 500 nm dichroic mirror, 525/50 nm emission filter; Hoechst: 360/40 nm excitation wavelength, 400 nm dichroic mirror, 470/40 nm emission filter; PI: 515-560 nm

excitation wavelength, 580 nm dichroic mirror, LP 590 nm emission filter). We used a 5x/0.12 HCX FL Plan and a 10x/0.30 Ph1 HCX PL Floutar objective.

A Nikon Ti-E inverted microscope with a motorized xy-stage was used for bright-field imaging using a Hamamatsu ORCA Flash 4.0 camera with a 4x Plan Apo λ and a 10x Ph1 Plan Fluor objective. The light source for bright-field images was a CoolLED pE-100 (CoolLED Ltd., Andover, UK).

All microscopes were equipped with an environmental box (The Box, Life imaging services, Basel, Switzerland) that was connected to a temperature regulator system (The Cube, Life imaging services, Basel, Switzerland) that was set to 37 °C. A stage-top incubator was connected to a CO_2 and humidity regulator (The Brick, Life imaging services, Basel, Switzerland) and was set to 95% humidity and 5% CO_2 with 10 L h^{-1} air flow during imaging.

4.3.9 Image Analysis

Images were analyzed using ImageJ[59] and plug-ins for the import of confocal data from the Nikon software.[60] All pictures underwent linear modification of brightness and contrast, and were homogeneously treated for a set of measurements. A macro for ImageJ was used to facilitate the analysis of the time-lapse images of multiple positions. The macro can be found on GitHub.[61]

4.3.10 Statistical analysis

Albumin secretion of MTs was measured using two replicates for all individual conditions. These values were averaged prior to any further analysis. The albumin secretion in the perfused chips was measured on three chips. No significant difference was observed between the different perfused experiments. As the media were sampled from an entire chip, the measured albumin concentration constituted an average secretion value of six MTs. The albumin secretion under static conditions was measured from eight individual MTs. Two-way ANOVA was used for statistical analysis with a significance level of 0.01.

The ATP values were measured from single MTs that have been harvested from four individual chips, except for Mebiol Gel, where only two chips were utilized. Control MTs from the same batch were kept in well-plates and measured simultaneously with the experimental MTs. At least three MTs were used to obtain the control values. The average ATP content of the control was then calculated, and each ATP value of the MTs in hydrogel was consecutively normalized with respect to the average control value. The results of different sets of experiments for a given

hydrogel did not significantly differ. For this reason, the average ATP was calculated over all MTs for a certain hydrogel condition. One-way ANOVA with a significance level of 0.01 was used for statistical analysis.

Origin Pro 2017 was used to calculate the average and the standard deviation and to perform statistical analysis as well as to plot the data. The graphics of this paper were prepared with Adobe Illustrator CC.

4.4 Results and Discussion

4.4.1 Operation of the microfluidic system

The microfluidic hydrogel hanging-drop chip (Figure 1) is made out of a patterned polydimethylsiloxane (PDMS) layer that is placed on a microscope slide. The chip contains cylindrical culture chambers with a diameter of 3 mm and a pitch of 4.5 mm, which is identical to the standard 384-well plate format. The chambers are interconnected with small microfluidic channels to enable the perfusion of medium, staining solutions, or drugs. The chip was designed as a simple 1-by-6 arrangement (Figure 1a,b) and in an array format of 4-by-6 culturing chambers (Figure 1c) for higher throughput and multiplexed experiments. The system design and chamber arrangement is flexible so that the layout can be extended to realize even larger arrays.

Circular rim structures with a diameter of 2 mm are located at the ceiling of each culture chamber to define the position of the hydrogel drop. The medium is then perfused underneath the hanging hydrogel drops as soon as those have been solidified and the MTs have settled to the bottom of the hanging drops (Figure 1a). One common inlet can be used to simultaneously perfuse medium through all four lines of the 4-by-6 hydrogel hanging drop array. Each line can also be accessed through an individual inlet, which allows the perfusion of different media in the lines in parallel.

The microfluidic PDMS part is reversibly attached to a microscope glass slide using a vacuum channel that is integrated in the PDMS and surrounds the fluidic network. The vacuum ensures a tight seal between PDMS and glass during the entire experiment. At the same time, the vacuum enables a removal of potentially occurring air bubbles from the microfluidic channels through the porous PDMS, which ensures stable operation of the device (Figure S1a, Supporting Information). The reversible bonding allows for an easy loading of the chip at the beginning as well as for access to the MTs at the end of the experiment. The chips are operated

by one or more fluidic pumps and a vacuum connection, which reduces the complexity of the experimental setup to a minimum.

The initial filling of the 4-by-6 microfluidic chip and a medium exchange are shown in Figure S1b and in Movie S2 (Supporting Information), respectively. Complete filling of the 4-by-6 microfluidic chip was achieved by an optimized channel design of the inlet and outlet channels.[62] The inlet channel splits symmetrically up into two and finally four channels. Capillary stop valves on the outlet side stop the liquid until an equal filling of the channels across the chip occurred (Figure S1b, Supporting Information). The chip can be either placed on a microscope or operated in a regular incubator.

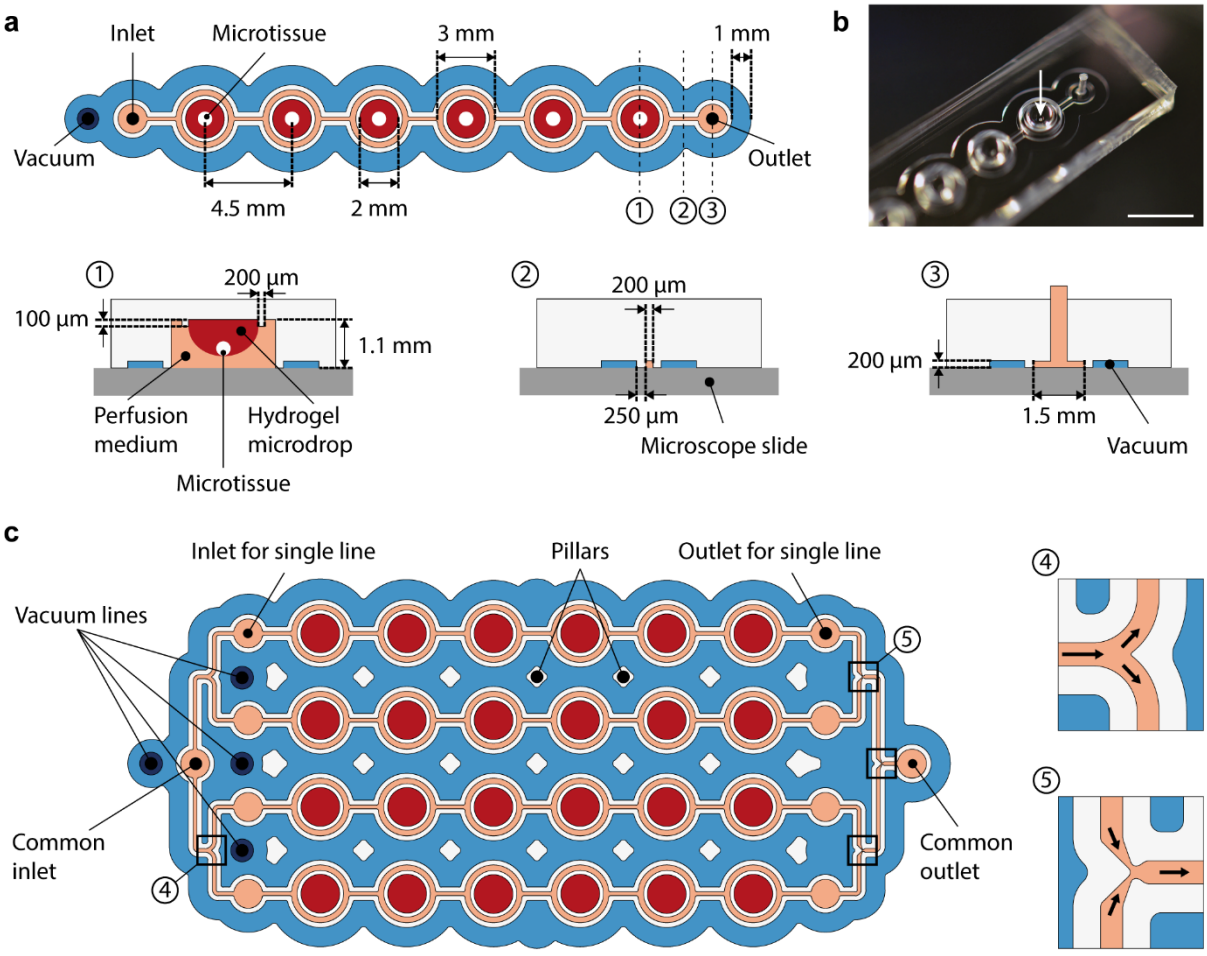

Figure 1 Schematic description of the microfluidic system. (**a**) Design of the 1-by-6 hydrogel hanging drop chip with one inlet and one outlet. Inset (1) shows the cross section of a culture chamber surrounded by a vacuum channel (blue), the culture medium (orange), the solid hydrogel (red) and the MT (white). Inset (2) shows the cross section of a micro-channel, and inset (3) the cross section of an in-/outlet. (**b**) Picture of the chip (scale bar = 5 mm). The wells are filled with hydrogel and glass beads (white arrow) to indicate the positions of the MTs. (**c**) Design of a 4-by-6 array. Pillar-like structures were added to reduce sagging of the PDMS due

to the vacuum. Inset (4) depicts the separation of the microchannels at the inlet and inset (5) shows the structures at the outlet, which enable complete and bubble-free filling of the chip.

4.4.2 Positioning of microtissues in hanging hydrogel drops

The loading of the chip is schematically shown in Figure 2a. A small volume of 2.5 μL liquid agarose, alginate, Mebiol Gel or poly(ethylene glycol) diacrylate (PEGDA) hydrogel is filled into the inner rim of each culture chamber using a 10 μL pipette tip. Then, a MT is aspirated with 10 μL medium from a GravityTRAP plate (InSphero, Schlieren, Switzerland) using a 200 μL pipette tip and left to sediment to the liquid-air interface of the pipette tip. Once the MT sedimented, the pipette tip is brought into contact with the hydrogel surface to transfer the MT into the liquid hydrogel drop without piston activation. The chip is then turned over and placed onto the microscope slide. Subsequently, the MT sediments to the liquid-air interface at the bottom of the liquid hydrogel hanging drop, and the hydrogel solidifies. Through this process, the MT is automatically located at the bottom center of the hanging drop before the hydrogel solidifies and immobilizes the MT. Alternatively, hydrogels with low viscosity, such as agarose, can also be premixed with MTs in the wells of a GravityTRAP plate and directly transferred to the chip using a 200 μL pipette tip. Hydrogel and MT are then loaded together. For both methods, the loading procedure only includes simple pipetting steps guided by the integrated ring structures that indicate the droplet positions on the chip. Once the MTs are loaded and immobilized, the chip is connected to tubing and can be perfused with culture medium. Flow rates of 200 μL min^{-1} (Movie S3, Supporting Information) down to 1 μL min^{-1} (Movie S4, Supporting Information**)** can be applied. The microfluidic chip was tested for flow rates up to 1 mL min^{-1} without observing any leakage.

This novel concept of using hanging hydrogel drops meets multiple requirements of time-lapse confocal imaging: i) the method reliably and precisely places the MT at the bottom-center of the drop so that the position is well defined and can be quickly localized at the start of the experiment; ii) it ensures spatiotemporal stability of the MT to avoid the use of a time-consuming autofocus; iii) it enables high-quality time-lapse image acquisition due to the stable immobilization of the MT; iv) the MT is located close to the objective for the use of high-magnification objectives with low working distances; and v) the method ensures MT viability and functionality due to constant nutrients supply and removal of waste products of the entire MT through the hydrogel, which enables diffusion.

We tested the loading procedure with various types of hydrogels, differing in their type of solidification. Two temperature-driven gels were used: Mebiol Gel and agarose. Mebiol Gel is liquid at 15 °C and solid at 37 °C. Low gelling temperature agarose solutions show a hysteresis behavior, melting at 65 °C and remaining liquid upon cooling down to 28 °C. This feature enables to load the MTs in liquid hydrogels at 37 °C and, after a short cooling step, to cultivate them at 37 °C in the solidified gel. The PEGDA solution was cross-linked using a photoinitiator and ultraviolet (UV) light. Finally, alginate, a commonly used hydrogel for cell encapsulation,[63] was solidified through the use of a $CaCl_2$ solution. The chip was loaded with alginate, and MTs were loaded into the liquid drops. The chip was then placed in the salt solution for 5 min to allow for crosslinking of the hydrogel.

First, we assessed the position of the MTs in x-y direction in the drop for all hydrogel types after loading (Figure 2b). A reliable and precise positioning of the MTs in the chip is beneficial for setting up an experiment on a microscope. The position of the first MT needs to be defined, and the positions of the remaining MTs can then be found according to the coordinates of a typical 384-well plate matrix format. The MTs turned out to be well centered in the droplet upon using 0.5% agarose (x-standard deviation = 47 μm / y-standard deviation = 39 μm), 1.0% agarose (24 μm / 35 μm), Mebiol Gel (48 μm / 56 μm), 5% PEGDA (39 μm / 100 μm) and 10% PEGDA (41 μm / 63 μm). In alginate, the MT positions were more scattered due to the solidification process, for which the alginate drops were dipped in $CaCl_2$ solution. This led to a flattening of the alginate droplets.

Second, we measured the focal plane and position stability of six MTs cultured over 9 days in 0.5% agarose. Figure 2c shows that the position of the individual MTs was very stable over time. Further, we measured the positions of the MTs in other hydrogels at the beginning and the end of experiments that lasted for at least 41 h (Figure 2d). For Mebiol Gel and alginate, a somewhat larger position change occurred during the first 2 h after loading, while the positions remained very stable from 6 h postloading on (Figure S5, Supporting Information). Overall, agarose, Mebiol Gel and alginate hydrogels featured little position variation over time, which renders them highly suitable for imaging without the need of an autofocus system, once the focus has been manually set (Figure S5, Supporting Information). The temporal stability of PEGDA gels could not be assessed with functional MTs due to the low viability of the MTs upon culturing in this type of hydrogel.

In summary, Mebiol Gel, PEGDA, and agarose showed the best results with respect to reliable and stable positioning of the MTs in x,y-direction in the drop. Alginate yielded higher variations in the MT position within the drop. In the z-direction, especially Mebiol Gel, but also agarose yielded good results with MTs being placed very close to the surface of the microscope slide. In the case of agarose, we observed more variation, which may be due to the direct loading of microtissues in only 2.5 µL hydrogel using a relatively large 200 µL pipette tip. This large tip opening entails decreased precision of the manually transferred comparably small volume, but is necessary to allow gentle pickup of the relatively large MT.

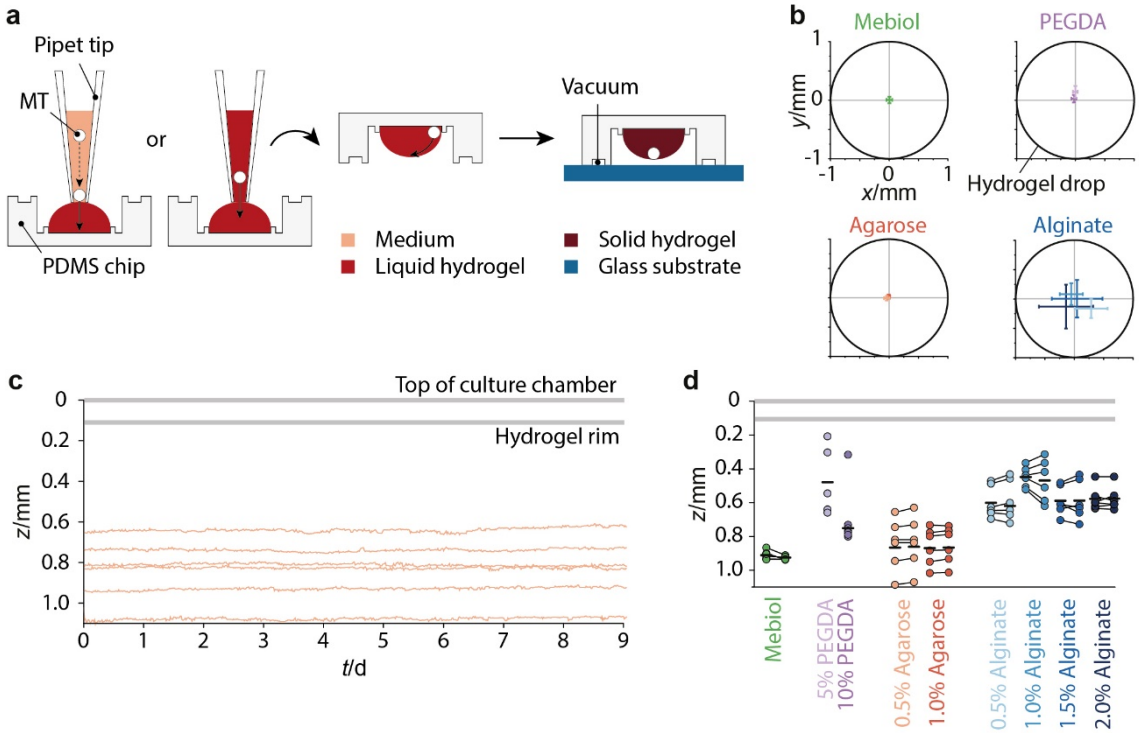

Figure 2 Chip loading, positioning of microtissues, and stability of the hydrogel. (**a**) Procedure used for the loading of microtissues into the chip. (**b**) Placement of the microtissues in x-y direction in the hydrogel drop after loading (Mebiol Gel n=6; PEGDA n=6; 0.5 and 1.0% agarose n=6; 0.5 and 1.0% alginate n=5; 1.5 and 2.0% alginate n=6, mean ± standard deviations). (**c**) Evolution over time of the focus height of six microtissues placed in 0.5% agarose. (**d**) Summary of the data in panel (**c**) and Figure S5 (Supporting Information) displaying only the point at the beginning of the experiment (left starting point) and the point at the end (right end point). Two linked points represent the data of one MT. Experiment duration was 41 h for Mebiol Gel, 216 h for 0.5% agarose, 42 h for 1% agarose and 69.5 h for alginate.

4.4.3 Microtissue viability and functionality

Preserved functionality and viability of the MTs in the device is key for biological applications. We used primary human liver MTs as a sensitive model system and cultured the MTs over several days while the culture medium coming out of the system was sampled. The samples were used to determine the secretion rate of albumin of the tissues (Figure 3a). Albumin is a widely known liver-specific functional marker.[64] Liver microtissues that were cultured in agarose hanging drops secreted on average 40-55 ng $MT^{-1}day^{-1}$ of albumin under perfused conditions. Similar secretion rates were measured in the static control sample. Overall, the tissues remained highly functional over more than 9 days. Their morphology concords with those results, as the tissues showed smooth edges and a compact appearance (Figure S6a, Supporting Information**)**. At the end of the experiment, the MTs were individually removed from the chips, and the relative adenosine triphosphate (ATP) content was measured to further assess their viability. Figure 3b presents the ATP values relative to the static control sample, cultured in parallel in a well plate. Liver MTs did not show any significant difference in their ATP content in agarose and alginate hydrogels. MTs that were immobilized in Mebiol Gel showed significantly reduced viability. The viability of MTs in PEGDA was not quantified but assessed with a propidium iodide (PI) staining (Figure S6b, Supporting Information). Their tattered morphology and the high PI signal indicated a very low viability.

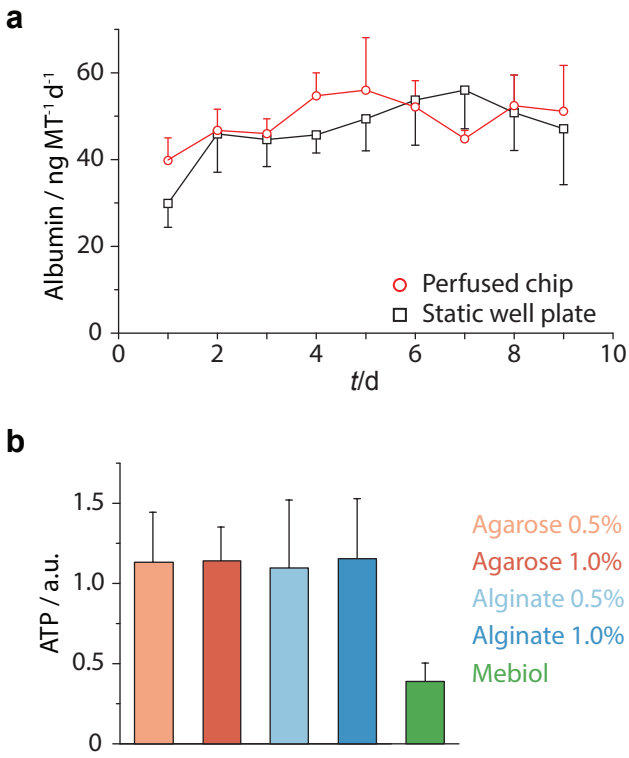

Figure 3 Functionality and viability measurements of hLiMTs. (**a**) Albumin production per MT and per day. MTs were cultivated over 9 d in the perfused hydrogel chip (red, n=3 chips with 6 MTs each, mean ± standard deviations) and in a static well plate (black, n=8 MTs, mean ± standard deviations). The culture medium was sampled every day for albumin quantification. (**b**) The relative ATP content of the hLiMTs was measured to determine their viability in different hydrogels in comparison to the static control (agarose 0.5% n=20; agarose 1.0% n=20; alginate 0.5% n=16; alginate 1.0% n=17; Mebiol Gel n=5, mean ± standard deviations). Data bars represent means ± standard deviations.

4.4.4 Imaging quality of the chip

Imaging quality of MTs in the microfluidic chips is commonly reduced by trapping or well structures, which introduce artefacts and shadowing effects. Images of MTs in agarose were found to be clear and undisturbed (Figure 4a). Slight artifacts were observed in alginate, whereas Mebiol Gel showed even larger artefacts and significant background fluorescence (Figure S7, Supporting Information). This background fluorescence and the reduced viability of MTs in Mebiol Gel and PEGDA was the reason why we discontinued doing experiments with those two hydrogels. Alginate was eliminated for subsequent experiments because of the less precise x-y placement and position of the MT (Figure 2b). The results reported on below were, therefore, achieved with agarose.

Figure 4a shows a clear, artifact-free bright-field image of a HCT-116 MT that was taken with a 5x objective in an agarose hydrogel hanging-drop on an inverted microscope. The right-hand side picture shows the same microtissue with a 10x objective. The hydrogel is nearly invisible, since its refractive index (n=1.34)[65] is similar to that of the culture medium (n=1.338)[66] and water (n=1.328).[67] MTs could be imaged with objectives up to 40x in this device. Objectives with working distances (WD) of 1 mm were commonly used for these experiments. However, one could also image the tissues using objectives of 500 µm WD.

Confocal imaging of MTs is classically performed under static conditions at a single time point. Conjoint continuous and long-term imaging and culturing of MTs in microfluidic chips is of great interest to reveal details of the cellular structures and superstructures, and to track dynamic changes upon drug perfusion over longer periods of time. Exposing non-immobilized MTs to flow induces movements, which make the acquisition of image stacks and time-lapse imaging impossible. Moreover, large distances between the sample and the substrate may obviate the use of high-magnification objectives. Our system overcomes these limitations. Figure 4b shows confocal imaging of liver MTs within our microfluidic platform with an extralong working distance (ELWD) 40x air objective. The picture displays the maximal intensity projection of 3 slices of a human liver MT located between 12 µm and 30 µm depth. The bile canaliculi, stained with CellTracker green 5-chloromethylfluorescein diacetate (CMFDA), are clearly visible within the MT. A zoom-in shows the resolution of single canaliculi. Canaliculi are intercellular structures, formed by hepatocytes. Their small diameter (≈1 µm[68]) makes it usually difficult to image them under perfusion conditions in a microfluidic chip environment. Here, the hydrogel immobilizes the tissue so that even such small structures within the MT can be visualized under continuous flow and varying flow conditions.

Studying dynamic processes in the microtissues requires time-lapse imaging. Figure 4c shows a confocal time-lapse series of a HCT-116 MT embedded in hydrogel in the chip. The MT expresses enhanced green fluorescent protein (eGFP) and was additionally perfused with a low concentration of PI in order to visualize the dead cells. The immobilization of MTs in the hydrogel permitted tracking of single cells and dynamic cellular processes. For instance, we present an example of cell death in real time (Figure 4c, white arrow). In the first hour, one can observe a cell with a globular morphology, a strong eGFP signal and no PI signal. After two hours, the PI signal increases around the cell and after four hours, the entire eGFP signal disappears. Because of the presence of PI, we can deduce that the cell underwent cell death.

However, as this marker is present in both, necrotic and apoptotic cells,[69] it is not possible to distinguish between the two situations.

Multi-channel, multi-position imaging on a confocal microscope was realized using the 4-by-6 chamber design, in which we loaded eGFP-induced HCT-116 MTs and stained them with Hoechst and PI on the chip. Three different sizes of MTs were loaded into specific culture chambers (750, 500, and 250 cells MT^{-1}, initial cell count for MT formation). Figure 4d shows a stitched image of all MT positions, where each MT is represented by the maximal projection of the z-stack acquired over the lower half of the MT. This image shows that the chip enables confocal imaging of a larger array of MTs in the same microfluidic setup. Different MTs can be placed into specific culturing chambers, here we used MTs of different sizes. The confocal microscope setup allowed to achieve an interval of 30 min for imaging through all 24 positions while acquiring a z-stack over the entire MT (267 μm in total, 7.5 μm steps) and doing image acquisition in 3 channels. In order to achieve faster scanning rates to visualize rapid cellular processes in multiple MTs in parallel, this system is compatible with spinning-disc confocal microscope setups.

Tissue clearing is a process that enables the imaging of structures deeper in the tissue. In normal tissue, light scattering occurs at all refractive-index boundaries. Clearing solution helps to match the index of the inside of a cell with its surrounding, so that less incoherent light scattering occurs. Clearing solutions, such as Scale U2,[56] are highly viscous and, therefore, require high pressure to be driven through a microfluidic network, which may lead to system failure. Scale U2 was perfused through our device. Figure 4e,f shows an HCT-116 MT before and after the clearing treatment. The penetration depth of light was dramatically increased, which enabled the observation of the hypoxic, low nutrient inner region of the MT: the necrotic core. Imaging of this region is of great relevance for the development of cancer drugs, as it is often resistant to the common therapies. Drug testing often take place on highly proliferative cells, placed in high nutrient and high oxygen environment which completely exclude the less proliferative cells from analysis.[70] During the clearing procedure, the diameter of the MTs increased on average 1.38 fold, as previously shown,[56] from an average of 439 μm to 607 μm.

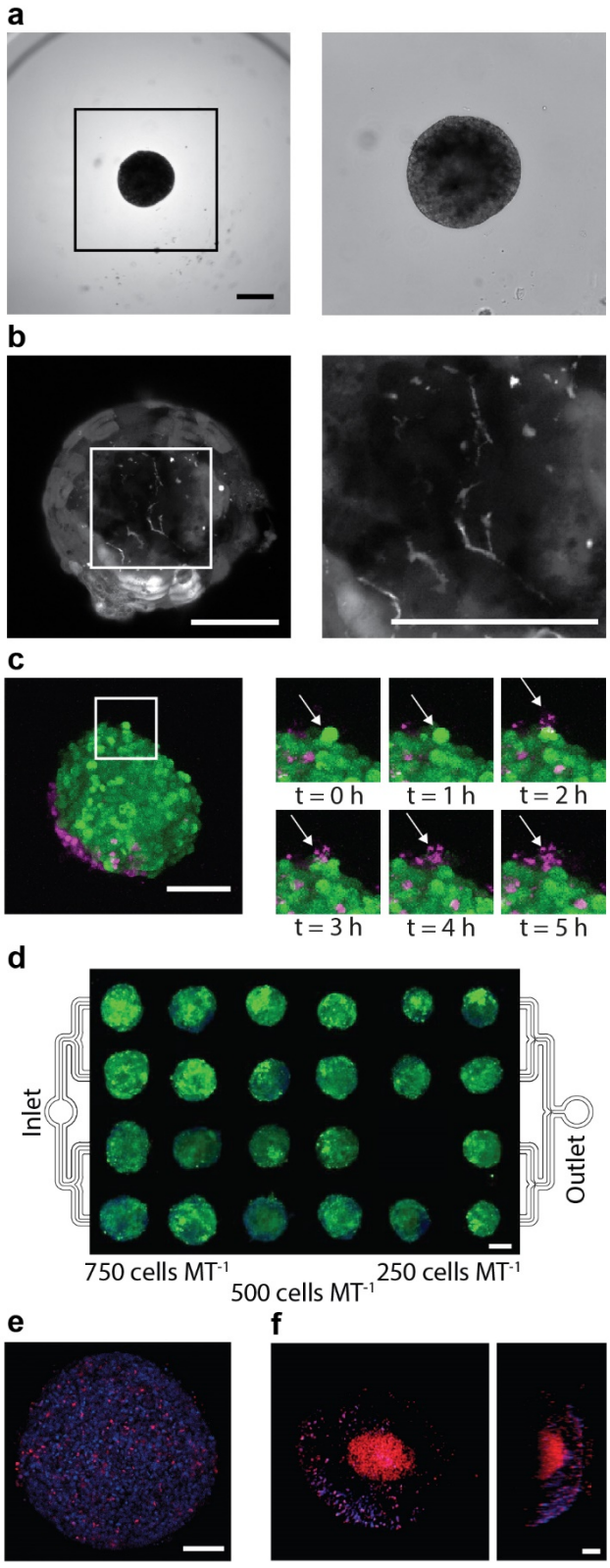

Figure 4 Imaging performance with the microfluidic hydrogel hanging drop chip. (**a**) A wide-field image of a HCT-116 MT in 1.0% agarose is shown using a 5x objective. The picture on the right-hand side shows the same MT with a 10x objective. (**b**) Confocal imaging of a hLiMT stained with CMFDA CellTracker Green reveals bile canaliculi between the hepatocytes. The

right-hand side shows a zoom-in of the same picture. (**c**) Time-lapse confocal imaging. A HCT-116 MT expressing eGFP (green) was stained with PI (purple) and imaged over time. The right-hand side shows a time-lapse of the top part of the MT. The course of apoptosis of one cell can be observed over 5 h. (**d**) Confocal images (maximal projection of z-stack of the lower half of the MT) of 23 tissues loaded into the 4-by-6-droplet design. Images show overlays of GFP, Hoechst nuclear stain, and PI dead stain. The system allows for imaging of several MTs in the same setup. A full-resolution picture is available in Figure S8 (Supporting Information). Confocal images (**e**) before and (**f**) after clearing. A HCT-116 MT was stained with PI and Hoechst. After clearing with Scale U2, also the center of the MT becomes clearly visible showing the necrotic core. Scale bars = 100 μm.

A brief summary of all tested hydrogels and their respective advantages and disadvantages is given in Table 1. We tested four different ways of solidifying the hydrogels: temperature (increase and decrease), UV, and $CaCl_2$ crosslinking. We observed reduced viability of human liver microtissues (hLiMTs) in Mebiol Gel and a very low viability in PEGDA, whereas MTs were perfectly viable in agarose and alginate. MTs could be encapsulated in all types of hydrogels, but the positioning at the droplet bottom center was most precise in agarose and Mebiol Gel. Imaging was possible with all types of hydrogels. However, the clearest images were taken with agarose, while Mebiol Gel and alginate showed artifacts. The imaging properties were not investigated in detail with PEGDA due to the low viability of MTs in this hydrogel. Overall, the results show that the presented platform and method is compatible with most types of hydrogels, while the best results were achieved for using agarose.

Table 1 Characteristics of the different hydrogels

	Mebiol Gel	PEGDA	Agarose	Alginate
Polymerizing type	Temperature	UV	Temperature	$CaCl_2$
Used concentrations	10%	5%, 10%	0.5, 1.0%	0.5, 1.0, 1.5, 2.0%
Positioning in x-y	+++	+++	+++	–
Positioning in z	+++	+	+++	+
Stability of z over time	++	not assessed	++	+
Hydrogel handling	++	+	++	++
Imaging characteristics	–	++	+++	++
Viability of MTs	–	– – –	+++	+++

4.4.5 Imaging the effect of cytochalasin D in liver microtissues

Cytochalasin D (CCD) is a toxin obviating the polymerization of actin, which strongly affects the dynamics and morphology of cells. So far, CCD effects on MTs were only imaged at discrete time points before and after drug exposure,[71] which does not provide any information on drug kinetics, or responses and dynamics of the cells. Real-time observation requires a dedicated setup that is compatible with high-resolution time-lapse confocal imaging. We stained hLiMTs with CMFDA in a well plate and introduced them in two 1-by-6 single-lane chips using 0.5% agarose. Both chips were filled with human liver maintenance medium TOX (hLiMM-TOX) medium (InSphero AG, Schlieren, Switzerland) and SiR-actin staining solution. After complete filling of the chip, the medium of one of the chips was exchanged for a solution containing CCD. A z-stack of the lower half of the MT was taken every 15 min.

The effect of CCD on hLiMTs is shown in Figure 5. We observed three major changes: i) a change of the morphology of the bile canaliculi, ii) a significant decrease in the motility of the hepatocytes, and iii) a swelling of the entire hLiMT (Movie S9, Supporting Information). Figure 5a shows a time-lapse imaging of two canaliculi with and without addition of CCD over 45 min. The images show the reported effects of this compound,[72] namely, that the morphology of the canaliculi, visualized by the stain CMFDA, changed from a filamentous to a saccular shape. The images nicely demonstrate the need to immobilize the MTs for imaging small structures that are 40 μm long and 1 μm thin and need to be imaged and tracked over time within a 300 μm large MT.

Figure 5b shows the morphological changes of the hLiMTs over 10 h. Two effects could be observed and confirmed: the increase of the SiR-actin staining,[73,74] and the increase of MT size.[75–78] Pictures at t = 10 h of higher resolution are shown in Figure S10 (Supporting Information). Additionally, dynamic changes could be measured using our platform (Movie S9, Supporting Information) during the exposure to CCD. The movie shows a total arrest of inter-cellular movements shortly after the exposition to CCD, due to a complete blockage of actin polymerization. This effect is observable 1 h and 30 min after the start of the perfusion. The examples in Figure 5 show how the developed platform enables to resolve dynamic cellular processes through confocal, time-lapse imaging of location-stabilized microtissues.

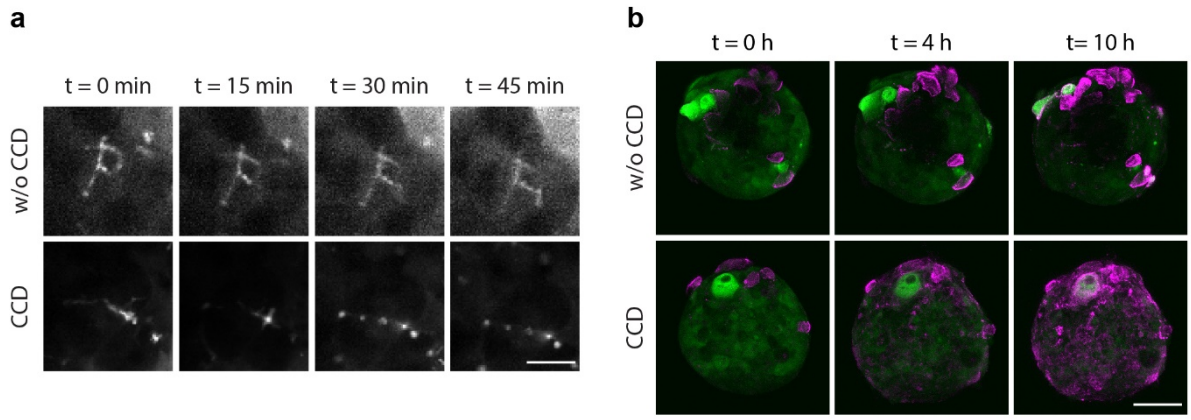

Figure 5 Effects of cytochalasin D (CCD) on primary human liver MTs detected by confocal imaging. (**a**) CellTracker Green CMFDA dye was used to visualize the canaliculi of the MT. The top shows the control MT, where the morphology of the canaliculi remained unchanged. CCD induced a change of the filamentous structure of the canaliculi into a string-of-pearls-like structure. Scale bar = 20 μm. (**b**) The effect of cytochalasin D on the entire MT visualized by CMFDA (green) and SiR-actin (purple). The upper series of images shows the control MT, where the purple stain becomes brighter in all dead cells of the MT. MTs that were treated with CCD show a much stronger increase of SiR-actin signal over time. A picture with higher resolution is available in Figure S10 (Supporting Information). Furthermore, the cells within the tissue stop moving on infusion of the drug (see Movie S9, Supporting Information). Scale bar = 100 μm.

4.5 Conclusion

We presented a robust microfluidic chip, engineered for the culturing of MTs in a perfused and controlled hydrogel environment. Single microtissues were immobilized in hanging hydrogel drops, which enabled their reliable, precise, and stable placement in a perfused culturing chamber. The system is very versatile, as different types of microtissues and hydrogels can be used. The transparent nature of the hydrogels provides excellent microscopy conditions. Compared to existing systems, there is no need of additional trapping structures, which then may interfere with the MTs and the imaging.

Experiments can be run in parallel with different perfusion conditions and drug exposure protocols, either by using several 1-by-6 chips in parallel or by using the 4-by-6 array chip. Setting up experiments is fast and simple, 3D microtissues are straightforward to handle, and many MT types are commercially available in the meantime.

We showed culturing and continuous imaging of 3D microtissues for more than nine days, we continuously collected medium samples at the system outlet for further analysis and harvested the MTs at the end of the experiment for endpoint analysis. Furthermore, the developed system was used to monitor biological processes at different spatiotemporal scales using a wide range of microscopy configurations including bright-field, fluorescence, and confocal microscopy. The microfluidic device enabled studying 3D microtissues at cellular and even subcellular level in real-time and was used to assess effects of compounds, while the cells were kept in a representative 3D microenvironment. The culturing environment can be adapted to closely reproduce *in vivo* conditions of various cell types and scenarios, ranging from healthy primary cells to diseased cancer microtissues, which opens up a large range of biological applications. The individually accessible and fluidically interconnected culture chambers allow for culturing different types of microtissues in multi-tissue arrangements.

4.6 Acknowledgements

E.A.A. and P.M.M. contributed equally to this work. Financial support of the Swiss National Science Foundation (SNF project 2-77079-16 “Infected body on a chip”) and the Swiss Commission for Technology and innovation (CTI project 18024.1 PFLS-LS “Microfluidic two-tissue platform for combined drug efficacy and toxicity testing”) is acknowledged. We would like to thank Christian Lohasz for his support during the albumin ELISA, Philipp Koch (Bioprocess Laboratory, D-BSSE, ETHZ) for providing the alginate hydrogel and Jonas Fürstenberger (I-Math, UZH) for his recommendations regarding the statistical analysis. Additionally, we would like to thank Kasper Renggli for his scientific advice regarding the use of PEGDA, and his input for the introduction of this paper. We also thank the Single Cell Facility at D-BSSE, ETH Zurich for microscopy assistance. Furthermore, we would like to thank Spirochrome AG Switzerland for providing the SiR-actin stain and we acknowledge InSphero AG, Schlieren, Switzerland for providing primary human liver microtissues and cell culture medium.

4.7 Supporting Information

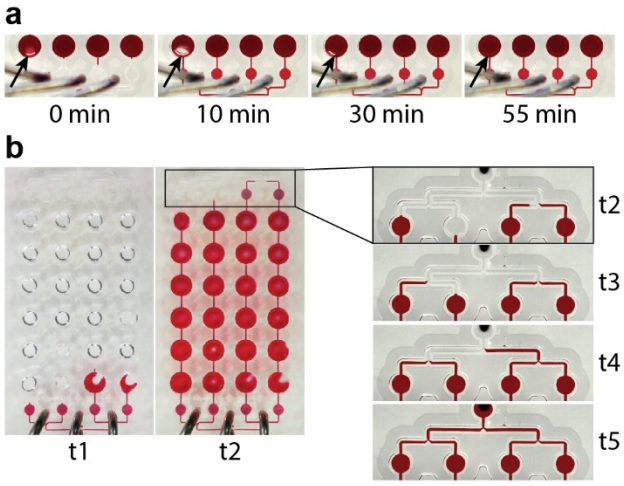

Figure S1 Microfluidics of the chip. (**a**) Removal of an air bubble (arrow), which was trapped in the first culturing chamber during the filling of the chip. Despite its large size, the bubble was removed after 55 min. (**b**) Filling of the chip, using an array of 4 lines in parallel. At the time point t2, the chip was filled homogeneously. The insets from time t2 on show a close-ups of the stop valves placed at the outlet side.

Movie S2 Movie of a 4-by-6 chip, loaded with 0.5% agarose droplets that was initially filled with amaranth food dye. The proper filling of the channels is clearly visible. Once filled, the liquid was exchanged with DI water, and the stain that was also present in the hydrogel droplets was slowly removed through diffusion. The chip was perfused at a flow rate of 30 µL min^{-1}, and pictures were taken at an interval of 12.5 sec.

Movie S3 Movie of a 1-by-6 chip, loaded with 0.5% agarose droplets, being perfused with amaranth food dye, followed by perfusion of DI water. The agarose droplets take up the dye, which is still visible when water is perfused through the channels and culture chambers. The coloration of the agarose droplets fades out over time. The chip was perfused at a flow rate of 200 µL min^{-1}, pictures were taken at an interval of 5 sec for a total of 14 min.

Movie S4 Movie of a 1-by-6 chip, loaded with 0.5% agarose droplets. The perfusion rate was 1 µL min^{-1}, which is a typical flow rate used for biological experiments. The diffusion rate of the food dye out of the agarose droplets is comparable to the exchange rate of the DI water and the remaining food dye in the microfluidic chip. Pictures were taken at an interval of 20 sec for a total of 54 min and 40 sec.

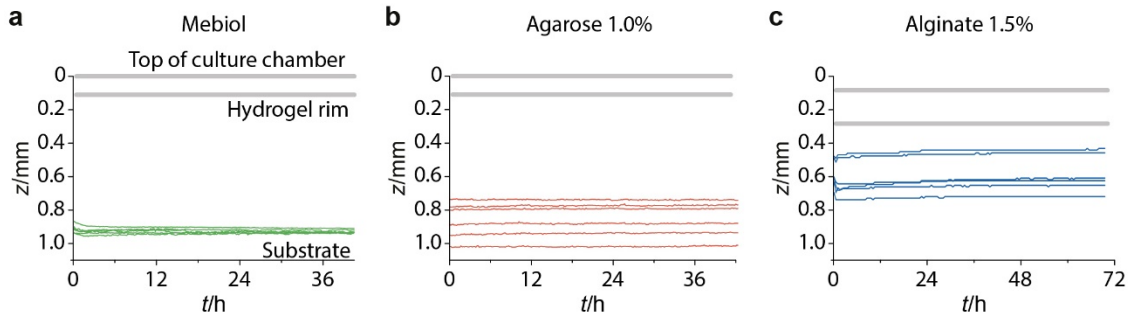

Figure S5 The focal plane of six MTs in different hydrogels measured over 2-3 days. (**a**) Mebiol (**b**) Agarose 1.0% and **c**) Alginate 1.5%.

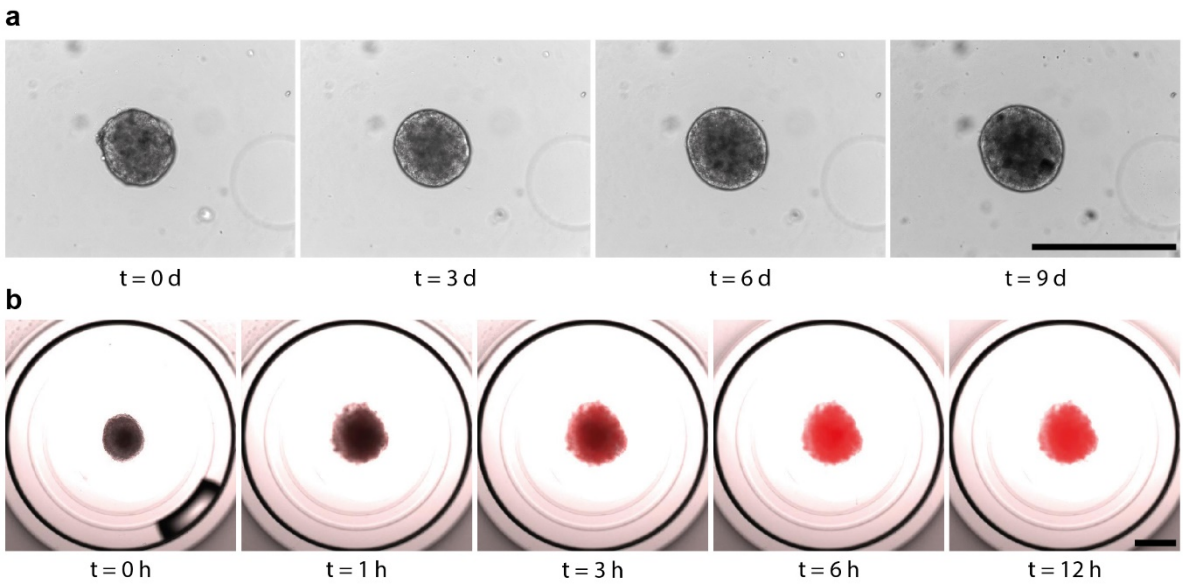

Figure S6 Images and morphology of MTs in various hydrogels. (**a**) 10X images of one hLiMT immobilized in an agarose hanging drop. The edges of the MT remained smooth over 9 days of culture in the microfluidic chip, which demonstrates the viability of the MT under these conditions. (**b**) Time-lapse imaging of one HCT-116 MT in PEGDA over 12 h with a 4X objective. PI dead stain was perfused through the chip. The rapid increase of the PI signal and the fuzzy edges of the MT indicate a very limited viability of the MT over time. Scale bars = 500 μm.

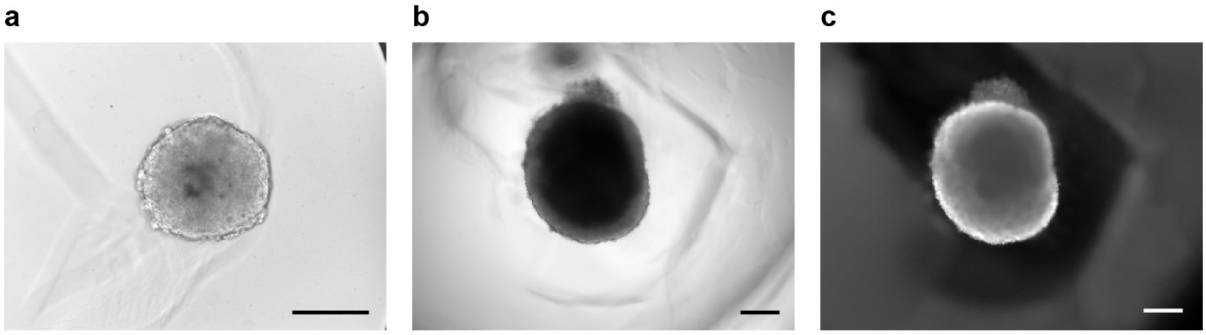

Figure S7 Artefacts caused by Mebiol and alginate hydrogels. (**a**) Bright-field image of a HCT-116 MT in alginate. Some shadows are present around the microtissue, but no background fluorescence was observed. (**b**) Bright-field image and (**c**) fluorescence image of Hoechst of a 14-day old HCT-116 microtissue after 8h of culturing in Mebiol. Shadows can be observed in the bright-field image, and background fluorescence is visible in the Hoechst image. Scale bar = 200 μm.

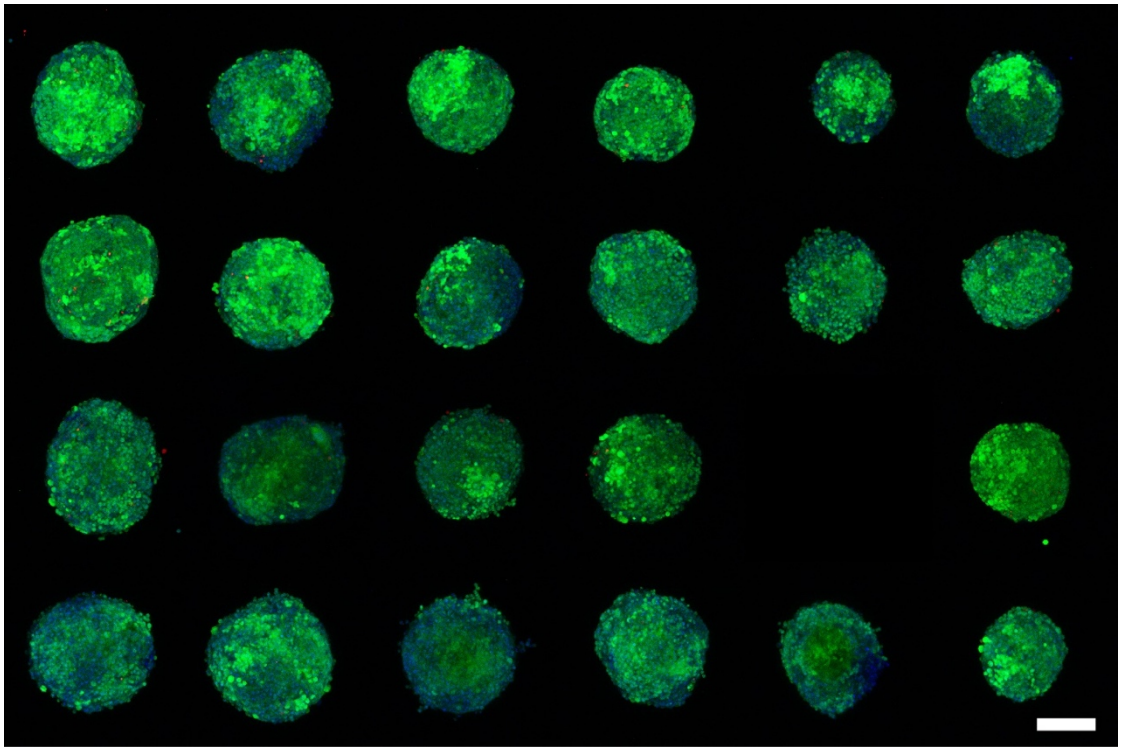

Figure S8 Stitched image of all 24 position of a 4-by-6 chip at full resolution. Every position is a maximal projection of the acquired z-stacks. The first two columns were loaded with large MTs (750 cells MT^{-1}), the two center columns were loaded with average-size MTs (500 cells MT^{-1}) and the two right columns were loaded with small MTs (250 cells MT^{-1}). The number of cells per MT was determined at the time point of seeding. Scale bar = 100 μm.

Movie S9 Confocal time-lapse movie of 2 hLiMTs in agarose 0.5% that were imaged over 10 h. Both tissues were stained with CMFDA (green) and SiR-actin (purple). The hLiMT on the left-hand side was the control, while the one on the right-hand side was perfused with CCD. After 1h 30 min of perfusion, we can see a decreased motility of the cells of the right MT. After 3h, the actin signal started to increase in the entire tissue. During this time, the cells continued to move in the control sample, and the actin signal did not change. The flow rates in both chips were 1 µL/min, pictures were taken every 15 min.

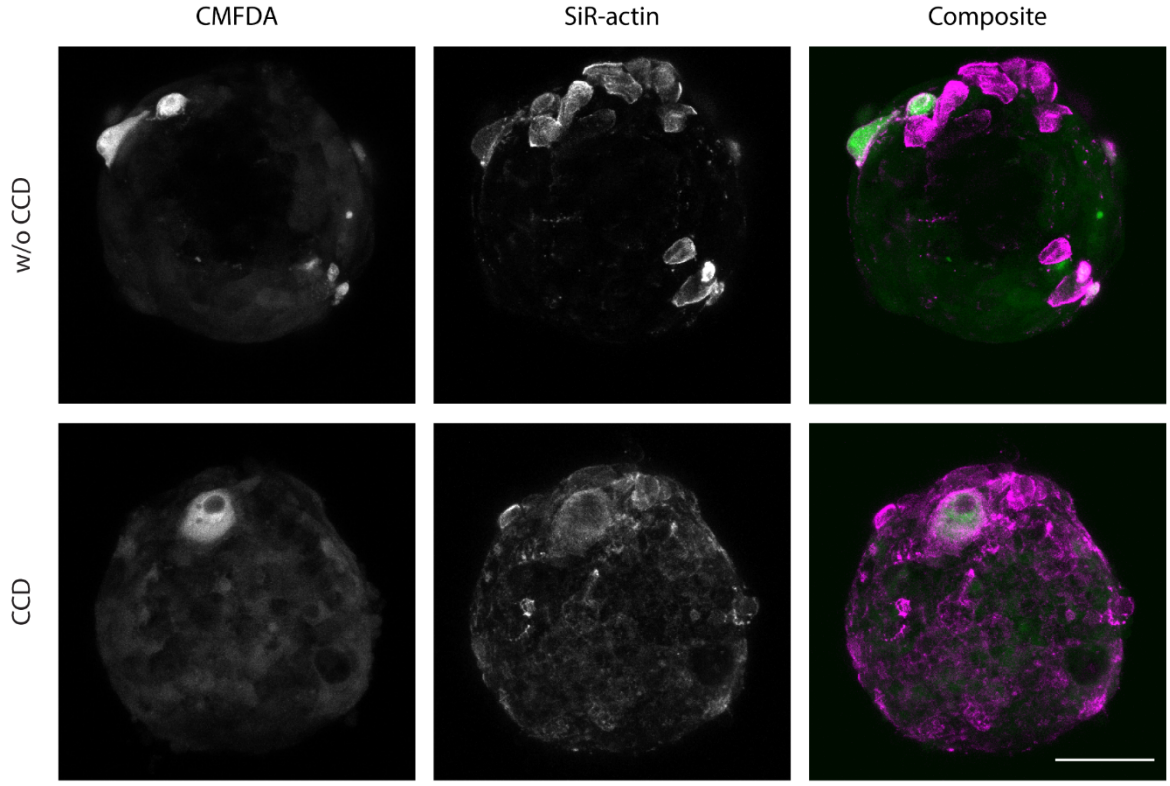

Figure S10 Higher-resolution images of the final results in Figure 5. This image shows two MTs at t = 10 h, perfused with normal medium (w/o CCD) and with medium supplemented with CCD. Both channels, CellTracker Green CMFDA and SiR-actin are displayed separately for better visibility. The actin signal in CCD shows a different localization than in the control. Scale bar is 100 µm.

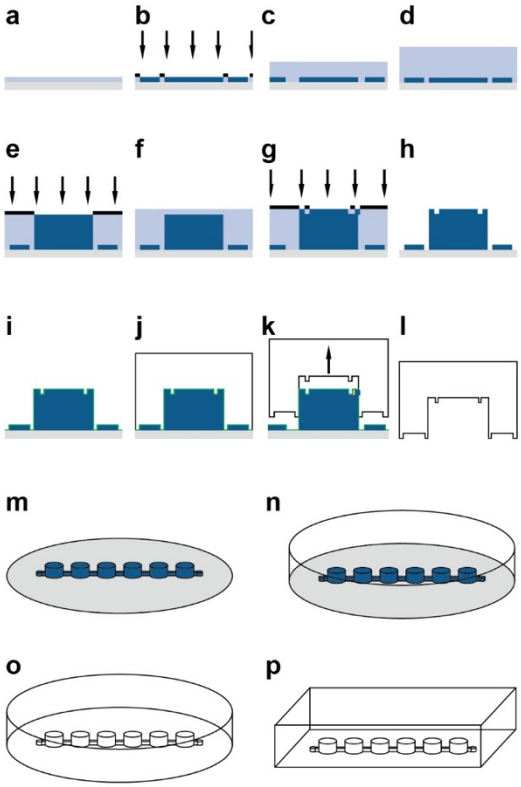

Figure S11 This figure shows the fabrication process of the microfluidic chips. (**a-h**) summarizes the photolithography process with subsequent steps of spin coating of SU-8 (blue) on silicon wafers (gray), exposure, and, finally, development of the mold. **i**) Silanization (green) of the SU-8 mold to avoid adhesion. (**j**) Soft lithography, casting PDMS (white) onto the mold. (**k**) and (**l**) Removal of the cured PDMS from the mold and the final PDMS chip. (**m-p**) Final steps of the fabrication in a 3D fashion. (**m**) The master mold is processed. (**n**) PDMS is poured over the master mold and cured. (**o**) The entire PDMS block is removed from the SU-8 master mold. (**p**) The PDMS piece is cut to size.

4.8 References

1. Antoni, D., Burckel, H., Josset, E. & Noel, G. Three-dimensional cell culture: a breakthrough in vivo. *Int. J. Mol. Sci.* **16,** 5517–27 (2015).

2. Edmondson, R., Broglie, J. J., Adcock, A. F. & Yang, L. Three-dimensional cell culture systems and their applications in drug discovery and cell-based biosensors. *Assay Drug Dev. Technol.* **12,** 207–18 (2014).

3. Ravi, M., Paramesh, V., Kaviya, S. R., Anuradha, E. & Solomon, F. D. P. 3D cell culture systems: advantages and applications. *J. Cell. Physiol.* **230,** 16–26 (2015).

4. Pampaloni, F. & Stelzer, E. Three-dimensional cell cultures in toxicology. *Biotechnol. Genet. Eng. Rev.* **26,** 117–38 (2010).

5. Lee, J., Cuddihy, M. J. & Kotov, N. A. Three-dimensional cell culture matrices: state of the art. *Tissue Eng. Part B. Rev.* **14,** 61–86 (2008).

6. Rimann, M. & Graf-Hausner, U. Synthetic 3D multicellular systems for drug development. *Curr. Opin. Biotechnol.* **23,** 803–9 (2012).

7. Khan, F., Tare, R. S., Oreffo, R. O. C. & Bradley, M. Versatile biocompatible polymer hydrogels: scaffolds for cell growth. *Angew. Chem. Int. Ed. Engl.* **48,** 978–82 (2009).

8. Huh, D., Torisawa, Y., Hamilton, G. A., Kim, H. J. & Ingber, D. E. Microengineered physiological biomimicry: organs-on-chips. *Lab Chip* **12,** 2156–64 (2012).

9. Domansky, K. *et al.* Perfused multiwell plate for 3D liver tissue engineering. *Lab Chip* **10,** 51–8 (2010).

10. Khademhosseini, A., Langer, R., Borenstein, J. & Vacanti, J. P. Microscale technologies for tissue engineering and biology. *Proc. Natl. Acad. Sci. U. S. A.* **103,** 2480–7 (2006).

11. Huh, D. *et al.* Reconstituting organ-level lung functions on a chip. *Science* **328,** 1662–8 (2010).

12. Benam, K. H. *et al.* Small airway-on-a-chip enables analysis of human lung inflammation and drug responses in vitro. *Nat. Methods* **13,** 151–7 (2016).

13. Lee, P. J., Hung, P. J. & Lee, L. P. An artificial liver sinusoid with a microfluidic endothelial-like barrier for primary hepatocyte culture. *Biotechnol. Bioeng.* **97,** 1340–6 (2007).

14. Jang, K.-J. & Suh, K.-Y. A multi-layer microfluidic device for efficient culture and

analysis of renal tubular cells. *Lab Chip* **10,** 36–42 (2010).

15. Kim, H. J., Huh, D., Hamilton, G. & Ingber, D. E. Human gut-on-a-chip inhabited by microbial flora that experiences intestinal peristalsis-like motions and flow. *Lab Chip* **12,** 2165 (2012).

16. Esch, M. B. *et al.* On chip porous polymer membranes for integration of gastrointestinal tract epithelium with microfluidic 'body-on-a-chip' devices. *Biomed. Microdevices* **14,** 895–906 (2012).

17. Booth, R. & Kim, H. Characterization of a microfluidic in vitro model of the blood-brain barrier (μBBB). *Lab Chip* **12,** 1784 (2012).

18. Blundell, C. *et al.* A microphysiological model of the human placental barrier. *Lab Chip* **16,** 3065–73 (2016).

19. Kelm, J. M. & Fussenegger, M. Microscale tissue engineering using gravity-enforced cell assembly. *Trends Biotechnol.* **22,** 195–202 (2004).

20. Tung, Y.-C. *et al.* High-throughput 3D spheroid culture and drug testing using a 384 hanging drop array. *Analyst* **136,** 473–8 (2011).

21. Hirschhaeuser, F. *et al.* Multicellular tumor spheroids: an underestimated tool is catching up again. *J. Biotechnol.* **148,** 3–15 (2010).

22. Friedrich, J., Ebner, R. & Kunz-Schughart, L. a. Experimental anti-tumor therapy in 3-D: spheroids--old hat or new challenge? *Int. J. Radiat. Biol.* **83,** 849–71 (2007).

23. Hamilton, G. Multicellular spheroids as an in vitro tumor model. *Cancer Lett.* **131,** 29–34 (1998).

24. Ramaiahgari, S. C. *et al.* A 3D in vitro model of differentiated HepG2 cell spheroids with improved liver-like properties for repeated dose high-throughput toxicity studies. *Arch. Toxicol.* **88,** 1083–95 (2014).

25. Kim, J. Bin. Three-dimensional tissue culture models in cancer biology. *Semin. Cancer Biol.* **15,** 365–77 (2005).

26. Khaitan, D., Chandna, S., Arya, M. B. & Dwarakanath, B. S. Establishment and characterization of multicellular spheroids from a human glioma cell line; implications for tumor therapy. *J. Transl. Med.* **4,** 12 (2006).

27. Beauchamp, P. *et al.* Development and Characterization of a Scaffold-Free 3D Spheroid

Model of Induced Pluripotent Stem Cell-Derived Human Cardiomyocytes. *Tissue Eng. Part C. Methods* **21,** 852–61 (2015).

28. Messner, S., Agarkova, I., Moritz, W. & Kelm, J. M. Multi-cell type human liver microtissues for hepatotoxicity testing. *Arch. Toxicol.* **87,** 209–213 (2013).

29. Kelm, J. M., Timmins, N. E., Brown, C. J., Fussenegger, M. & Nielsen, L. K. Method for generation of homogeneous multicellular tumor spheroids applicable to a wide variety of cell types. *Biotechnol. Bioeng.* **83,** 173–80 (2003).

30. Rimann, M. *et al.* An in vitro osteosarcoma 3D microtissue model for drug development. *J. Biotechnol.* **189,** 129–35 (2014).

31. Kostrzewski, T. *et al.* Three-dimensional perfused human in vitro model of non-alcoholic fatty liver disease. *World J. Gastroenterol.* **23,** 204 (2017).

32. Cooper, G. M. *The Cell: A Molecular Approach, Cell-Cell Interactions.* (Sinauer Associates, 2000).

33. Jacobs, C. R., Huang, H. & Kwon, R. Y. *Introduction to Cell Mechanics and Mechanobiology*. (Garland Science, 2012).

34. *The Extracellular Matrix: an Overview*. (Springer-Verlag Berlin Heidelberg, 2011). doi:10.1007/978-3-642-16555-9

35. Fang, Y. & Eglen, R. M. Three-Dimensional Cell Cultures in Drug Discovery and Development. *SLAS Discov. Adv. life Sci. R D* **22,** 456–472 (2017).

36. Young, E. W. K. & Beebe, D. J. Fundamentals of microfluidic cell culture in controlled microenvironments. *Chem. Soc. Rev.* **39,** 1036–48 (2010).

37. Kovarik, M. L. *et al.* Micro total analysis systems for cell biology and biochemical assays. *Anal. Chem.* **84,** 516–40 (2012).

38. El-Ali, J., Sorger, P. K. & Jensen, K. F. Cells on chips. *Nature* **442,** 403–11 (2006).

39. Ruppen, J. *et al.* A microfluidic platform for chemoresistive testing of multicellular pleural cancer spheroids. *Lab Chip* **14,** 1198–205 (2014).

40. Torisawa, Y. S. *et al.* A multicellular spheroid array to realize spheroid formation, culture, and viability assay on a chip. *Biomaterials* **28,** 559–566 (2007).

41. Wu, L. Y., Di Carlo, D. & Lee, L. P. Microfluidic self-assembly of tumor spheroids for

anticancer drug discovery. *Biomed. Microdevices* **10,** 197–202 (2008).

42. Hsiao, A. Y. *et al.* Microfluidic system for formation of PC-3 prostate cancer co-culture spheroids. *Biomaterials* **30,** 3020–7 (2009).

43. Frey, O., Misun, P. M., Fluri, D. A., Hengstler, J. G. & Hierlemann, A. Reconfigurable microfluidic hanging drop network for multi-tissue interaction and analysis. *Nat. Commun.* **5,** 4250 (2014).

44. Misun, P. M., Rothe, J., Schmid, Y. R. F., Hierlemann, A. & Frey, O. Multi-analyte biosensor interface for real-time monitoring of 3D microtissue spheroids in hanging-drop networks. *Microsystems Nanoeng.* **2,** 16022 (2016).

45. Schmid, Y. R. F., Bürgel, S. C., Misun, P. M., Hierlemann, A. & Frey, O. Electrical Impedance Spectroscopy for Microtissue Spheroid Analysis in Hanging-Drop Networks. *ACS Sensors* **1,** 1028–1035 (2016).

46. Rismani Yazdi, S. *et al.* Adding the 'heart' to hanging drop networks for microphysiological multi-tissue experiments. *Lab Chip* **15,** 4138–47 (2015).

47. Wagner, I. *et al.* A dynamic multi-organ-chip for long-term cultivation and substance testing proven by 3D human liver and skin tissue co-culture. *Lab Chip* **13,** 3538–47 (2013).

48. Kim, J.-Y., Fluri, D. A., Kelm, J. M., Hierlemann, A. & Frey, O. 96-well format-based microfluidic platform for parallel interconnection of multiple multicellular spheroids. *J. Lab. Autom.* **20,** 274–82 (2015).

49. Kim, J.-Y. *et al.* 3D spherical microtissues and microfluidic technology for multi-tissue experiments and analysis. *J. Biotechnol.* **205,** 24–35 (2015).

50. van Duinen, V., Trietsch, S. J., Joore, J., Vulto, P. & Hankemeier, T. Microfluidic 3D cell culture: from tools to tissue models. *Curr. Opin. Biotechnol.* **35,** 118–126 (2015).

51. Tibbitt, M. W. & Anseth, K. S. Hydrogels as extracellular matrix mimics for 3D cell culture. *Biotechnol. Bioeng.* **103,** 655–63 (2009).

52. Caliari, S. R. & Burdick, J. A. A practical guide to hydrogels for cell culture. *Nat. Methods* **13,** 405–14 (2016).

53. Ahmed, E. M. Hydrogel: Preparation, characterization, and applications: A review. *J. Adv. Res.* **6,** 105–121 (2015).

54. Peppas, N. A., Hilt, J. Z., Khademhosseini, A. & Langer, R. Hydrogels in biology and medicine: from molecular principles to bionanotechnology. *Adv. Mater.* **18,** 1345–1360 (2006).

55. Zhao, H. *et al.* Rationale for the real-time and dynamic cell death assays using propidium iodide. *Cytometry. A* **77,** 399–405 (2010).

56. Hama, H. *et al.* Scale: a chemical approach for fluorescence imaging and reconstruction of transparent mouse brain. *Nat. Neurosci.* **14,** 1481–8 (2011).

57. Cooper, J. A. Effects of cytochalasin and phalloidin on actin. *J. Cell Biol.* **105,** 1473–8 (1987).

58. Lang, M., Rudolf, F. & Stelling, J. Use of YouScope to Implement Systematic Microscopy Protocols. *Curr. Protoc. Mol. Biol.* **98,** 14.21.1-14.21.23 (2012).

59. Schneider, C. A., Rasband, W. S. & Eliceiri, K. W. NIH Image to ImageJ: 25 years of image analysis. *Nat. Methods* **9,** 671–5 (2012).

60. Kiriyama, S. Nikon ND2 Reader. (2014). at <https://imagej.nih.gov/ij/plugins/nd2-reader.html>

61. Aeby, E. A. ImageJ macro for stitching of time-lapse imaging. (2017). at <https://github.com/EAAeby/ImageJ_TimeLapse_Montage>

62. Hagmeyer, B., Zechnall, F. & Stelzle, M. Towards plug and play filling of microfluidic devices by utilizing networks of capillary stop valves. *Biomicrofluidics* **8,** 56501 (2014).

63. Andersen, T., Auk-Emblem, P. & Dornish, M. 3D cell culture in alginate hydrogels. *Microarrays* **4,** 133–161 (2015).

64. Buyl, K., De Kock, J., Bolleyn, J., Rogiers, V. & Vanhaecke, T. Measurement of Albumin Secretion as Functionality Test in Primary Hepatocyte Cultures. *Methods Mol. Biol.* **1250,** 303–8 (2015).

65. Lee, T.-M. *et al.* Optical Characterization of Contrast Agents for Optical Coherence Tomography. *Proc. SPIE* **4967,** 1546–1548 (2003).

66. Chan, C. J., Whyte, G., Boyde, L., Salbreux, G. & Guck, J. Impact of heating on passive and active biomechanics of suspended cells. *Interface Focus* **4,** 20130069 (2014).

67. Thormählen, I., Straub, J. & Grigull, U. Refractive index of water and its dependence on wavelength, temperature, and density. *J. Phys. Chem. Ref. Data* **14,** 933–945 (1985).

68. Boyer, J. L. in *Comprehensive Physiology* (ed. Terjung, R.) (John Wiley & Sons, Inc., 2013). doi:10.1002/cphy.c120027

69. Cummings, B. S. & Schnellmann, R. G. in *Current Protocols in Pharmacology* (John Wiley & Sons, Inc., 2004). doi:10.1002/0471141755.ph1208s25

70. Däster, S. *et al.* Induction of hypoxia and necrosis in multicellular tumor spheroids is associated with resistance to chemotherapy treatment. *Oncotarget* **8,** 1725–1736 (2017).

71. Letzsch, S., Boettcher, K., Kelm, J. M. & Messner, S. Quantifying Efflux Activity in 3D Liver Spheroids. *Genet. Eng. Biotechnol. News* **35,** 14–15 (2015).

72. Watanabe, N., Tsukada, N., Smith, C. R. & Phillips, M. J. Motility of bile canaliculi in the living animal: implications for bile flow. *J. Cell Biol.* **113,** 1069–80 (1991).

73. Milroy, L.-G. *et al.* Selective chemical imaging of static actin in live cells. *J. Am. Chem. Soc.* **134,** 8480–6 (2012).

74. Mortensen, K. & Larsson, L.-I. Effects of cytochalasin D on the actin cytoskeleton: association of neoformed actin aggregates with proteins involved in signaling and endocytosis. *Cell. Mol. Life Sci.* **60,** 1007–12 (2003).

75. Ujihara, Y., Miyazaki, H. & Wada, S. Morphological study of fibroblasts treated with cytochalasin D and colchicine using a confocal laser scanning microscopy. *J. Physiol. Sci.* **58,** 499–506 (2008).

76. Kovacs, E. M. & Yap, A. S. Cell-cell contact: cooperating clusters of actin and cadherin. *Curr. Biol.* **18,** R667–R669 (2008).

77. Angres, B., Barth, A. & Nelson, W. J. Mechanism for transition from initial to stable cell-cell adhesion: kinetic analysis of E-cadherin-mediated adhesion using a quantitative adhesion assay. *J. Cell Biol.* **134,** 549–57 (1996).

78. Tzanakakis, E. S., Hansen, L. K. & Hu, W. S. The role of actin filaments and microtubules in hepatocyte spheroid self-assembly. *Cell Motil. Cytoskeleton* **48,** 175–89 (2001).

5 Uniform Reaggregated Pancreatic Islets in Microfluidic Hanging-Drop Perfusion System Enable to Study Insulin Release Dynamics at Single-Islet Level

The manuscript is in preparation for submission. The order of the authorship is preliminary and listed according to affiliation.

Patrick M. Misun[1], Felix Forschler[1], Nassim Rousset[1], Andreas Hierlemann[1]

Burçak Yesildag[2], Aparna Neelakandhan[2], Adelinn Biernath[2], Olivier Frey[2]

[1]ETH Zürich, Mattenstrasse 26, 4058 Basel, Switzerland

[2]InSphero AG, Wagistrasse 27, 8952 Schlieren, Switzerland

5.1 Abstract

Insulin is released from pancreatic beta cells in a biphasic and pulsatile manner in response to the presence of glucose. *In vitro*, the dynamic insulin release can be studied with islet perfusion assays. However, inherent tissue heterogeneity necessitates pooling of multiple islets, which entails a decreased resolution due to uncoordinated functioning of the different islets and the inefficient use of donor material. Here, we describe a novel method that enables single-islet perfusion assays for studying alterations in the dynamics of insulin release. We engineered a hanging-drop based microfluidic perfusion system, which facilitates rapid glucose switching, minimal sample dilution and short sampling intervals down to 30 seconds. We combined this microfluidic system with a standardized islet model – human islet microtissues, produced by controlled scaffold-free reaggregation of primary islet cells. The uniform size and cellular composition, the proper functioning of the islet microtissues as well as their robust and long-term glucose responsiveness resulted in highly reproducible dynamic glucose-stimulated insulin secretion (GSIS) assays with a prominent first phase and a sustained, pulsatile second phase that varied across donors. The developed platform also enabled the study of compound effects on both phases of insulin secretion as shown by two different classes of insulin secretagogues; tolbutamide and exendin-4. Our results demonstrate that the combination of the presented microfluidic hanging-drop system with uniform islet microtissues provides a unique method for studying physiologically relevant dynamic insulin secretion at comparably low variation and high temporal resolution.

5.2 Introduction

Islets of Langerhans are the endocrine micro-organs of the pancreas that secrete a set of tightly regulated hormones that are fundamental to normal glucose homeostasis.[1] Pancreatic β-cells, the most common endocrine cell type of the islets, uniquely respond to changing blood glucose concentrations by secreting adequate amounts of insulin, the central hormone to normoglycemia. Relative or absolute deficiency in insulin results in diabetes mellitus; a group of heterogeneous disorders characterized by chronic hyperglycemia.[2]

Insulin release from pancreatic β-cells in response to glucose is a highly dynamic process, which is biphasic and pulsatile.[3] Impairment of the dynamic insulin release can have a severe influence on glucose homeostasis and related physiological functions. Loss of the first phase, reduction of the second phase, and impairment of the oscillatory pattern of insulin secretion,

for example, are characteristic features of type 2 diabetes.[3] Thus, studying dynamic insulin secretion is a crucial component to understand the pathogenesis and pathophysiology of diabetes as well as to assess pharmacokinetics and potential mechanisms of action of anti-diabetic medication.

Dynamics of insulin release, including the two phases, and oscillations of glucose-stimulated insulin secretion (GSIS) can be investigated through time resolved assay systems, such as pancreatic islet perfusion platforms. Commercial systems (Biorep technologies, Miami Lakes, Florida) often require more than 20 islets to achieve quantifiable insulin concentrations. Additionally, the inherent heterogeneity in native islet size and endocrine cell composition necessitates pooling of multiple islets for each experimental condition in order to achieve a sample that is representative of the pancreas of origin. The pooling entails a decreased resolution due to uncoordinated functioning of the islets caused by the lack of neuronal and hormonal factors that would normally synchronize individual islets in the body.[4,5]

Microtechnology provides suitable tools for miniaturizing cell- and tissue-culturing devices. Microfluidic platforms allow for the manipulation of single cells and small cell aggregates, as well as for precise control of small liquid volumes at the micron scale.[6–8] They, therefore, are an ideal choice for constructing islet perfusion systems.

Microfluidic perfusion systems, developed to study dynamic insulin release from isolated pancreatic islets, either rely on calcium imaging to measure the intracellular Ca^{2+} response,[9,10] on the collection of medium samples for biochemical analysis of secreted insulin[11–13] or glucagon,[14] or on a combination of both, imaging and biochemical readouts.[15–18] Most previously conducted studies employed rodent islets, which do not represent all aspects of the human organism. Furthermore, the measurements were either limited in temporal resolution or comprised pools of islets to achieve quantifiable insulin concentrations. The relatively large volumes in these devices obviate rapid liquid exchange and, consequently, reduce both, spatial and temporal resolution of medium sampling. The integration of electroosmotic flow and an on-line electrophoresis immunoassay[19,20] as well as further miniaturization of the devices[21–23] enabled to resolve the highly dynamic and oscillatory secretion pattern of single islets.[24,25] The complexity of the experimental setups and the use of highly heterogenous native islets, however, limits reproducibility and obstructs the adoption of such systems in a larger community.

To address these issues, we developed an analytical microfluidic platform, engineered for a uniform islet model, produced by scaffold free reaggregation of primary human islet cells that featured homogeneous and native-like distribution of endocrine cells within each aggregate. The microfluidic system benefits of all advantages of the hanging-drop technology.[26,27] The completely open microfluidic chip design allows for an easy loading of the islet microtissues and their damage-free retrieval after the assay for further analysis. Islet microtissues are kept at the liquid-air interface at the bottom of a hanging drop. Precise fluid control and the characteristic flow profile in hanging drops ensure a rapid liquid turnover, short delays and minimal dispersion so that rapid changes in the secretion patterns can be observed. The relatively small surface area of the chip that is in contact with the liquid phase entails little analyte absorption and adsorption.[28] The open chip design overcomes problems with bubble formation and ensures continuous oxygen supply, which is important to maintain islet functionality and viability *in vitro*.[29–33] Moreover, this design limits flow-induced shear stress on the microtissues.[34] Further, the transparent device is compatible with microscopy for simultaneous imaging. The design concept is simple and features low setup complexity.

The high sampling rates in combination with the optimized chip design enabled us to resolve the physiologically characteristic biphasic and pulsatile insulin release from individual primary human islet microtissues. The device was used to study the effects of two different classes of insulin secretagogues, exendin-4 and tolbutamide. Both compounds altered the insulin release pattern during the different secretion phases. The corresponding measurements show the importance of precise islet perfusion systems, specifically designed to get better insights into the mechanism of action of anti-diabetic compounds. The developed system offers a wide and parameter range that can be tuned in such assays, which renders studies on islets more efficient and meaningful and increases their information content.

5.3 Materials and Methods

5.3.1 Re-aggregated human islets

InSphero 3D InSight™ human islet microtissues were produced by scaffold-free reaggregation of dispersed primary human islets obtained through Prodo Laboratories Inc. Irvine, CA. Consent was obtained from all donors, and there was no information on the identity of the donor for ethical and privacy reasons. Islet microtissues were maintained in 3D InSight™ Human Islet Maintenance Medium.

5.3.2 Microfluidic chip fabrication

Microfluidic chips have been fabricated using a SU-8 mold and casting poly(dimethylsiloxane) (PDMS, Sylgard 184, Dow Corning GmbH, Wiesbaden, Germany). A 4-inch silicon wafer was used as a substrate in a multi-layer photolithographic process. The wafer was consecutively spin-coated with two layers of negative photoresist SU-8 100 (Microchem Corp., Newton, MA, USA) at a thickness of 250 µm for each layer. The wafer was soft-baked after deposition of each layer and UV exposed through a transparency mask for cross-linking. A post-exposure baking step followed for each layer. The wafer was developed in mr-Dev 600 (Micro resist technology GmbH, Berlin, Germany) to dissolve all unexposed SU-8 and afterwards coated with trichloro(1H,1H,2H,2H-per-fluorooctyl)silane (Sigma-Aldrich, Buchs, Switzerland) to reduce adhesion during PDMS casting.

PDMS was prepared by mixing the elastomer and curing agent in a 10:1 ratio. PDMS was poured onto the SU-8 mold resulting in a 3-mm-thick layer and cured for 2 h at 80 °C. Individual chips were cut, and access holes were punched on the outlet and inlet side for the fluidic connection. Finally, the PDMS chip was bonded to a microscope slide featuring corresponding access holes by oxygen plasma activation of both parts.

5.3.3 Device preparation

The microfluidic chip was cleaned with water and soap, rinsed with isopropanol and dried with an air gun. The microfluidic structures were treated with oxygen plasma for 35 s at 50 W (Diener Electronic GmbH & Co., Ebhausen, Germany) before any experiment to obtain a hydrophilic surface. Therefore, a thin PDMS mask with a small opening at the drop position was aligned to the hanging-drop chip. The mask covered the rim and allowed to activate only the drop structure and channels through the oxygen plasma. The activated hanging-drop chip was placed on a custom-made chip holder, which fits into a Nunc OmniTrayBox (Thermofisher Scientific, Reinach, Switzerland).

5.3.4 Microtissue loading

The chip was filled with pre-warmed (37 °C) Krebs Ringer Hepes Buffer (KRHB – 131 mM NaCl, 4.8 mM KCl, 1.3 mM CaCl2, 25 mM Hepes, 1.2 mMm Kh2PO4, 1.2 mM MgSO4, 0.5% Bovine serum albumin). The microtissues were aspirated from an Akura™ 96 plate (InSphero AG, Schlieren, Switzerland) and transferred from the pipette tip into the chip via passive sedimentation. The drop height was adjusted to 800 µm prior to each experiment. The height

is defined as the distance between the PDMS rim structure of the chip and the focal plane of the microtissue.

5.3.5 Experimental setup

The chip was placed on a microscope (DMI6000B, Leica Microsystems, Germany) and covered with a top-stage incubator (The Brick, Life Imaging Services, Basel Switzerland) to ensure >95% humidity and 5% CO_2. A liquid reservoir on the chip holder and a wet cotton pad at the bottom of the OmniTrayBox increased the humidity to minimize evaporation. Temperature was kept at 37 °C by an environmental box (The Cube, Life Imaging Services, Basel Switzerland).

5.3.6 Perfusion system

Syringe pumps (neMESYS, Cetoni GmbH, Korbussen, Germany) were connected to the inlet of the chip. Polytetrafluoroethylene (PTFE) tubing (ID 0.3 mm, OD 0.6 mm, Bola GmbH, Grünsfeld, Germany) and metal connecting pieces, obtained from standard luer lock syringe-tubing connectors (22 GA ½" Bent 90 Deg, APM Technica AG, Heerbrugg, Switzerland), were connected together by short flexible silicone tubing (Tygon R3607, ID 0.25 mm, wall 0.91 mm, Idex Health & Science GmbH, Wertheim, Germany). A flow splitter enabled the connection of multiple syringes to a single inlet of the hanging-drop chip and a heatable perfusion cannula (PH01&TC02, Multichannel Systems, Reutlingen, Germany) ensured a constant temperature of 37 °C of the infused medium.

A peristaltic pump (peRISYS-S, Cetoni GmbH) was connected in the same way to the outlet of the microfluidic chip. Peristaltic tubing (Tygon S3 E-LFL, ID 0.27 mm, wall 0.91 mm, Idex Health & Science GmbH) was used for the peristaltic pump.

The final part of the tubing was attached to the sampling arm of the rotAXYS system (Cetoni GmbH) using fluid connectors (Upchurch Scientific Products, Oak Harbor, USA). A needle (facet cut, 0.15 mm ID, 0.3 mm OD, 16 mm length, Unimed, Lausanne, Switzerland) was connected at the end of the sampling tubing. All tubing was filled with medium before being connected to the chip.

Inflow rates of the syringe pumps were set to 15 µl min^{-1} and controlled by YouScope software [35] (Version: R2016-03). A controller implements a feedback loop, that continuously adjusts the inflow rate based on the information of the actual and initially-set drop height to bring drops back to their initial size. The peristaltic pump withdraws medium from the outlet at a constant

rate of 15 µl min^{-1}. The integrated feedback pump controller ensures constant flow rates and drop sizes throughout the experiment. The tubing caused a 4-min delay for the liquid to reach the islet microtissue in the hanging drop after switching between the different buffer solutions. The delay has been corrected in all graphs so that the time starts when the medium reaches the islet.

5.3.7 Automated sampling

A programmable positioning and sampling system (rotAXYS, Cetoni GmbH) was used to collect outflow samples in predefined time intervals of down to 30 seconds. The Qmix Elements Software (Cetoni GmbH) was used to create a sampling script. An insulating Styrofoam box was placed underneath the sampling arm and filled with dry ice to cool down and freeze the samples. A multiwell plate (384-well, V-bottom, polypropylene, Thermo Fisher Scientific, USA) was sealed with a plate sealing foil (Platesealer EasySeal, Greiner Bio-One, Frickenhausen, Germany) inserted into the Styrofoam box and used for collecting the samples. The plates were stored and kept at -20 °C until analysis.

5.3.8 Microfluidic characterization

The microfluidic hanging-drop chip has been validated using a fluorescent Rhodamine 6G solution (Sigma-Aldrich, Buchs, Switzerland) at a concentration of 50 mg/l. DI water was first perfused at a flow rate of 15 µl min^{-1} for 60 min, then, the fluorescent dye was introduced into the chip at the same flow rate. The withdrawal flow rate at the outlet was set to 15 µl min^{-1}. Fluorescence within the hanging-drop was tracked over time by taking fluorescence images (GFP channel) every 10 seconds. Fluorescence in the central drop region around a glass bead was analyzed using ImageJ. A glass bead of similar size was used instead of an islet microtissue for drop-height regulation in the validation experiments.

5.3.9 Static GSIS and quantification of insulin and ATP

Culture media were removed, islet microtissues were washed twice with 70 µL KRHB containing 2.8 mM glucose and equilibrated for 1 hour in the same solution. Glucose-stimulated insulin secretion (GSIS) was performed in the Akura™ 96 well-plate in 50 µL KRHB containing the respective glucose concentrations during 2 hours. The supernatant was collected for ELISA analysis. After GSIS, the tissues were lysed to analyze total ATP content using CellTiter-Glo® Luminescent Cell Viability Assay (Promega, with protease inhibitor cocktail (Promega, G6521)) and a microplate reader (Infinite M1000, TECAN, Switzerland).

The lysates were then used for assessment of total insulin content. After proper dilutions in KRHB were performed, total and secreted insulin was quantified using Stellux® Chemi Human Insulin ELISA (Alpco, 80-INSHU-CH10).

5.3.10 Perfusion GSIS

Islet microtissues were transferred to a special preconditioning medium (hIsPCM, InSphero AG, Schlieren, Switzerland) 12 h before the experiment. A 100 µM exendin-4 stock solution and 25 mM tolbutamide in DMSO were diluted in KRHB shortly before experiments. Four 2.5 mL glass syringes were loaded with 2.8 mM glucose + 0.1% DMSO (control), 16.7 mM glucose + 0.1% DMSO (control), 2.8 mM glucose + compound (100 nM exendin-4 or 25 µM tolbutamide) and 16.7 mM glucose + compound (100 nM exendin-4 or 25 µM tolbutamide). These buffers were consecutively perfused through the hanging drop in the following order; 90 min 2.8 mM glucose + 0.1% DMSO for equilibration, 30 min 2.8 mM glucose + compound (100 nM exendin-4 or 25 µM tolbutamide) for compound baseline secretion, 60 min 16.7 mM glucose + compound (100 nM exendin-4 or 25 µM tolbutamide) for compound stimulation secretion and 70 min with 2.8 mM glucose + compound (100 nM exendin-4 or 25 µM tolbutamide) for post-GSIS secretion.

5.3.11 Microscopy

Islet microtissues were continuously monitored with an inverted wide-field microscope (Leica DMI6000, Leica Microsystems, Switzerland) using a 10x objective and a 0.70x c-mount. Bright-field and fluorescence images were taken with a Leica DFC 340FX CCD camera. A mercury arc lamp was used as a light source for fluorescence imaging.

5.3.12 Data analysis

For each sampling interval, the average insulin secretion rate per microtissue [fmol $IEQ^{-1}min^{-1}$] was calculated from the known flow rate and the insulin concentration in the sample. To ensure that experiments were comparable, this value was normalized to islet microtissue size in islet equivalents (IEQs), with one IEQ corresponding to the volume of a sphere with a diameter of 150 µm, yielding the secretion rate in [fmol $IEQ^{-1}min^{-1}$].

5.3.13 Diffusion-convection transport model

Diffusive-convective transport of molecules through the liquid phase was modeled numerically using the finite-element method. Dimensions of the chip and drops were reproduced in COMSOL Multiphysics® software (COMSOL AB, Stockholm, Sweden).

The fluid dynamics model included the viscosity and density of the medium at 37 °C, which were assumed to be identical to water. Slip and no-slip boundary conditions were assumed at the liquid-air and liquid-PDMS interfaces respectively. A constant flow of 15 µl min^{-1} and a null pressure at the inlet and outlet boundaries were assumed. A log scale color mapping of the resulting flow was incorporated in Figure 2, showing that flow speed at the islet site was significantly lower than in the channel, which reduces shear stress while direct molecule transport is enabled. These date were used to model the convective transport of molecules.

The diffusion-convection model was applied for Rhodamine 6G and insulin with diffusion coefficients of 4.14×10^{-4} m^2 s^{-1},[36,37] and 0.15×10^{-9} m^2 s^{-1} [33], respectively. From the determined diffusion coefficient at 25°C, we derived its value at 37°C using the Stokes-Einstein equation and the viscosity of water. For the case of Rhodamine 6G (Figure 2c), a normalized concentration influx was applied at the inlet and both, the average concentration in the entire hanging drop and at the islet were computed over time. For the case of insulin (Figure 2d), a short insulin secretion burst from an islet was simulated. We took the values from a measurement (Figure 3a) and simulated a total release of 2.5 fmol IEQ^{-1} insulin within one burst and assumed a fast secretion within one second, such that the secretion averages 5 fmol IEQ^{-1} min^{-1} over one sampling interval of 30 s. The concentration at the outlet was probed over time to investigate sampling aliasing due to various boundary conditions at the liquid-air interface.

5.4 Results and Discussion

5.4.1 The standardized pancreatic islet model – human islet microtissues

The experimental use of isolated native islets has multiple limitations due to the inherent heterogeneity in size and function, the varying endocrine cell composition, and low the purity. Additionally, quickly after isolation, islets decline in viability and functionality with regard to their glucose responsiveness.[38,39] It has long been known that dissociated isolated islets can spontaneously reaggregate into islet-like clusters, with native-like endocrine cell composition, architecture and secretory function.[40–43] The reaggregation process also provides control over

the islet size, which enables the generation of smaller islets. The smaller islets display superior glucose-stimulated insulin secretion in perfusion assays and more favorable glycemic outcomes after transplantation *in vivo*.[44,45]

3D InSight™ Islet microtissues were produced by enzymatic dissociation and controlled scaffold-free hanging-drop-based reaggregation of primary islet cells to obtain a standardized islet size of around 150 µm (Figure 1a). The resulting uniform islet microtissues are cultured in a one-islet per well format in 3D-cell culture optimized 96-well microwell plates (Akura™ 96, InSphero AG). Islets microtissues have a composition, which closely resembles that of the human pancreas[46,47] with 55.1% β-cells, 36.1% α-cells and 6.5% δ-cells (Figure 1b). The islet size was reproducible over several aggregations (Figure 1c), and microtissues featured sustained viability (indicated by the total ATP content, Figure 1d) during 28 days in culture. The insulin content, on the other hand, increased with culture time (Figure 1e). Throughout these 4 weeks, islet microtissues also showed robust glucose-stimulated insulin secretion (Figure 1f).

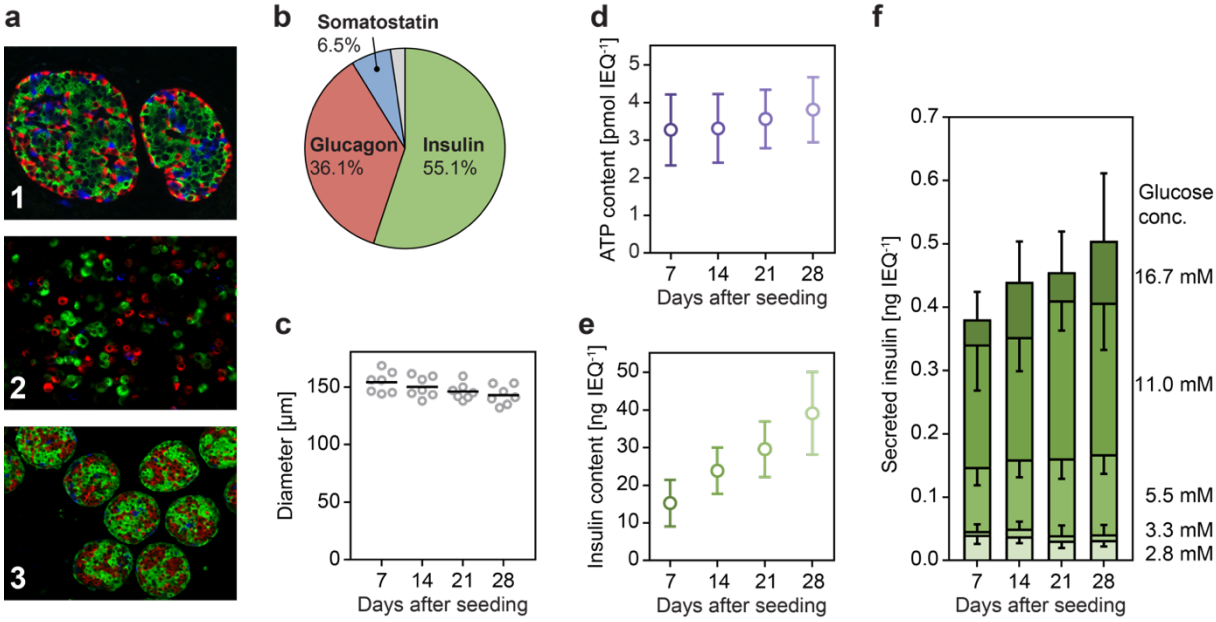

Figure 1 Characterization of reaggregated islet microtissues. (**a**) Stages of islet microtissue production displayed through immunofluorescence stainings for insulin (green), glucagon (red), and somatostatin (blue). Panels show (1) isolated native islets, (2) dissociated islets, and (3) scaffold-free re-aggregated islets. (**b**) Endocrine cell compositions of the islet microtissues were calculated from morphometric analysis of the microtissue sections from 2 individual donors. **c**) Cross-sectional diameter, (**d**) total ATP content, (**e**) total insulin content, and (**f**) GSIS of human islet microtissues were assessed on days 7, 14, 21 and 28 post production. ATP

content, insulin content and secreted insulin were normalized to the islet size in islet equivalents (IEQs), which is an islet of 150 µm diameter. Data in panel (**c**), (**d**) and (**f**) have been obtained from islets of 7 individual donors, while (**e**) includes data from islets of 4 individual donors, mean ± standard deviations.

5.4.2 The microfluidic perfusion system

The microfluidic hanging-drop chip was designed as an open microfluidic system. Figure 2a shows the layout and dimensions of the chip, and a cross-section is shown in Figure S1a (Supporting Information). A surface-patterned PDMS-layer was bonded onto a microscope slide, which ensured planarity and mechanical stability of the chip system. A small, 200-µm-wide and 500-µm-tall hydrophobic rim defines the fluidic structures, which feature one inlet, one outlet, two 200-µm-wide interconnecting channels and the circular hanging-drop structure with a diameter of 3 mm. Due to surface tension and capillary action, small liquid volumes can be guided underneath the surface-patterned PDMS substrate.

The loading procedure of the chip is simple and fast, which is important when working with sensitive primary microtissues. A single microtissue is directly loaded with a small liquid volume into the empty drop structure until a small standing drop is formed. The chip is then flipped upside-down to let the microtissue sediment to the bottom of the hanging drop and then placed on a microscope stage using a dedicated holder. The chip is completely transparent, which allows for real-time imaging.

Figure 2b shows the microfluidic setup. Three syringe pumps with different media are connected via adapters to the inlet of the chip and operated by a predefined perfusion script. Inflow rates of the syringe pumps were set to 15 µl min^{-1}. A peristaltic pump was set to withdraw medium from the outlet at a constant rate of 15 µl min^{-1}. An automated sampling system was used to collect medium samples into a 384-well plate. The medium flow caused a maximum shear stress of 2.97 mPa on the islet microtissue, when a flow rate of 15 µl min^{-1} was applied (Figure S1b, Supporting Information).

A trade-off between flow rate (dilution of secreted insulin) and minimal required sampling volume for ELISA defined the sampling frequency. The flow rate was optimized to reduce the dilution of secreted insulin so that it remained above the limit of detection of the ELISA (2 pg/ml) and to maximize the sampling frequency. A minimum volume of 5 µl is required to prepare the ELISA samples which limits the sampling rate to 3 samples per minute when applying a flow rate of 15 µl min^{-1}. Combining the automated sampling system with a flow-

rate controller ensured consistent sampling volumes and ensured continuous flow rates and drop sizes throughout the experiment (Figure S1c, Supporting Information).

The hanging-drop was used as a miniaturized microtissue culturing compartment with a volume of 6.5 µl (Figure S1a, Supporting Information). The microfluidic chip did not have any dead volume, and the completely open chip design reduced the PDMS surface area in contact with the liquid phase in order to lower the risk of analyte adsorption. Moreover this design ensured sufficient oxygenation of the medium and prevented bubble formation in the chip. The cultured islet microtissue was inherently fixed at the bottom of a hanging drop so that there was no need for trapping structures. Moreover, the tissue could not adhere to any chip surface. The precise and stable location of the microtissue at the bottom of the drop also ensured identical flow conditions in every experiment, which increased reproducibility. Finally the hanging drop features a characteristic flow profile and a rapid and efficient medium exchange around the microtissue (Figure 2c).

We measured the dynamics of the medium exchange in the hanging drop by switching from deionized water to a fluorescent dye (Rhodamine 6G) and then back to deionized water (Figure S1d, Supporting Information). Based on the resulting relative fluorescence data (Figure 2c), we modeled the average concentration of Rhodamine 6G in the hanging drop and around the islet microtissue. The medium exchange timescale – defined as time to go from 5 to 95% of analyte – amounts to 99 seconds in the hanging drop, with a good fit between model (dotted black line) and experiments (red line), and to 17 seconds in the region around the islet microtissue (black line). These results show that medium switching is faster than the sampling rate, which enables precise timing of the glucose-stimulation of pancreatic islets.

The hanging-drop setup has an additional advantage over more conventional closed microfluidic devices. The air-liquid interface near the secreting organ exhibits a slip-boundary that enables to transport metabolites more rapidly than the no-slip-boundary of closed microfluidic devices. This enables resolving much sharper changes in the secretion dynamics. To demonstrate this, a sharp 1-s-wide insulin secretion burst at the pancreatic islet was simulated (Figure 2d). The results show that, with the slip-boundary, one can detect this sharp peak within one 30 s sample, whereas with a no-slip-boundary the true signal from the islet is widened 5 times. Sampling that is in-phase and out-of-phase of a secretion event is shown in Figure S2a,b (Supporting Information). Numerical modeling results of the concentrations through the chip along a cross section demonstrate the transport characteristics of secreted insulin within the hanging-drop (Movie S3, Supporting Information).

In summary, the miniaturized system is ideal for islet microtissue perfusion - optimized for maximal functionality and minimal complexity.

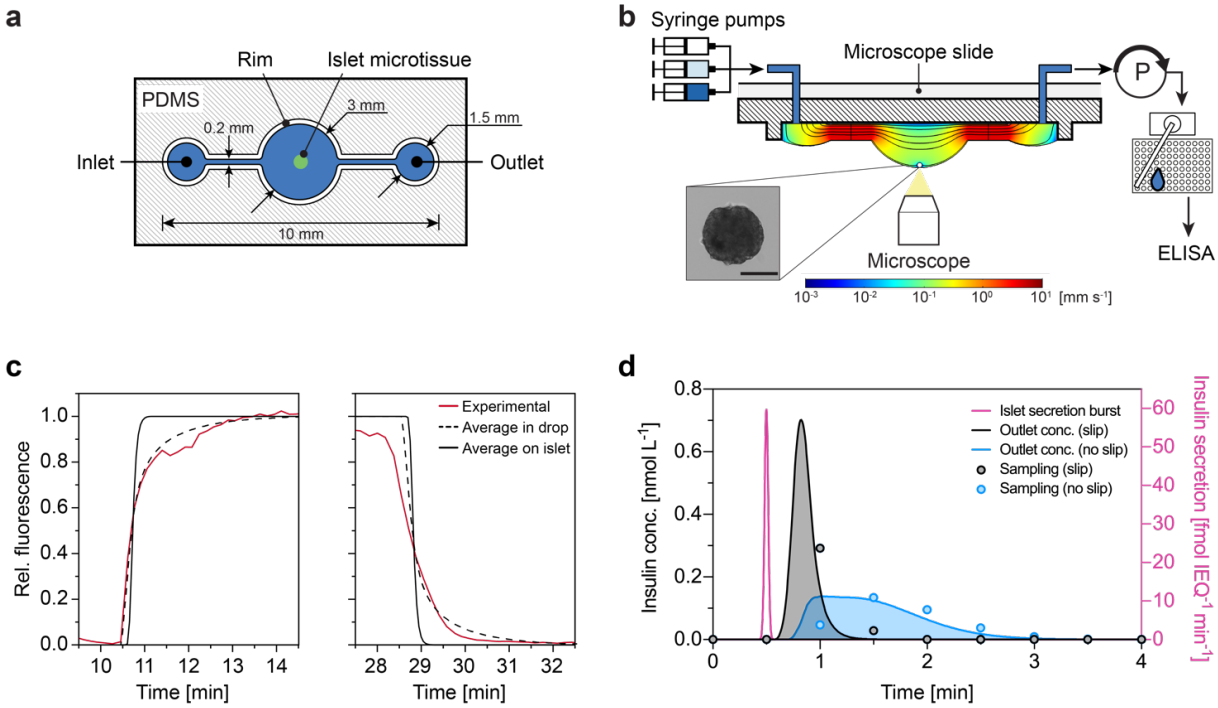

Figure 2 Microfluidic hanging-drop device and flow characteristics. (**a**) Layout of the hanging-drop chip showing a top view of the hydrophobic PDMS rim structure (white), which guides the medium (blue). The chip consists of one inlet, and one outlet and a circular hanging-drop structure with a diameter of 3 mm hosting the microtissue. (**b**) Microfluidic perfusion setup and schematic cross-sectional view along the hanging-drop chip. The microtissue is located at the bottom of the hanging drop. The chip is operated on a microscope. Multiple syringes are connected to the inlet of the chip, and a peristaltic pump is actively withdrawing the medium from the outlet. An automated sampling system collects the medium in a 384-well plate for down-stream ELISA. (**c**) Experimental measurements and simulation of the concentration changes in the hanging drop. Experimental data (red) of the average relative fluorescence in the hanging drop upon switching from deionized water to Rhodamine 6G solution (left), and back to deionized water (right). A corresponding simulation shows the average concentration in the drop (dotted black) and the average concentration around the islet microtissue (black). A fast medium switching near the islet microtissue is observed. (**d**) Modeling result of the insulin concentration at the chip outlet following a sharp 1-s-wide insulin secretion burst (purple) at the islet with a total release of 2.5 fmol IEQ^{-1} insulin. This is equivalent to an experimentally measured average secretion rate of 5 fmol IEQ^{-1} min^{-1} over one sample interval (see Figure 3a). The resulting outlet concentration has been calculated

assuming either a slip- (black) or no-slip (blue) boundary condition at the bottom of the drop. The resulting expected experimental data points are shown for a sampling rate of two samples per minute for both slip- (black dots) and no-slip (blue dots) boundary conditions.

5.4.3 Insights in islet secretion dynamics, mechanistic function and biology

Insulin is secreted from healthy β-cells of pancreatic islets in a glucose-dependent manner. The physiological release of insulin is highly dynamic and results in a characteristic biphasic and pulsatile insulin secretion pattern.[3] The robust first phase of the biphasic insulin secretion is mediated by the limited readily releasable pool of insulin granules, which are docked to the cell membrane. The second phase of glucose-stimulated insulin secretion is sustained by the granules that are transported from the intracellular reserves.[3]

We used a microfluidic glucose-stimulated insulin secretion (FlowGSIS) protocol with precise timing and sampling to characterize the secretion dynamics of single human islet microtissues. Figure 3a shows a typical insulin secretion pattern of a single islet microtissue. The time-resolved insulin secretion curve allowed us to define a large set of parameters that can be extracted from such a FlowGSIS assay, shown in Table S4 (Supporting Information).

A glucose enriched Krebs-Ringer buffer was constantly perfused at a flow rate of 15 µl min^{-1}. Glucose concentration was first kept low at 2.8 mM for 105 min and then switched to high 16.7 mM for 60 min before returning back to 2.8 mM for 60 min. The low liquid volume minimized dilution effects of secreted hormones and allowed for a sampling every 30 seconds.

During the initial phase, basal secretion values show low variation along the time axis with a standard deviation of ± 0.05 fmol IEQ^{-1} min^{-1} proving good reproducibility between samples. A fast increase in glucose concentration from 2.8 to 16.7 mM glucose induced a reproducible biphasic insulin secretion pattern with a prominent first phase and a sustained, pulsatile second phase. The observed oscillatory secretion of insulin indicated an intact intercellular communication and a synchronized release of insulin from the β-cells present in the islet microtissues. While perfusion of a single islet microtissue enabled detection of very distinct and reproducible pulsations, we could not detect clear oscillations when multiple islet microtissues were used. This was most likely a result of the averaging of asynchronous insulin secretion patterns of the individual islets (Figure S5, Supporting Information). We also observed a reduced peak and total secretion in the first phase and a reduced secretion in the second phase when pooling islets.

We were able to extract various parameters of dynamic insulin release from single-islet-microtissue perfusion experiments including the basal insulin secretion rate, the peak secretion and the total secreted insulin during a full GSIS assay. In the presented case, the basal insulin secretion from a single islet microtissue was 0.25 fmol IEQ^{-1} min^{-1} for low glucose (2.8 mM). Interestingly, we observed a short (~3 min) but distinct dip in insulin secretion when switching to high glucose (16.7 mM) prior to the start of the first phase in which the secretion rates increased rapidly to 7.0 fmol IEQ^{-1} min^{-1} within 2.5 min. This prominent 1st peak lasted for 8 min. In the 2nd phase, we observed pulsatile insulin secretion with 5.5-min oscillations for 20 min, followed by prolonged 11-min oscillations for 40 min. Peaks of insulin secretion decreased from initially 5.0 to 1.5 fmol $IEQ^{-1}min^{-1}$. Prolonged low frequency, pulsatile secretion lasted for 15 min after switching back to low glucose medium (2.8 mM). The simulations in Figure 2d show that we can resolve insulin oscillations down to a frequency of 1 cycle min^{-1} if we sample in phase, and down to 0.5 cycles min^{-1}, if we sample out of phase (Figure S2a and b, Supporting Information). Consequently, the measurement does not provide any information about the dynamics of secretion events within the sampling interval of 30 s.

Figure 3b shows the average secretion rates and the distribution of insulin release in all different phases of the FlowGSIS represented in Figure 3a. Obviously, the highest secretion rate occurs during the first phase with a total insulin release of 31.9 fmol. In the second phase, the insulin secretion rate drops significantly, which provides information on the intracellular synthesis and transport of insulin granules to the cell membrane. The total insulin in this phase depends on the duration of the high-glucose phase. The respective measurements of islets from different donors are shown in Figure S9 and S10 (Supporting Information).

Figure 3c presents timing and duration of every phase of the FlowGSIS assay. Islets across different donors show a very precise timing and respond highly reproducible to high glucose stimulation, which can be attributed to the beta cell function and mechanisms that are involved in the release of insulin. Islets responded in average within 4.57 ± 0.98 min ($t_{Response}$) to high glucose levels. They reached a peak secretion rate of 11.23 ± 6.56 fmol $IEQ^{-1}min^{-1}$ in the 1st phase 3.57 ± 0.84 min (t_{Peak}) after stimulation. The 1st phase (t_{Ph1}) lasted in total for 9.86 ± 1.38 min. Islets showed a delayed response after switching to low glucose levels. This relaxation time ($t_{Relaxation}$) was 19.71 ± 11.13 min. Especially the response time, the time to reach peak secretion and the duration of the 1st phase were very reproducible over different donors, whereas the peak secretion rate and the relaxation time showed higher variations across islets from different donors.

Islet microtissues can easily be removed from the hanging drop after GSIS for downstream analysis. Islets that were perfused during the FlowGSIS have a lower ATP content (2.62 ± 0.82 pmol/MT) compared to the static GSIS (3.61 ± 0.86 pmol/MT) (Figure S6b, Supporting Information). Reduced ATP levels in islets which are measured directly after GSIS assays can be attributed to the highly dynamic regulation of intracellular ATP concentration.[48]

Additionally, the system allows to perform different perfusion scenarios, including multiple FlowGSIS sequences over time. Figure S7 (Supporting Information) presents insulin secretion dynamics of islet microtissues over 24 hours. Microtissues responded repeatedly to seven low-high glucose cycles. Peak rates decreased over time, while increased basal secretion rates indicated that microtissues may not have recovered fully after each cycle.

Compared to the standard static GSIS, the mean secretion rate over both high-glucose phases is in average 7.6-fold higher in the perfusion system (4.03 ± 3.07 fmol IEQ $^{-1}$min^{-1} in the FlowGSIS compared to 0.53 ± 0.35 fmol IEQ $^{-1}$min^{-1} in the static GSIS). However, the stimulation-level factor from basal secretion at 2.8 mM glucose to the average secretion at high glucose levels (16.7 mM) remains the same under both, static (15.97 ± 8.85) and FlowGSIS conditions (15.37 ± 10.06) (Figure 3d).

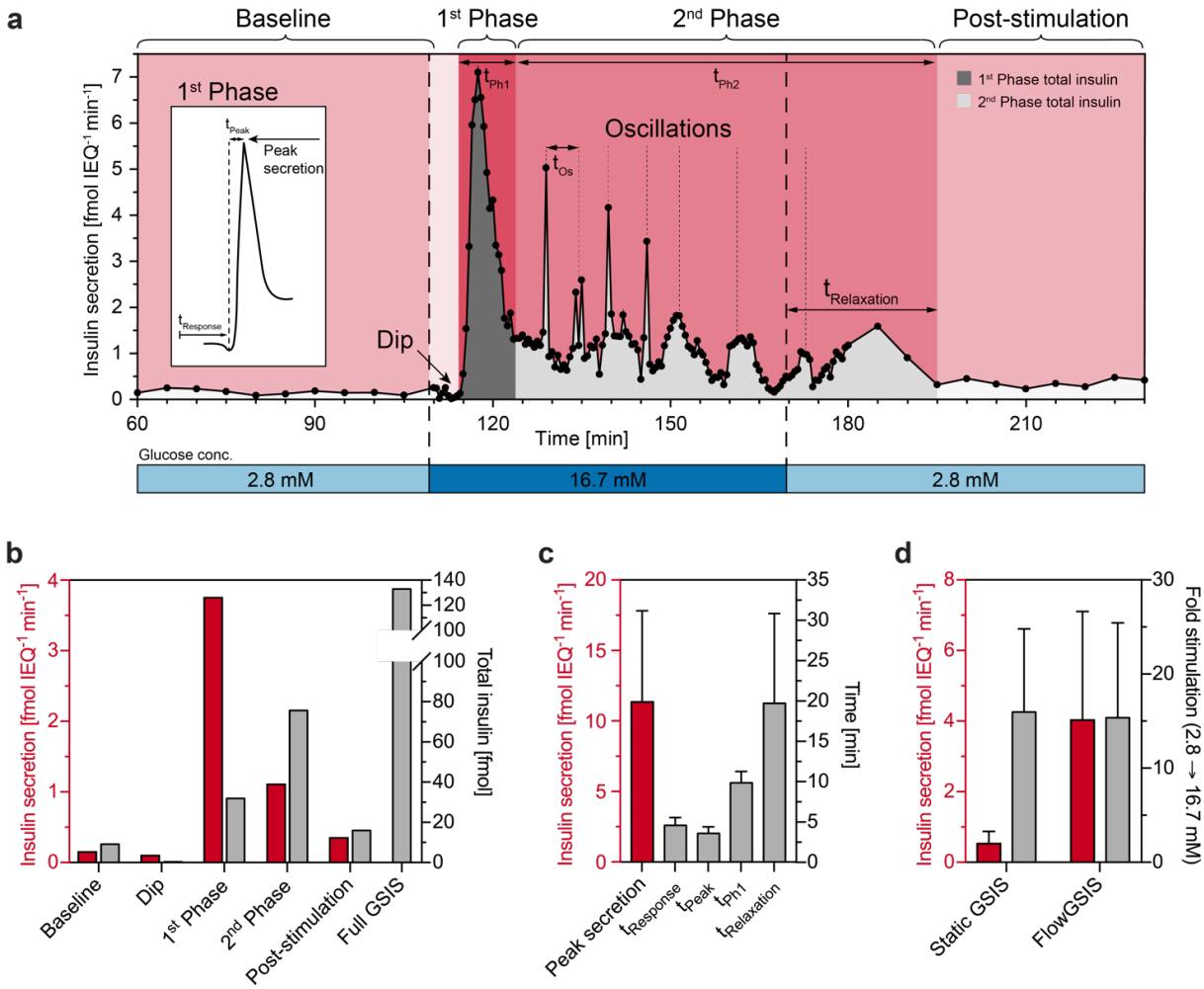

Figure 3 (**a**) High-resolution microfluidic FlowGSIS measurement of a single human islet microtissue. A change from low (2.8 mM) to high (16.7 mM) glucose concentrations stimulates insulin secretion in a bi-phasic pattern. Samples were continuously taken every 5 min during low-glucose conditions (60-110 min and 180-230 min) and every 30 s in the high-glucose phase (110-180 min). Islets secreted insulin at a low level and constantly at low glucose concentrations (basal secretion). High glucose concentrations induced highly dynamic insulin secretion with a dip at the beginning, a prominent 1st phase, which was followed by a sustained, pulsatile 2nd phase. The inset shows the characteristic shape of the first secretion peak and the parameters that can be extracted from the curve. (**b**) Insulin secretion rate (red) and the total secreted insulin (grey) in each phase of the FlowGSIS are represented in panel (**a**). (**c**) Characteristic timing of insulin release (grey) and the maximum secretion rate in the 1st phase (red), (n=7 islets from 4 different donors). (**d**) Flow-induced increase of insulin secretion (red) and the respective stimulation-level factor from baseline to high glucose (grey), static GSIS (n=9 donors), FlowGSIS (n=5 donors). Data represent mean ± standard deviations.

5.4.4 The islets recapitulate *in vivo* compound response

In order to verify, whether the assay platform can be used to study compound-stimulation mechanisms for insulin secretion, we have treated the islet microtissues with two different classes of insulin secretagogues: tolbutamide, a sulfonylurea-class compound and exendin-4, a glucagon-like-peptide-1 (GLP-1) receptor agonist.

The effect of sulfonylureas is based on blocking the ATP-sensitive K^+ (KATP) channels on the surface of pancreatic beta cells, which leads to membrane depolarization, opening of the voltage-gated Ca^{2+} channels (VGCC) and the consecutive rise in intracellular calcium levels.[49] Elevated calcium levels results in increased fusion of insulin granules and higher levels of insulin secretion (even under low levels of glucose).[49] In the static glucose-stimulated insulin secretion experiments, addition of tolbutamide resulted in a substantial increase in insulin secretion for all tested glucose concentrations (Figure 4a). The secretion rate was increased by 0.21–0.37 fmol $IEQ^{-1}min^{-1}$ from 2.8 to 8.0 mM glucose in comparison to the vehicle control and remained constant at 0.68 fmol $IEQ^{-1}min^{-1}$ from 8.0 to 16.7 mM glucose. Similarly, tolbutamide increased basal insulin secretion at 2.8 mM glucose in the high-resolution FlowGSIS experiment (Figure 4b). Tolbutamide increased the baseline secretion rate at 2.8 mM glucose from 0.16 to 0.89 fmol $IEQ^{-1}min^{-1}$ and caused a partial attenuation of the following first phase of glucose-stimulated insulin secretion from 7.1 to 5.1 fmol $IEQ^{-1}min^{-1}$ (maximum secretion rate) in comparison to the vehicle control. A potential reasoned may be an early exhaustion of the readily releasable pool of insulin granules. The total amount of glucose-stimulated insulin release in the second phase was comparable for the first 30 min (140-170 min) for tolbutamide (42.1 fmol insulin) and solvent-only treated islets (41.3 fmol insulin). Addition of tolbutamide helped to sustain higher levels of insulin secretion for elongated exposure (170-195 min) to high glucose levels (tolbutamide: 41.8 fmol insulin, vehicle control: 18.7 fmol insulin).

GLP-1, an incretin hormone, is secreted from the intestinal L-cells in response to elevated glucose concentrations and activates the GLP-1 receptors on the pancreatic β-cells.[50] The activated GLP-1 receptor (GLP-1R), engages with the trimeric G-protein complex and consequently augments insulin secretion through multiple mechanisms including but not restricted to: i) potentiation of glucose-initiated cell membrane depolarization, ii) delay of membrane repolarization, iii) increased permeability of the voltage-gated calcium channel (VGCC), iv) promotion of calcium-induced calcium release (CICR), iv) increased ATP production in the presence of glucose, vi) promotion of larger releasable insulin pools and the

refilling of depleted pools.[50] GLP-1R-promoted insulin secretion is dependent upon glucose-initiated events, and is thus only pronounced through glucose stimulation.

As expected, in the static GSIS experiments, exendin-4 potentiated insulin secretion in a glucose-dependent manner displaying the first small but significant increase in insulin secretion at 5.5 mM glucose with increasing effects at higher glucose concentrations, e.g., from 0.40 to 0.91 fmol IEQ^{-1} min^{-1} at 16.7 mM glucose (Figure 4c). Similarly, addition of exendin-4 did not influence basal insulin secretion at 2.8 mM glucose in perfusion experiments (Figure 4d). During this pre-stimulation phase (80-110 min) the total secreted insulin was in average 3.5 fmol in the vehicle control and 4.0 fmol for exendin-4. An increase in glucose-stimulated insulin secretion was mostly present in the second phase (120-180 min). The total secreted insulin was on average 83.7 fmol in the vehicle control and 128.0 fmol for exendin-4.

Further, the measurements in Figure 4 show, that islets in the perfused hanging drop secrete insulin at higher rates compared to the static well plate condition. The baseline secretion of untreated islets under static conditions is 0.01 fmol IEQ^{-1} min^{-1} at 2.8 mM glucose and 0.40 fmol IEQ^{-1} min^{-1} at 16.7 mM glucose. Untreated islets under perfused conditions secrete insulin at an average rate of 0.13 fmol IEQ^{-1} min^{-1} at 2.8 mM glucose and 1.56 fmol IEQ^{-1} min^{-1} at 16.7 mM glucose. Tolbutamide and exendin-4 increased insulin secretion under perfusion in the high-glucose phase to 1.65 fmol IEQ^{-1} min^{-1} and 2.30 fmol IEQ^{-1} min^{-1} respectively. Figure S6a (Supporting Information) shows that the viability of islets was not affected by the compounds for concentrations of 25 µM tolbutamide, 100 nM exendin-4 and 0.1% DMSO as the vehicle control.

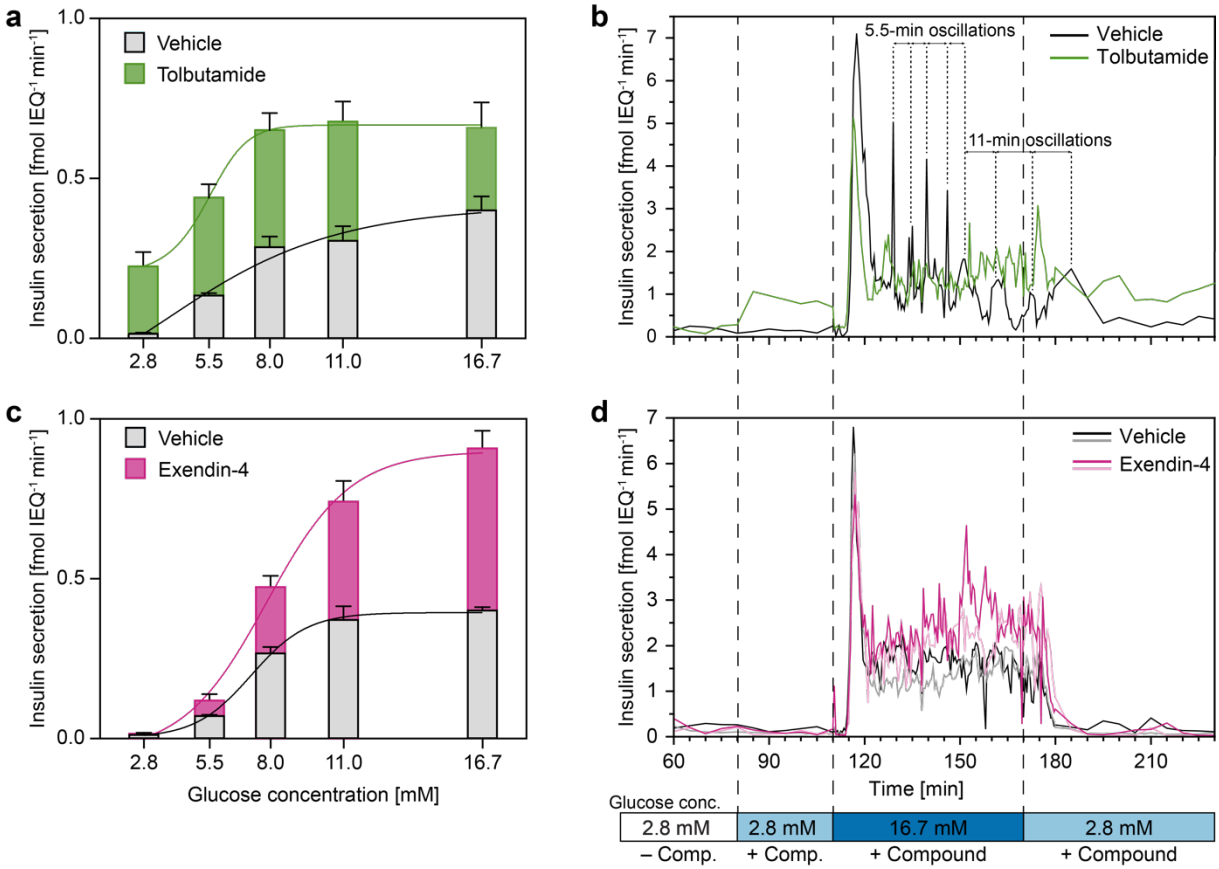

Figure 4 Static well plate and high-resolution FlowGSIS experiments on single human islet microtissues. The secretion of insulin was stimulated with different glucose concentrations ranging from 2.8 mM up to 16.7 mM. (**a**) Insulin secretion under static conditions with 25 µM tolbutamide (green, n=5 islets for each condition) and (**c**) 100 nM exendin-4 (red, n=6 islets for each condition). (**b**) Resolving the insulin secretion dynamics by using single islets treated with tolbutamide (green) and (**d**) exendin-4 (purple). More FlowGSIS measurements for tolbutamide (different donors) are shown in Figure S8 (Supporting Information). Islets from two different donors were used (Donor A for tolbutamide, Donor D for exendin-4), and the measurements were compared to control islets from the same donor without compound dosage (black and grey). More details are shown in Figure S9 and S10 (Supporting Information). The highly dynamic biphasic insulin secretion with a prominent first phase and a sustained, pulsatile second phase was detected under all conditions. Data obtained under static conditions represent mean values ± standard deviations.

5.4.5 Compounds influence mechanistic parameters

Exendin-4 and tolbutamide altered the dynamics of insulin release of islets in FlowGSIS assays. We analyzed the data by looking at characteristic parameters, which we extracted from

the high-resolution FlowGSIS measurements to get more insights in how both compounds change the insulin secretion pattern of islets.

Figure 5a describes the distribution of total secreted insulin in all phases of insulin release during FlowGSIS. This analysis provides information about the shape of the GSIS curve and it shows how compounds change this characteristic insulin release pattern. In general, insulin was predominantly released during the high-glucose phase (1st phase and 2nd phase). The baseline secretion was not affected by the compounds. Tolbutamide increased insulin release in the pre-stimulation phase and in the post-stimulation phase at low glucose levels (2.8 mM). The early release of insulin in the pre-stimulation phase reduced insulin release in the high-glucose phase (16.7 mM), which was especially pronounced in the 2nd phase. This shows that tolbutamide altered the dynamics of insulin release during GSIS, whereas exendin-4 did not change the shape of the insulin secretion patterns in comparison to the control. The total amount of secreted insulin in all phases depends on the duration and timing of the low and high glucose conditions in the GSIS.

Figure 5b shows how exendin-4 and tolbutamide affect the insulin secretion rate in each phase of the FlowGSIS. Tolbutamide increased the secretion rate of insulin at low glucose (2.8 mM) concentrations – the pre-stimulation phase –12.9 ± 7.7 fold, and in the post-stimulation phase 3.67 ± 3.32 fold. The peak secretion rate and the secretion rate during high-glucose phases (predominantly 1st phase) were reduced by 0.72 ± 0.01 and 0.84 ± 0.26, respectively. Exendin-4 had no effect on the secretion rate in the pre-stimulation phase (1.12 ± 0.29). The peak secretion and the 1st phase were not affected (0.93 ± 0.11 and 0.94 ± 0.04). Exendin-4 increased the insulin secretion rate in the high-glucose phase (predominantly 2nd phase) 1.53 ± 0.16 fold, and reduced the secretion in the post-stimulation phase 0.57 ± 0.27 fold.

Figure 5c describes how both compounds affect the timing of insulin release during FlowGSIS relative to the control. The response time ($t_{Response}$, exendin-4: 0.85 ± 0.31; tolbutamide: 0.98 ± 0.21) and the duration of the 1st phase (t_{Ph1}, exendin-4: 0.92 ± 0.04; 0.91 ± 0.10) were not affected by the compounds, whereas exendin-4 reduced (0.70 ± 0.42) and tolbutamide increased (1.23 ± 0.61) the time to reach peak secretion (t_{peak}). Exendin-4 had no effect on the relaxation time ($t_{Relaxation}$) (0.97 ± 0.04), whereas tolbutamide largely extended this phase (2.85 ± 1.83).

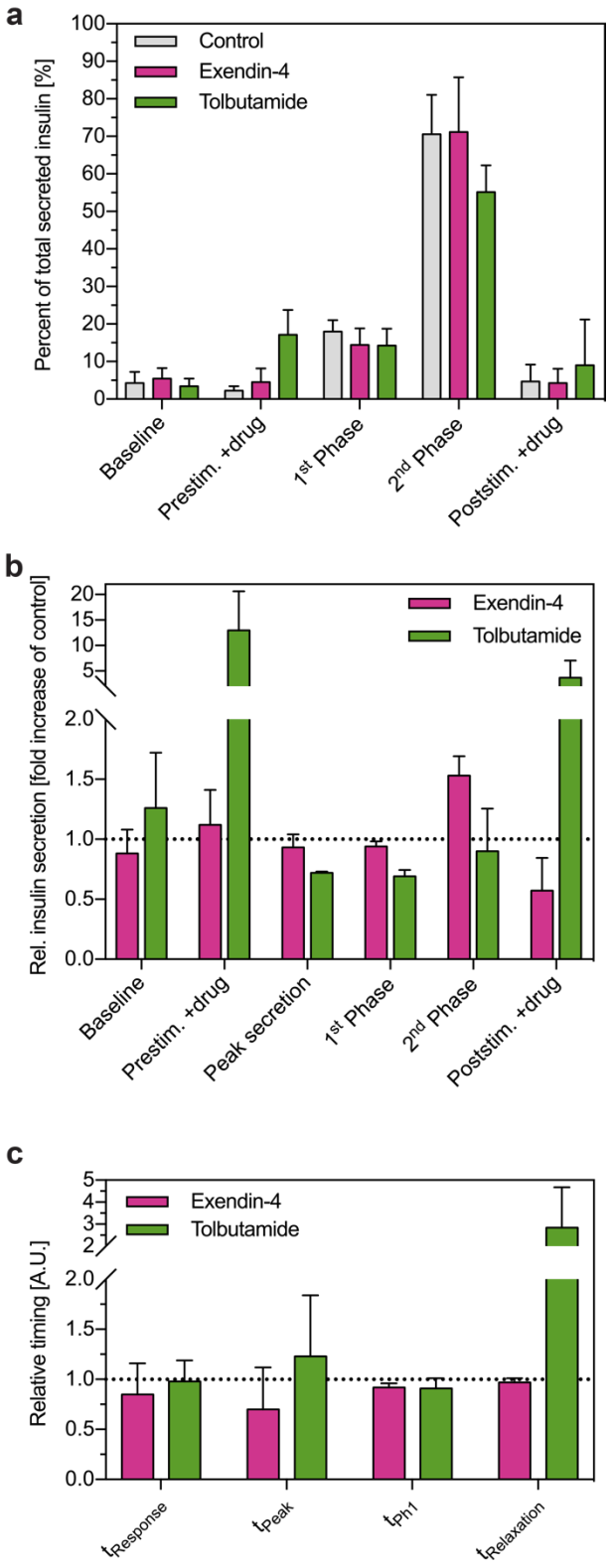

Figure 5 Effects of exendin-4 (red) and tolbutamide (green) on the dynamics of insulin secretion. (**a**) Distribution of insulin secretion in different phases of insulin release during FlowGSIS assays. The data represent the amount of insulin that was secreted in each phase relative to the total secreted insulin of the full FlowGSIS (control n=5 islets; exendin-4 n=3

islets; tolbutamide n=3 islets). (**b**) Effects of compounds on the secretion rate in different phases of GSIS. The data represent average insulin secretion rates during each phase of a FlowGSIS relative to the control of the same donor (exendin-4 n=2 islets; tolbutamide, n=3 islets). (**c**) Effects of compounds on the average timing of insulin release relative to the control of the same donor (exendin-4, n=2 donors; tolbutamide, n=3 donors). Data represent mean values ± standard deviations.

5.5 Conclusion

We presented a standardized human islet model in combination with a microfluidic hanging-drop perfusion system to study the insulin secretion dynamics of single islets. Re-aggregated islets showed highly reproducible and robust GSIS with stable function and viability over weeks. The miniaturized perfusion system enabled us to study GSIS from such individual islets in a precise manner at high temporal resolution. The use of the hanging-drop technology overcomes dispersion effects and sample dilution in closed microfluidic systems. The technology enables rapid medium switches and short sampling intervals, which, in turn, facilitates to resolve fast changes in the secretion dynamics of islets. At the same time, the islet microtissues are easy to load and retrieve from the perfusion chamber, i.e., the hanging drop, the liquid-air interface of which helps to preserve microtissue morphology and enables controlled oxygen supply. Due to gravity, the microtissues are inherently located at the bottom of the drop and experience the same flow conditions during the experiments, which promotes reproducibility.

The newly developed high-resolution FlowGSIS assay enabled us to resolve the native biphasic and pulsatile insulin release of single islet microtissues and to better characterize this release by extracting distinct dynamic parameters. In general, culturing islets under perfusion results in higher secretion rates of insulin compared to static culturing. We observed a high reproducibility of the bi-phasic insulin secretion across islets from different donors and we resolved the oscillatory release of insulin of single islets. The timing of GSIS, especially the response time and the duration of the 1st phase, was well preserved across different islets. More variability was seen in the average secretion rates across islets from different donors.

Further, we studied the effects of two pharmaceutical compounds and investigated how they altered the insulin release dynamics of islet microtissues. Compared to a standard GSIS, performed in well plates, the perfusion results enabled to better assign compound-related

stimulation effects to the respective secretion phases and so that physiologically relevant information on the single-islet level could be extracted.

The presented assay platform combines reproducible human islet microtissue technology with an application-specific microfluidic perfusion system for precise and reproducible insulin secretion analysis. The platform enables deeper insight in the release mechanisms and physiology of pancreatic islets and constitutes a promising tool for diabetes research.

5.6 Acknowledgements

This work was financially supported by the Swiss CTI (grant 18024.1 PFLS-LS) and the Swiss National Science Foundation (SNF 2-77079-16 Infected body-on-chip).

5.7 Supporting Information

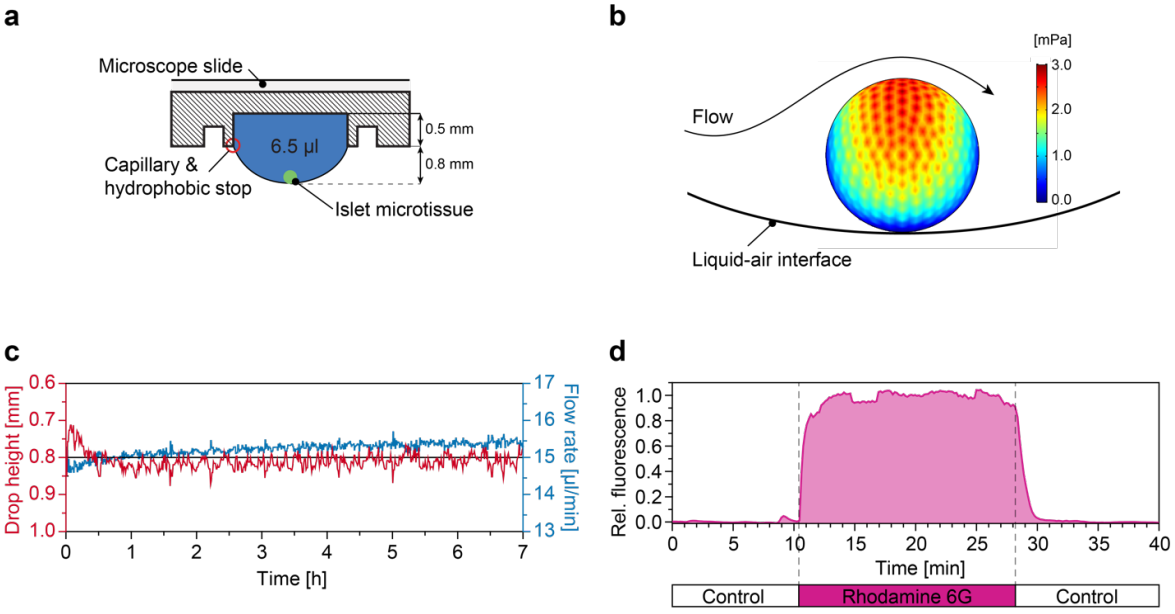

Figure S1 (**a**) Cross-section through a microfluidic hanging drop chip hosting an islet microtissue. The islet is located at the liquid-air interface at the bottom of the hanging drop and is fully accessible. (**b**) Modeling results of shear-stress on the islet microtissue (150 µm diameter) in a hanging drop (0.8 mm in height), caused by medium perfusion at 15 µl min^{-1}. (**c**) Stable operation of the perfused hanging drop. The height of the hanging drop was set to 0.8 mm and was kept stable, while it was perfused at a constant flow rate of 15 µl min^{-1}. (**d**) A fluorescent dye (Rhodamine 6G) was infused into the chip, and the fluorescence in the drop was measured every 10 seconds. A full medium exchange in the hanging drop was reached after ~2 min.

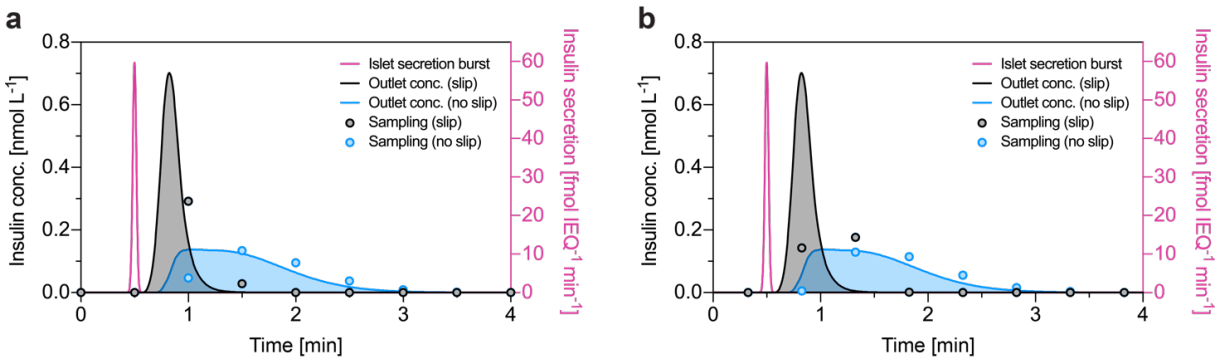

Figure S2 Modeling results of insulin concentration at the outlet of the chip following a sharp 1-s-long insulin secretion burst at the islet (purple), which is equivalent to an experimentally measured secretion of 2.5 fmol over one sample interval. The resulting outlet concentration were obtained assuming either slip (black) or no-slip (blue) boundary conditions at the bottom of the drop. The resulting expected experimental sample points are shown for a sampling rate of two samples per minute for both, slip (black dots) and no-slip (blue dots) boundary conditions. (**a**) In-phase sampling. A secretion peak was resolved with one sampling point (black dots). (**b**) Out-of-phase sampling. A secretion peak was resolved with two sampling points (red dots).

Movie S3 (**a**) Insulin secretion from an islet microtissue and the flow-mediated transport of secreted insulin at the liquid-air surface for slip (black) and no-slip (blue) conditions. A sharp 1-s-long secretion burst of 2.5 fmol insulin of the islet was simulated. (**b**) Modeling of insulin concentration at the outlet of the chip. The resulting concentration at the outlet was obtained assuming either slip- (black) or no-slip (blue) boundary conditions at the bottom of the drop for in-phase sampling. (**c**) The resulting sample points and concentrations are shown for a sampling rate of two samples per minute for both, slip- (black dots) and no-slip (blue dots) boundary conditions.

Table S4 Characteristics and parameter set that can be extracted from high-resolution FlowGSIS assays.

Glucose concentration	GSIS Phases	Characteristics of insulin release dynamics
2.8 mM	**Baseline**	Average secretion rate
		Total secreted insulin
		Variability of secretion rate
	Pre-stimulation	Response time
		Average secretion rate
		Total secreted insulin
		Variability of secretion rate
16.7 mM	**Dip**	Appearance of dip
		Dip (minimal) secretion
	1st Phase	Response time
		Average secretion rate
		Total secreted insulin
		Time to reach peak
		Peak (maximum) secretion
	2nd Phase	Average secretion rate
		Total secreted insulin
		Appearance of oscillations!?
		Frequency of oscillations
		Insulin depletion (relaxation in insulin release)
		Relaxation time after switching to low glucose
2.8 mM	**Post-stimulation**	Response time (Relaxation)
		Average secretion rate
		Total secreted insulin
		Variability of secretion rate

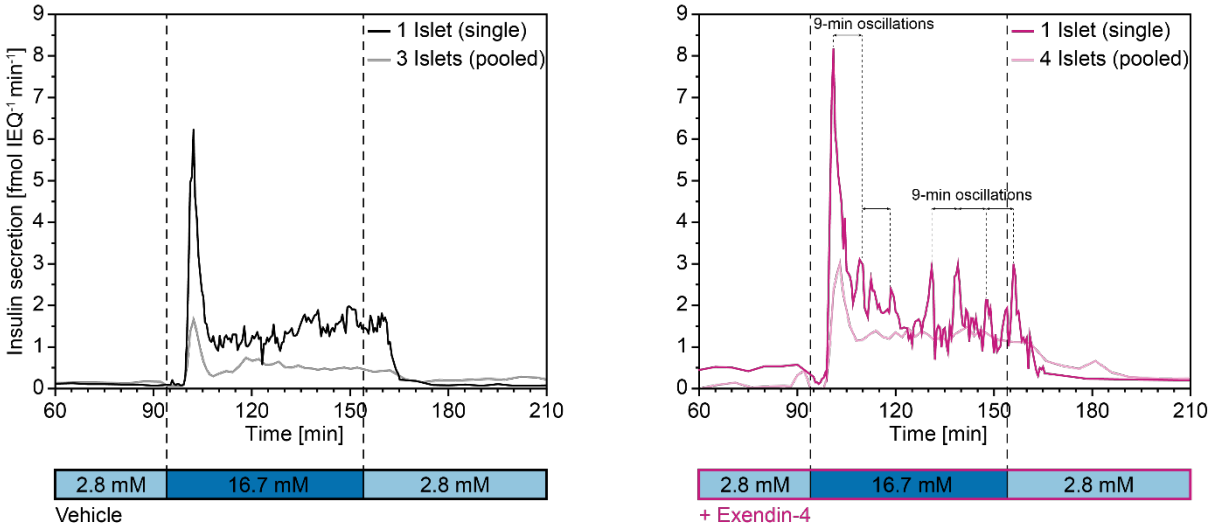

Figure S5 FlowGSIS with single islets vs. pooled islets for a control GSIS (left) and a GSIS with exendin-4 (right). A switch from low (2.8 mM) to high (16.7 mM) glucose concentrations induced highly dynamic insulin secretion in a bi-phasic manner with a dip at the beginning, a prominent 1st phase, which was followed by a sustained, pulsatile 2nd phase. Islets from two different donors were used for the GSIS in the vehicle control (left). Islets from a single donor were used for GSIS with exendin-4 (right). GSIS with single islets showed higher insulin secretion rates compared to pooled islets under both conditions. Exendin-4 stimulated insulin secretion in both, 1st and 2nd phase for both, the single islets and the pooled islets, compared to the vehicle control. Continuous sampling for single islet measurements every 5 min during low-glucose conditions (60-95 min and 165-230 min) and every 30 s in the high-glucose phase (95-165 min). GSIS with pooled islets was measured at lower temporal resolution. Samples were taken every 5 min during low glucose (60-95 and 150-210 min), every 1 min (95-110 min), and every 2 mins (110-150 min) in the high-glucose phase.

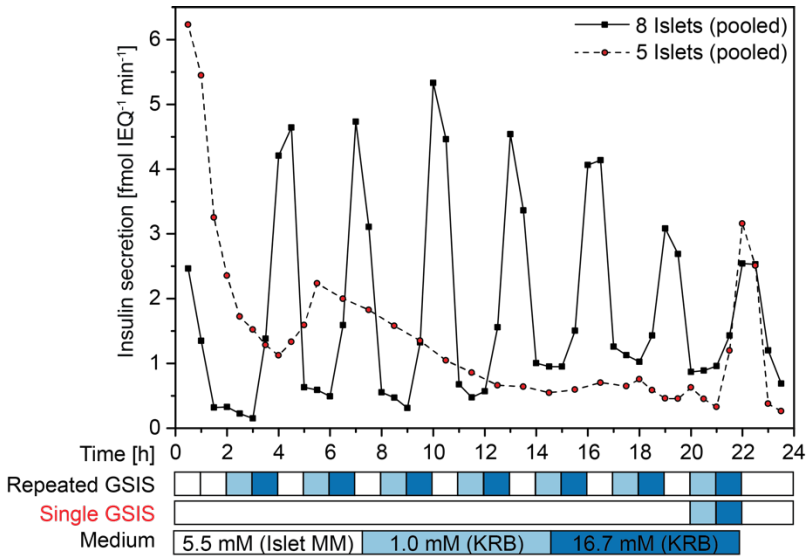

Figure S7 Repeated FlowGSIS. Islets were subjected to seven FlowGSIS (black). Pooled islets (8 islets for the seven FlowGSIS, and 5 islets for the single FlowGSIS) were successively exposed to 5.5 mM, 1 mM and 16.7 mM glucose for 1 h. The medium was continuously perfused at a flow rate of 5.5 µl min^{-1}, and samples were collected every 30 min.

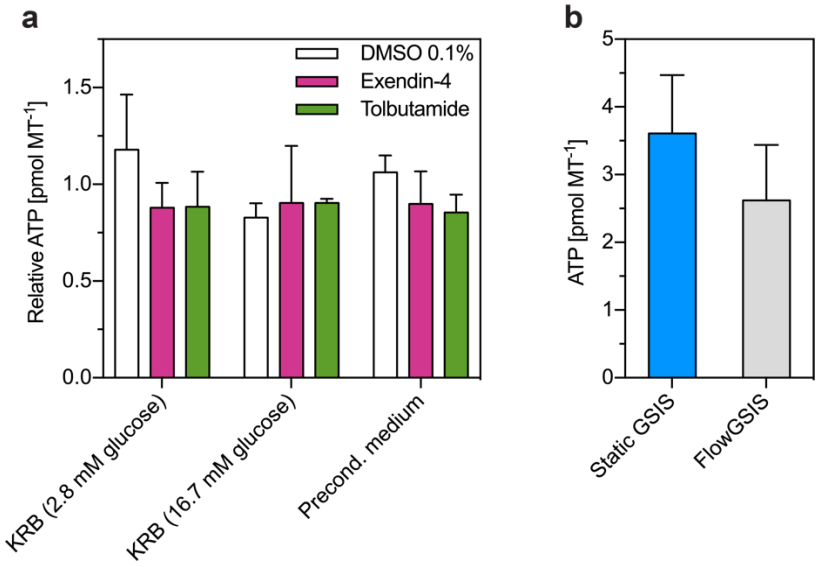

Figure S6 Viability of human islet microtissues. (**a**) Relative ATP content in human islet microtissues after exposure to compounds in different media. Islets were cultured in a static well plate for 310 min. The ATP content was normalized to that of islets that were cultured in pure medium for each condition (2.8, 16.7 mM glucose (KRB) and preconditioning medium). Three islets were analyzed for each condition (n=3 islets). (**b**) Absolute ATP content in human islet microtissues. The data shows the ATP content after the static GSIS (n=36 islets), and after the FlowGSIS (n=3 islets). Data represent mean values ± standard deviations.

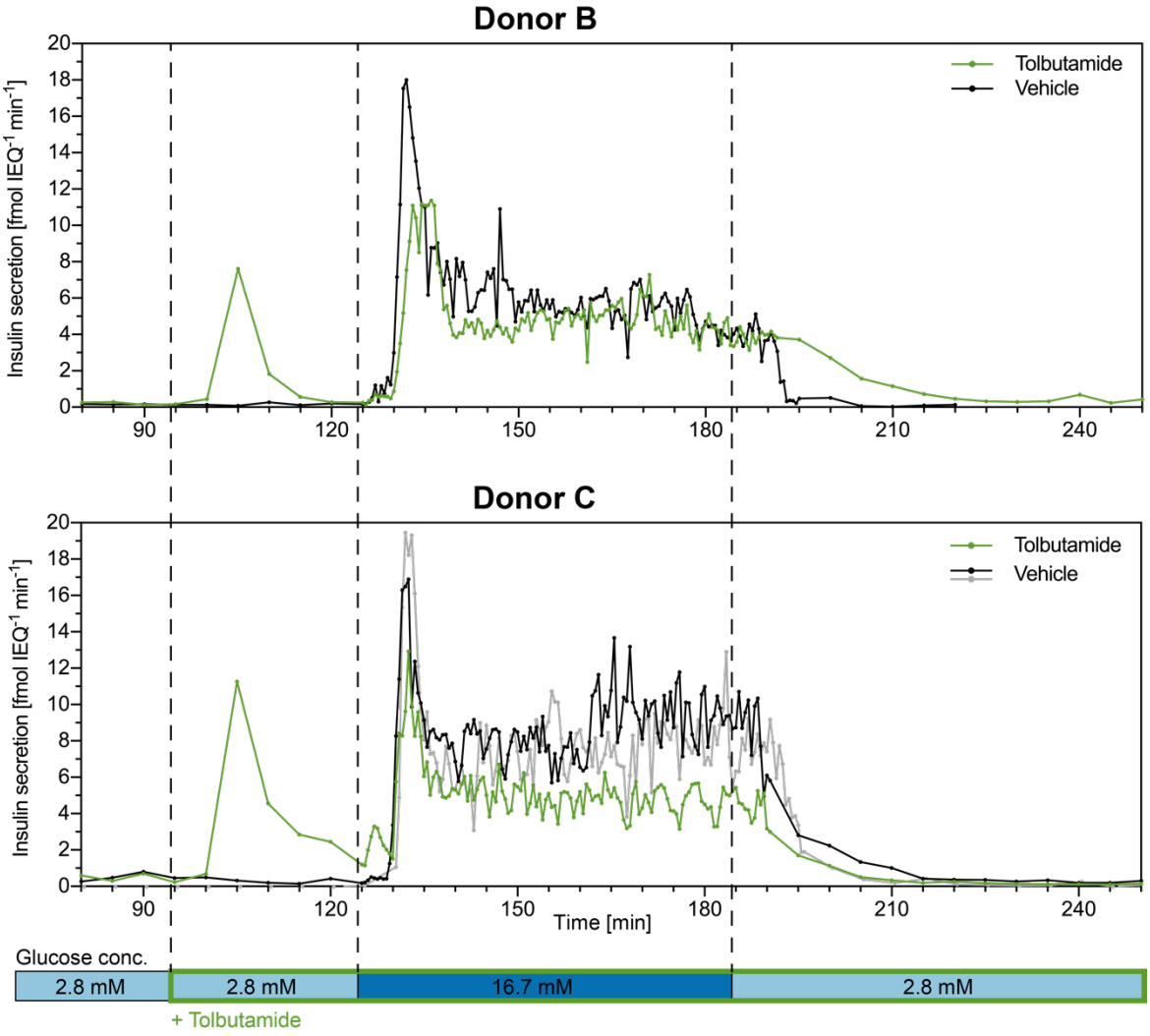

Figure S8 High-resolution FlowGSIS measurements on single islet microtissues from two individual donors (B and C). Islets were treated with 25 µM tolbutamide (green) to assess its effects in comparison to the vehicle control (black and grey). Samples were continuously taken every 5 min during low-glucose conditions (80-125 min and 195-250 min) and every 30 s in the high-glucose phase (125-195 min).

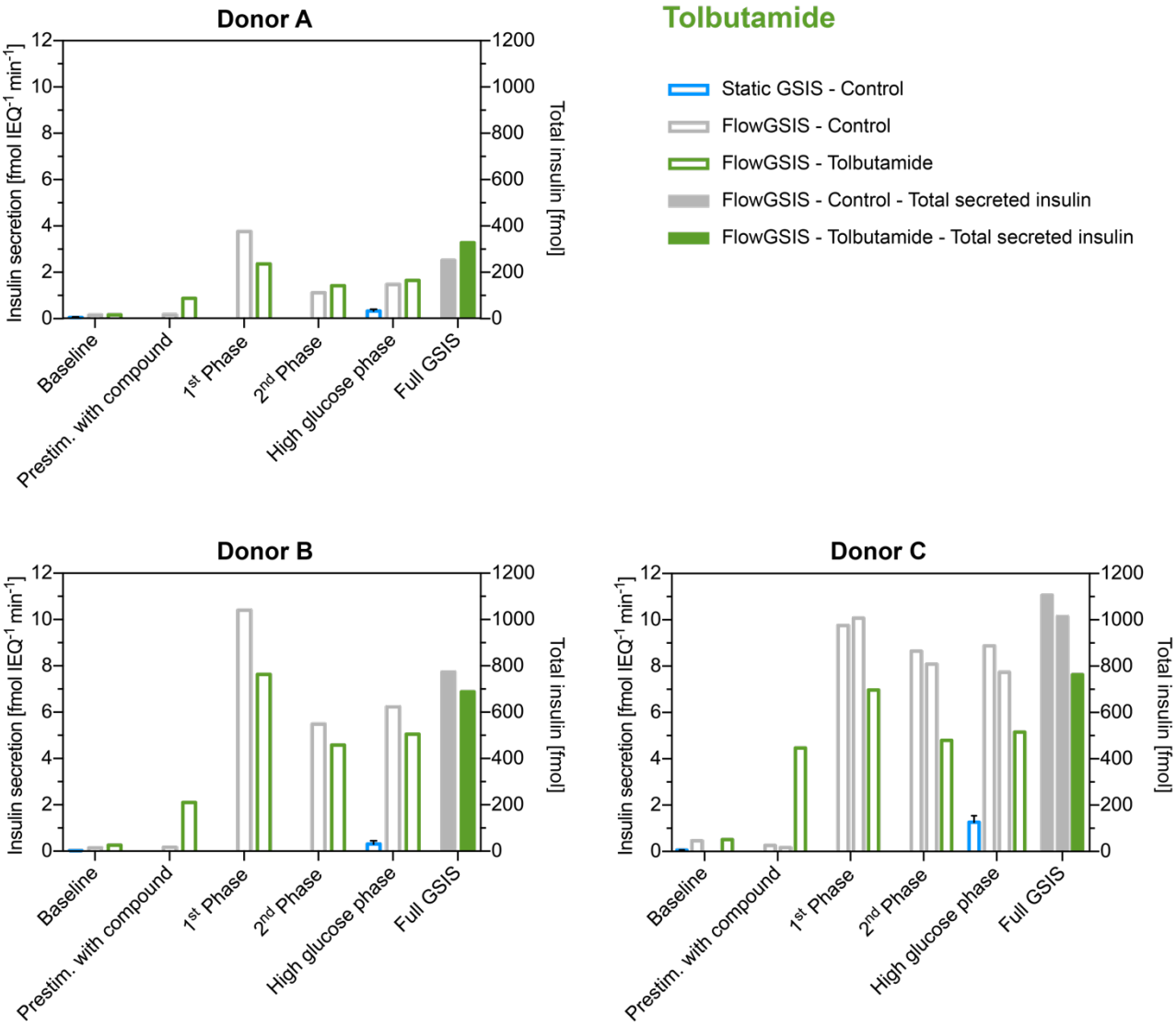

Figure S9 Average insulin secretion rate in each phase of the GSIS (left y-axis), and the total secreted insulin during the full GSIS (right y-axis). Effects of tolbutamide (green) vs. vehicle control (grey) were measured under perfused and static conditions and with islets of three individual donors (A, B and C).

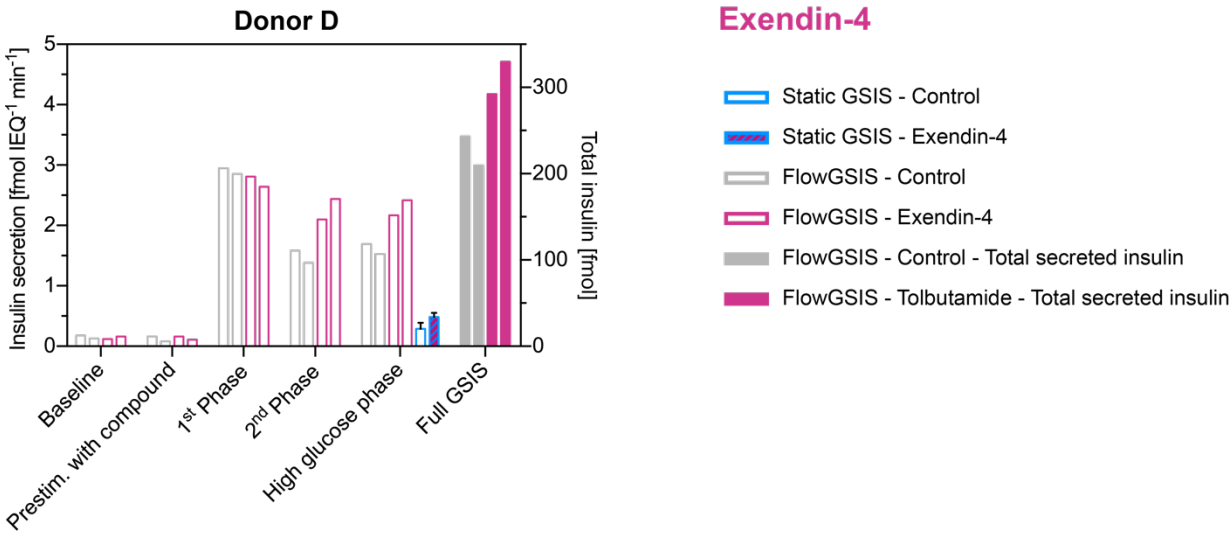

Figure S10 Average insulin secretion rate in each phase of GSIS (left y-axis), and the total secreted insulin during the full GSIS (right y-axis). Effects of 100 nM exendin-4 (purple) vs. vehicle control (grey) were measured under perfused and static conditions with islets of one individual donors (D).

5.8 References

1. In't Veld, P. & Marichal, M. in *The Islets of Langerhans* (ed. Islam, M. S.) **654,** 1–19 (Springer Netherlands, 2010).
2. Bell, G. I. & Polonsky, K. S. Diabetes mellitus and genetically programmed defects in beta-cell function. *Nature* **414,** 788–91 (2001).
3. Seino, S., Shibasaki, T. & Minami, K. Dynamics of insulin secretion and the clinical implications for obesity and diabetes. *J. Clin. Invest.* **121,** 2118–25 (2011).
4. Ahrén, B. Autonomic regulation of islet hormone secretion--implications for health and disease. *Diabetologia* **43,** 393–410 (2000).
5. Rutter, G. A. & Hodson, D. J. Minireview: intraislet regulation of insulin secretion in humans. *Mol. Endocrinol.* **27,** 1984–95 (2013).
6. El-Ali, J., Sorger, P. K. & Jensen, K. F. Cells on chips. *Nature* **442,** 403–11 (2006).
7. Dittrich, P. S. & Manz, A. Lab-on-a-chip: microfluidics in drug discovery. *Nat. Rev. Drug Discov.* **5,** 210–8 (2006).
8. Kovarik, M. L. *et al.* Micro total analysis systems for cell biology and biochemical assays. *Anal. Chem.* **84,** 516–40 (2012).
9. Rocheleau, J. V, Walker, G. M., Head, W. S., McGuinness, O. P. & Piston, D. W. Microfluidic glucose stimulation reveals limited coordination of intracellular Ca2+ activity oscillations in pancreatic islets. *Proc. Natl. Acad. Sci. U. S. A.* **101,** 12899–903 (2004).
10. Nourmohammadzadeh, M. *et al.* A microfluidic array for real-time live-cell imaging of human and rodent pancreatic islets. *Lab Chip* **16,** 1466–72 (2016).
11. Brooks, J. C., Ford, K. I., Holder, D. H., Holtan, M. D. & Easley, C. J. Macro-to-micro interfacing to microfluidic channels using 3D-printed templates: application to time-resolved secretion sampling of endocrine tissue. *Analyst* **141,** 5714–5721 (2016).
12. Heileman, K. *et al.* Microfluidic platform for assessing pancreatic islet functionality through dielectric spectroscopy. *Biomicrofluidics* **9,** 044125 (2015).
13. Godwin, L. a *et al.* Passively operated microfluidic device for stimulation and secretion sampling of single pancreatic islets. *Anal. Chem.* **83,** 7166–72 (2011).
14. Shackman, J. G., Reid, K. R., Dugan, C. E. & Kennedy, R. T. Dynamic monitoring of

glucagon secretion from living cells on a microfluidic chip. *Anal. Bioanal. Chem.* **402,** 2797–2803 (2012).

15. Adewola, A. F. *et al.* Microfluidic perifusion and imaging device for multi-parametric islet function assessment. *Biomed. Microdevices* **12,** 409–17 (2010).

16. Mohammed, J. S., Wang, Y., Harvat, T. a, Oberholzer, J. & Eddington, D. T. Microfluidic device for multimodal characterization of pancreatic islets. *Lab Chip* **9,** 97–106 (2009).

17. Lenguito, G. *et al.* Resealable, optically accessible, PDMS-free fluidic platform for ex vivo interrogation of pancreatic islets. *Lab Chip* **17,** 772–781 (2017).

18. Cabrera, O. *et al.* Automated, high-throughput assays for evaluation of human pancreatic islet function. *Cell Transplant.* **16,** 1039–48 (2008).

19. Dishinger, J. F., Reid, K. R. & Kennedy, R. T. Quantitative monitoring of insulin secretion from single islets of Langerhans in parallel on a microfluidic chip. *Anal. Chem.* **81,** 3119–27 (2009).

20. Dishinger, J. F. & Kennedy, R. T. Serial immunoassays in parallel on a microfluidic chip for monitoring hormone secretion from living cells. *Anal. Chem.* **79,** 947–54 (2007).

21. Nunemaker, C. S. *et al.* Glucose metabolism, islet architecture, and genetic homogeneity in imprinting of [Ca2+](i) and insulin rhythms in mouse islets. *PLoS One* **4,** e8428 (2009).

22. Ritzel, R. A., Veldhuis, J. D. & Butler, P. C. Glucose stimulates pulsatile insulin secretion from human pancreatic islets by increasing secretory burst mass: dose-response relationships. *J. Clin. Endocrinol. Metab.* **88,** 742–7 (2003).

23. Yi, L. *et al.* Integrated perfusion and separation systems for entrainment of insulin secretion from islets of Langerhans. *Lab Chip* **15,** 823–832 (2015).

24. Roper, M. G., Shackman, J. G., Dahlgren, G. M. & Kennedy, R. T. Microfluidic chip for continuous monitoring of hormone secretion from live cells using an electrophoresis-based immunoassay. *Anal. Chem.* **75,** 4711–4717 (2003).

25. Shackman, J. G., Dahlgren, G. M., Peters, J. L. & Kennedy, R. T. Perfusion and chemical monitoring of living cells on a microfluidic chip. *Lab Chip* **5,** 56–63 (2005).

26. Frey, O., Misun, P. M., Fluri, D. A., Hengstler, J. G. & Hierlemann, A. Reconfigurable microfluidic hanging drop network for multi-tissue interaction and analysis. *Nat. Commun.* **5,** 4250 (2014).

27. de Groot, T. E., Veserat, K. S., Berthier, E., Beebe, D. J. & Theberge, A. B. Surface-tension driven open microfluidic platform for hanging droplet culture. *Lab Chip* **16,** 334–344 (2016).

28. Toepke, M. W. & Beebe, D. J. PDMS absorption of small molecules and consequences in microfluidic applications. *Lab Chip* **6,** 1484–6 (2006).

29. Ohta, M., Nelson, D., Nelson, J., Meglasson, M. D. & Erecińska, M. Oxygen and temperature dependence of stimulated insulin secretion in isolated rat islets of Langerhans. *J. Biol. Chem.* **265,** 17525–32 (1990).

30. Dionne, K. E., Colton, C. K. & Yarmush, M. L. A microperifusion system with environmental control for studying insulin secretion by pancreatic tissue. *Biotechnol. Prog.* **7,** 359–68 (1991).

31. Nourmohammadzadeh, M. *et al.* Microfluidic array with integrated oxygenation control for real-time live-cell imaging: effect of hypoxia on physiology of microencapsulated pancreatic islets. *Anal. Chem.* **85,** 11240–9 (2013).

32. Lo, J. F. *et al.* Islet preconditioning via multimodal microfluidic modulation of intermittent hypoxia. *Anal. Chem.* **84,** 1987–93 (2012).

33. Buchwald, P. A local glucose-and oxygen concentration-based insulin secretion model for pancreatic islets. *Theor. Biol. Med. Model.* **8,** 20 (2011).

34. Silva, P. N., Green, B. J., Altamentova, S. M. & Rocheleau, J. V. A microfluidic device designed to induce media flow throughout pancreatic islets while limiting shear-induced damage. *Lab Chip* **13,** 4374–84 (2013).

35. Lang, M., Rudolf, F. & Stelling, J. Use of YouScope to implement systematic microscopy protocols. *Curr. Protoc. Mol. Biol.* **Chapter 14,** Unit 14.21.1-23 (2012).

36. Kapusta, P. in *Application Note* (PicoQuant GmbH, Berlin, 2010).

37. Müller, C. B. *et al.* Precise measurement of diffusion by multi-color dual-focus fluorescence correlation spectroscopy. *EPL (Europhysics Lett.* **83,** 46001 (2008).

38. Ichii, H. *et al.* Shipment of human islets for transplantation. *Am. J. Transplant* **7,** 1010–

20 (2007).

39. Kin, T. *et al.* Risk factors for islet loss during culture prior to transplantation. *Transpl. Int.* **21,** 1029–35 (2008).

40. Halban, P. A., Powers, S. L., George, K. L. & Bonner-Weir, S. Spontaneous reassociation of dispersed adult rat pancreatic islet cells into aggregates with three-dimensional architecture typical of native islets. *Diabetes* **36,** 783–90 (1987).

41. Kuo, C. Y., Herrod, H. G. & Burghen, G. A. Formation of pseudoislets from human pancreatic cultures. *Pancreas* **7,** 320–5 (1992).

42. Matta, S. G., Wobken, J. D., Williams, F. G. & Bauer, G. E. Pancreatic islet cell reaggregation systems: efficiency of cell reassociation and endocrine cell topography of rat islet-like aggregates. *Pancreas* **9,** 439–49 (1994).

43. Shizuru, J., Trager, D. & Merrell, R. C. Structure, function, and immune properties of reassociated islet cells. *Diabetes* **34,** 898–903 (1985).

44. Wolf-Jochim, M., Wöhrle, M., Federlin, K. & Bretzel, R. G. Comparison of the survival of fresh or cultured pancreatic islets, pseudoislets and single cells following allotransplantation beneath the kidney capsule in non-immunosuppressed diabetic rats. *Exp. Clin. Endocrinol. Diabetes* **103 Suppl,** 118–22 (1995).

45. Tze, W. J. & Tai, J. Allotransplantation and xenotransplantation of pseudoislets in diabetic rats and mice. *Transplantation* **38,** 438–40 (1984).

46. Cabrera, O. *et al.* The unique cytoarchitecture of human pancreatic islets has implications for islet cell function. *Proc. Natl. Acad. Sci. U. S. A.* **103,** 2334–9 (2006).

47. Pisania, A. *et al.* Quantitative analysis of cell composition and purity of human pancreatic islet preparations. *Lab. Invest.* **90,** 1661–75 (2010).

48. Tsuura, Y., Fujimoto, S., Kajikawa, M., Ishida, H. & Seino, Y. Regulation of intracellular ATP concentration under conditions of reduced ATP consumption in pancreatic islets. *Biochem. Biophys. Res. Commun.* **261,** 439–44 (1999).

49. Proks, P., Reimann, F., Green, N., Gribble, F. & Ashcroft, F. Sulfonylurea stimulation of insulin secretion. *Diabetes* **51 Suppl 3,** S368-76 (2002).

50. Doyle, M. E. & Egan, J. M. Mechanisms of action of glucagon-like peptide 1 in the pancreas. *Pharmacol. Ther.* **113,** 546–93 (2007).

6 CONCLUSION

Novel 3D cell-culture systems, such as 3D spherical microtissues, are an emerging and relevant *in vitro* model system. Microfluidic hanging-drop platforms provide a suitable and versatile tool for the culture and analysis of spherical 3D microtissues.

Enabling Features of Hanging Drops

The main common feature of the presented platforms is the hanging-drop structure, which enables seeding, formation, long-term culturing, and imaging of 3D microtissues. Hanging-drops are also readily accessible for harvesting of the tissues for further downstream analysis. Microtissues are inherently positioned at the bottom of the hanging drop, and their precise placement is achieved without the need for additional traps or guiding structures. This feature is especially important for providing undisturbed culturing of the tissues and to avoid microtissue-surface interactions, which could affect tissue integrity and functionality. Moreover, open microfluidic hanging drops provide the advantage of ensuring optimal gas exchange and avoiding bubble formation.

Microfluidic hanging drops can be perfused with high precision. This is an important feature, as it enables controlled transport of nutrients, removal of waste and of secretory products from the microtissues. Further, through hanging drops, tissue viability is supported by maintaining minimal shear stress. Additionally, perfusion allows for the interconnection of multiple hanging-drop compartments to host different tissue types within a single network. This configuration enables the study of multi-tissue interactions for body-on-a-chip applications. Finally, all presented platforms are optically and fluidically accessible making them versatile tools that can be augmented with additional microfluidic features including gradient generators, valves and pumps.

In this thesis, I presented the fabrication, characterization and operation of three different hanging-drop network platforms, which have been designed for specific readout and application purposes: (i) to monitor the metabolism of single microtissues by using integrated biosensors, (ii) to observe the morphology of microtissues at different spatiotemporal scales

through microscopy imaging, and (iii) to measure the dynamic release of secretory products of single microtissues by optimized liquid handling.

Biosensing in Hanging-Drop Networks

Hanging-drop networks with integrated electrochemical biosensors for real-time *in situ* monitoring of glucose and lactate metabolism of human colon cancer microtissues were presented. The sensors were integrated by using a hybrid-system integration approach, which potentially allows for incorporation of a wide variety of sensor types.

Hanging drops ensured the stable positioning of microtissues in close proximity to the biosensor electrodes, without the use of physical microtissue traps. This feature is fundamental for producing an undisturbed culturing environment, and consequently for enabling accurate and reproducible measurements.

The platform featured sensors for continuous *in situ* measurements of metabolite consumption and molecule secretion of single microtissues for several hours. Such a high level of sensitivity was possible owing to the small culture volumes and the close proximity of the sensors to the microtissues. These features are necessary to measure concentration changes that originate from small biological samples and occur on a time scale of minutes. In contrast to existing analysis methods using discrete sampling and analysis, continuous measurements through integrated sensors reduce the risk to miss important events, which may go undetected if the sampling interval is too long.

Consequently, the platform can be used to provide new insights into the metabolism of cancer microtissues by precisely measuring their glucose consumption and lactate secretion. However, the long-term stability of the electrochemical sensors still remains a challenge, and an optimization of the functional layer needs to be carried out to monitor processes extending over multiple days.

High-Resolution Imaging in Hanging-Drop Networks

A hanging-drop platform for the precise and stable immobilization of 3D microtissues in a perfused and controlled microenvironment was presented. The stable immobilization of microtissues is essential for high-resolution time-lapse imaging. The immobilization was achieved by embedding the microtissues in hanging hydrogel drops in a microfluidic channel.

The fabrication of the microfluidic chips is straightforward, the operation is simple and robust, and the setup complexity is kept to a minimum. The use of standard laboratory equipment, such as pipettes for loading of the hydrogel and tissues and syringe pumps for perfusion, is sufficient to operate the platform, which renders this approach readily applicable and affordable. The platform is compatible with many microscope technologies and setups including wide-field (bright-field and fluorescence) and confocal microscopy. The use of transparent materials, namely glass and PDMS, assures interference-free high-quality imaging to observe biological processes at various spatiotemporal scales. Perfusion enables *in situ* staining and imaging of the microtissues with minimal background signal, as washing of the tissue and hydrogel can be performed without disconnecting the chip and removing the hydrogel drops. The non-permanent bonding of the fluidic structure to the glass substrate allows for simple manual harvesting of the tissues for downstream analysis.

The platform is especially suited for microtissue cultures that require hydrogels to better mimic the *in vivo* microenvironment. The combination of multiple interconnected drops enables multi-tissue experiments, which, combined with the high imaging resolution attainable, opens up a large range of biological applications.

FlowGSIS in Hanging-Drops

A microfluidic hanging-drop perfusion system to precisely measure the secretion dynamics of endocrine microtissues at high temporal resolution was introduced in the last chapter of this thesis. Re-aggregated human pancreas islet microtissues were used as a model system, and insulin release at a single-islet level was measured. The precise control of the flow conditions in perfused and open microfluidic systems allowed for resolving fast concentration changes of insulin in the culture solution arising from the dynamics of insulin release of the pancreatic islets. Such a high temporal resolution was achieved by taking advantage of the slip boundary condition at the liquid-air surface of open microfluidic structures, which enables less axial sample distribution in the solution along the flow with respect to closed microfluidic channels. This minimal axial dispersion enables high-temporal-resolution detection of the insulin, released by the pancreatic islets, and fast medium exchange. Moreover, the structure-free trapping of the microtissue at the bottom of the drop enables homogeneous flow conditions around the microtissue, which promotes precise and reproducible measurements.

The hanging-drop perfusion system is highly suited for the quantification of small amounts of secretory products that are released from single microtissues at high temporal resolution. Here, this platform was used to resolve the biphasic and pulsatile release of insulin from single islets and was applied to assess the effects of anti-diabetic medication on the dynamics of insulin release. Consequently, the hanging-drop perfusion system is an excellent technological platform for islet and diabetes research.

To conclude, in this thesis I have introduced three hanging-drop platforms, which were specifically designed to get deeper insights into the biology of 3D microtissues and which could be operated with minimal experimental setup efforts and complexity. The developed platforms are compatible with different microtissue types and help to preserve tissue integrity, viability and functionality. The precise control of liquid and culturing conditions is possible through the use of microfluidics and open microfluidic structures for rapid exchange of media and analytes. All presented platforms support undisturbed culturing of the microtissues and feature minimal system effects on the readout.

Full characterization and validation of the platforms have been presented, as well as proof-of-concept examples of biological processes and mechanistic compound studies that are enabled by the developed novel tools.

7 OUTLOOK

The developed hanging-drop-based platforms are well suited for cell culturing and analysis of 3D microtissues. These platforms are highly versatile, and their layout can be easily adapted for different experimental conditions and configurations. The interconnection of multiple hanging-drop culturing compartments through microfluidic channels allows for co-culturing of different tissue types, and consequently for studying the interaction of different microtissues.

Sensors, which are integrated in hanging-drop networks, allow for continuously measuring changes in the metabolism not only of single-microtissues but also of different interacting tissue types. This can be of high interest to test prodrugs or to measure metabolic processes in which multiple tissue types are involved. Moreover, the detection of microtissue metabolic changes can be used to test drug compounds and to assess their effect on patient biopsies, which may reveal high variability and large donor-to-donor differences. In the future, improved biosensors will allow to perform experiments over longer time periods. The modular system integration of the biosensors can be used to expand the platform by integrating more electrodes and implementing other sensor types, which will augment the readout capability and consequently enable to extract more information from the system under study.

The hydrogel hanging-drop platform is optimized for long-term high-resolution imaging of microtissues, and can be operated with minimal experimental equipment. Hydrogels are used to precisely tune the microenvironment of the microtissues, which is needed for the culture of complex microtissue types, such as organoids or tissues obtained through biopsies. Therefore, hydrogel hanging-drop networks can be used to study inter-tissue communication to obtain more complex *in vitro* microtissue models. The design of the platform allows for using high-end confocal imaging systems, such as spinning-disk confocal and two-photon-excitation microscopes. Spinning disk microscopes represent a great tool to increase the scan-rate for higher imaging throughput, or to monitor very fast cellular events and responses of 3D microtissues. Two-photon excitation microscopes enable deep-tissue imaging, which is necessary for the relatively large 3D tissue structures (~300 μm in diameter).

The hanging-drop-based FlowGSIS assay can resolve the secretion dynamics of insulin of single human pancreas islets and, thus, opens up a wide range of applications in islet-, and diabetes research. The platform can be used to study the mechanisms of action of anti-diabetic medication. However, the platform currently offers limited throughput. Operation of the hanging-drop platform without the need to continuously monitor the hanging-drop size is key to enable parallelization of the assays. The needle-type outlet, presented in chapter 2, is a suitable solution but needs to be tested and validated to make sure that the needed temporal resolution and reproducibility can be achieved.